HISTORY MATCHING AND UNCERTAINTY QUANTIFICATION USING SAMPLING METHOD

A Dissertation

by

XIANLIN MA

Submitted to the Office of Graduate Studies of
Texas A&M University
in partial fulfillment of the requirements for the degree of

DOCTOR OF PHILOSOPHY

August 2008

Major Subject: Petroleum Engineering

HISTORY MATCHING AND UNCERTAINTY QUANTIFICATION USING SAMPLING METHOD

A Dissertation

by

XIANLIN MA

Submitted to the Office of Graduate Studies of
Texas A&M University
in partial fulfillment of the requirements for the degree of

DOCTOR OF PHILOSOPHY

Approved by:

Co-Chairs of Committee,	Akhil Datta-Gupta
	Yalchin Efendiev
Committee Members,	Daulat D. Mamora
	Behnam Jafarpour
Head of Department,	Stephen A. Holditch

August 2008

Major Subject: Petroleum Engineering

ABSTRACT

History Matching and Uncertainty Quantification Using Sampling Method.

(August 2008)

Xianlin Ma, B.S., China University of Geosciences, Wuhan, China;

M.S., University of Petroleum, Beijing, China;

M.S., University of Waterloo, Ontario, Canada

Co-Chairs of Advisory Committee: Dr. Akhil Datta-Gupta
Dr. Yalchin Efendiev

Uncertainty quantification involves sampling the reservoir parameters correctly from a posterior probability function that is conditioned to both static and dynamic data. Rigorous sampling methods like Markov Chain Monte Carlo (MCMC) are known to sample from the distribution but can be computationally prohibitive for high resolution reservoir models. Approximate sampling methods are more efficient but less rigorous for nonlinear inverse problems. There is a need for an efficient and rigorous approach to uncertainty quantification for the nonlinear inverse problems.

First, we propose a two-stage MCMC approach using sensitivities for quantifying uncertainty in history matching geological models. In the first stage, we compute the acceptance probability for a proposed change in reservoir parameters based on a linearized approximation to flow simulation in a small neighborhood of the previously computed dynamic data. In the second stage, those proposals that passed a selected criterion of the first stage are assessed by running full flow simulations to assure the rigorousness.

Second, we propose a two-stage MCMC approach using response surface models for quantifying uncertainty. The formulation allows us to history match three-phase flow simultaneously. The built response exists independently of expensive flow simulation, and provides efficient samples for the reservoir simulation and MCMC in the second stage.

Third, we propose a two-stage MCMC approach using upscaling and non-parametric regressions for quantifying uncertainty. A coarse grid model acts as a surrogate for the fine grid model by flow-based upscaling. The response correction of the coarse-scale model is performed by error modeling via the non-parametric regression to approximate the response of the computationally expensive fine-scale model.

Our proposed two-stage sampling approaches are computationally efficient and rigorous with a significantly higher acceptance rate compared to traditional MCMC algorithms.

Finally, we developed a coarsening algorithm to determine an optimal reservoir simulation grid by grouping fine scale layers in such a way that the heterogeneity measure of a defined static property is minimized within the layers. The optimal number of layers is then selected based on a statistical analysis.

The power and utility of our approaches have been demonstrated using both synthetic and field examples.

DEDICATION

To my wife Xiaofei Wu and my son Yueqian (David) Ma for their love, support, and encouragement.

ACKNOWLEDGMENTS

I would like to express my deep gratitude to my graduate advisor Dr. Akhil Datta-Gupta for his inspiration, thoughtful advice, academic guidance, financial support, time and efforts contributed to this project. This work would not have been possible without him for sure.

I would like to thank Dr. Efendiev for imparting some of his knowledge to me through our many meetings, discussions and classes.

I would like to thank Dr. Jafarpour and Dr. Mamora for serving on my committee. I acknowledge their helpful comments and suggestions in shaping this dissertation.

I would like to thank Chevron Energy Technology Company for providing me internship opportunities. Seongsik Yoon, Clair Jensen, Djuro Novakovic and Michael Shook were wonderful mentors in the summer jobs from whom I gained valuable experience and motivation for my research.

I would like to thank my colleagues in the model calibration and efficient reservoir imaging group for their precious help and discussion. Thank you for making my years in Texas A&M enjoyable.

I would like to acknowledge financial support from members of the Joint Industry Project on reservoir data integration and also from the U.S. Department of Energy. The facilities and resources provided by the Petroleum Engineering Department, Texas A&M University, are gratefully acknowledged.

TABLE OF CONTENTS

Page

ABSTRACT…… ……...…..iii

DEDICATION……. ……..v

ACKNOWLEDGMENTS… ……vi

TABLE OF CONTENTS…… …….vii

LIST OF FIGURES.....x

CHAPTER I INTRODUCTION AND STUDY OBJECTIVES.....1

1.1 Introduction.....1
1.1.1 Reservoir Data.....2
1.1.2 History Matching and Uncertainty Quantification.....3
1.2 Objectives……..... ……..……5
1.3 Dissertation Outline.....7

CHAPTER II TWO-STAGE MCMC WITH SENSITIVITY.....8

2.1 Introduction.....8
2.2 Approach….....10
2.2.1 Illustration of the Procedure: A Synthetic Example.....12
2.3 Theoretical Background.....14
2.3.1 Bayesian Framework.....14
2.3.2 Markov Chain Monte Carlo.....15
2.4 Proposal Generation.....16
2.4.1 Indpendent Sampler.....16
2.4.2 Random Walk Sampler.....17
2.4.3 Langevin Sampler.....17
2.5 Parameterization.....19
2.5.1 Karhunen–Loève Expansion.....19
2.5.2 Gradual Deformation Method.....21
2.6 Description of Two-stage MCMC Method.....21
2.6.1 Two-stage MCMC Algorithm.....23
2.7 Illustrative Example.....25
2.8 Synthetic Example.....27
2.9 Field Example.....30

CHAPTER III TWO-STAGE MCMC WITH RESPONSE SURFACE MODELS.....36

Page

3.1 Introduction....36
3.2 Bayesian Partition Modeling....38
3.3 Kriging....41
3.4 Two-stage MCMC Algorithm....42
3.5 Illustrative Example....43
3.6 2D Synthetic Example....47
3.7 Facies Type Example....52
3.7.1 Plurigaussian Simulation....52
3.7.2 Production Data Matching and Uncertainty Quantification....54
3.8 Field-scale Example....59
3.8.1 Reservoir Model Description....59
3.8.2 Uncertainty Assessment....62

CHAPTER IV TWO-STAGE MCMC WITH UPSCALING AND NONPARAMETRIC REGRESSION....68

4.1 Two-stage MCMC with Upscaling and Nonparametric Regression....68
4.1.1 Single Phase Upscaling....70
4.2 Convergence Diagnostics....72
4.2.1 Gelman and Rubin Method....72
4.2.2 Maximum Entropy Test....74
4.3 2D Synthetic Example....75
4.4 3D Synthetic Example....80

CHAPTER V OPTIMAL COARSENING OF 3D RESERVOIR MODELS....87

5.1 Introduction....88
5.2 Approach and Mathematical Formulation....91
5.2.1 Illustration of the Procedure: A Synthetic Example....95
5.3 Case Study of 2D Cross-Section....98
5.4 Case Study of 3D Channelized Reservoir....103

CHAPTER VI CONCLUSIONS AND RECOMMENDATIONS....115

6.1 Conclusions....115
6.2 Recommendations....117

NOMENCLATURE....118

REFERENCES....120

APPENDIX A CONVERGENCE OF MODIFIED MARKOV CHAIN....127

Page

APPENDIX B ACCEPTANCE PROPERTIES FOR LANGEVIN ALGORITHM IN LINEAR PROBLEMS 132

APPENDIX C SAMPLING PROPERTIES OF RML..... 134

VITA……..... 138

LIST OF FIGURES

FIGURE Page

2. 1 Two-stage MCMC flowchart. 11
2. 2 Nine-spot pattern example: reference and initial models. 13
2. 3 Reduction in RMS per simulation run. 14
2. 4 Comparison of acceptance rates for two-stage, full MCMC and Langevin algorithm. 14
2. 5 Histogram generated by two-stage MCMC matches to the posterior distribution that was to be sampled from. 26
2. 6 Reference (a) and initial (b) models of adjacent nine-spot example. 28
2. 7 Reduction in RMS per simulation run. 28
2. 8 Comparison of acceptance rates for two-stage, full MCMC and Langevin algorithm. 29
2. 9 Collected samples using two-stage MCMC in the adjacent example. 29
2. 10 Well configuration (a) and schedule (b) of the Goldsmith field case. 31
2. 11 3D Realizations generated by gradual deformation method. 31
2. 12 Acceptance rate for the full and two-stage MCMC. 32
2. 13 Two-stage MCMC: three collected samples. 32
2. 14 Permeability variance reduction. 34
2. 15 Initial and final water cut responses. 35
3. 1 2D Voronoi diagram 40
3. 2 Graphical representation of Rastrigin's function. 44
3. 3 Response surface built using Kriging. 45
3. 4 Response surface built using BPM. 45
3. 5 Functional value versus the number of iterations. 46
3. 6 History matching 3-phase model for a nine-spot heterogeneous case (a) reference and (b) initial model. 48
3. 7 Water cut match and uncertainty assessment. 48

FIGURE Page

3. 8 BHP match and uncertainty assessment....49
3. 9 GOR match and uncertainty assessment....50
3. 10 History matching 3-phase model for a nine-spot heterogeneous case: data misfit reduction....50
3. 11 Collected samples of history matching 3-phase model for a nine-spot heterogeneous case....51
3. 12 Simulation of lithofacies distribution using random Gaussian fields (Y1 and Y2) and rock type rule (a) exponential type random field; (b) Gaussian type field; (c) rock type rule (d) simulated facies map....53
3. 13 Reference and initial facies map....54
3. 14 Water cut match and uncertainty quantification....55
3. 15 BHP match and uncertainty quantification....56
3. 16 GOR match and uncertainty quantification....57
3. 17 Collected samples of facies type example....58
3. 18 Initial water saturation for SPE 9....59
3. 19 Solution gas/oil ratio and gas formation volume factor curves....60
3. 20 Relative permeability curves....60
3. 21 Gas saturation distribution at the end of simulation time (900 days)....61
3. 22 Two stage for SPE9: data misfit reduction....62
3. 23 Two stage for SPE9: water cut match....63
3. 24 Two stage for SPE9: BHP match (PROD 2 ~ PROD 16)....64
3. 25 Two stage for SPE9: BHP match (PROD 17 ~ PROD 26)....65
3. 26 Two stage for SPE9: GOR match (PROD 2 ~ PROD 16)....66
3. 27 Two stage for SPE9: GOR match (PROD 17 ~ PROD 26)....67
4. 1 Fine scale cells and coarse scale cell....71
4. 2 Reference, initial models and collected samples....76
4. 3 Error model of 2D synthetic example....77
4. 4 GOR misfits reduction of 2D synthetic example....77

FIGURE Page

4. 5 GOR match of 2D synthetic example. 78
4. 6 Brooks and Gelman diagnostic plot for 2D synthetic example. 79
4. 7 Reference and initial log permeability fields. 81
4. 8 Error model of 3D example. 82
4. 9 Water cut misfits reduction of 3D example 82
4. 10 Watercut match of 3D example. 84
4. 11 Horizontal permeability histogram for (a) inital model, (b)-(f) sampled inverted model starting from initial model. 85
4. 12 Convergence parameters for two-stage MCMC on 1000 proposals (a) entropy (b) variance of entropy. 86
5. 1 Error in velocity is introduced while upscaling; different fluid velocities are replaced by a single value. 90
5. 2 Between-variation heterogeneity analysis; the heterogeneity has been normalized to 100%. 94
5. 3 Fine scale model of 2D channelized reservoir. 96
5. 4 Between-layer variance and the determination of the optimal layer. 96
5. 5 18-layer optimal model using variance analysis. 97
5. 6 20-layer model using uniform upgridding. 97
5. 7 Distribution of inverse time of flight, showing fine scale (100 layers), the optimal (18 layers) and uniform (20 layers). 98
5. 8 The heterogeneity has 50x100 2D cross-section generated by sequential Gaussian simulation. 99
5. 9 Regression mean square error analysis. 100
5. 10 Distribution of inverse time of flight for 100 streamlines, showing the optimal (30 layers) and fine solutions (100 layers) 101
5. 11 QQ scatter-plot of averaged versus fine permeability. 102
5. 12 81 layer, 3D model permeability distribution. 104

FIGURE Page

5. 13 81 layer model, Sand A shows no channel definition. Sand B shows more channelized reservoir. Main sand shows highly channelized reservoir between pay/non-pay regions. 104
5. 14 36 Layers is determined to be the optimal number of layers due to the sharp change in slopes. 105
5. 15 Regression mean square error analysis is used to determine the minimum number of layers at 26 layers. 105
5. 16 36 layer, 3D model permeability distribution. 107
5. 17 36 layer model Sand A comparison of permeability distribution shows homogenization of the previous smeared distribution in 81 layer model. 108
5. 18 36 layer model Sand B permeability distribution shows that the channels are being smeared but the regions maintain a high permeability to maintain the pay/non-pay distinction. 108
5. 19 The field oil production rate is almost identical for both the 36 layer model and the fine 81 layer model. 109
5. 20 The water-cut matches in forecasting for both the fine and 36 layer model. 109
5. 21 The oil production rate and wate cut are closely matached for the BJ-U producer. 110
5. 22 The oil production rate and water cut are closely matched for the BJ_Q producer. 110
5. 23 The oil production rate and water cut are closely matched for the BJ_V producer. 111
5. 24 26 layer 3D model permeability distribution. 111
5. 25 26 layer model Sand A permeability distribution shows a homogenization of the smeared distribution shown the 81 layer model. 112
5. 26 26 layer model Sand B permeability distribution shows a greater removal of channel definition as compared to the 36 layer model. .. 112

FIGURE Page

5. 28 The oil production rate and water cut for the 26 layer model are severely deviated when compared to the fine scale model. 113

5. 29 The oil production rate and water cut for the 26 layer model deviates at approximately 2003 with the water cut significantly higher than the fine scale model causing under production of oil. 114

5. 30 The water cut in the 26 layer model is higher than the fine scale model starting around 2005 causing a deviation in the oil production rate and lowering the wells response. 114

C. 1 Geometric interpretation of RML. 137

CHAPTER I

INTRODUCTION AND STUDY OBJECTIVES

Subsurface uncertainty exists inherently in dynamic reservoir modeling because of several factors, the primary ones being modeling error, data noise and the non-uniqueness of inverse problems that causes several models to fit the dynamic data. By understanding and quantifying the uncertainty in production forecast, financial investment risks can be reduced and decision quality can be improved. A suite of acceptable history matched models, which have multiple combinations of model parameters, is required to obtain a probabilistic view of the reservoir performance. Once these models have been obtained, they are calibrated for predicting the future performance and assessment of uncertainty and risk associated with a particular development plan. Uncertainty quantification in history matching geological models is by far the most time-consuming aspect of the workflow for both geoscientists and engineers since many simulation runs may be required. This chapter presents the motivation and objectives of the research in this dissertation.

1.1 Introduction

History matching is a process that a reservoir model is altered to match the known production data such as oil, gas and water production rate as well as pressure so that the history matched reservoir model will more accurately predict future performance of the reservoir. The history matching is an inverse problem in which a reservoir engineer calibrates key geological/reservoir model parameters. The process is time consuming and difficult. First, multiple forward flow simulations (Aziz and Settari 1979) are required to perform a history matching, and it often takes hours or days to model flow

---

This dissertation follows the style and format of the *SPE Journal*.

and transport through high resolution geologic models. This leads to weeks or months to complete a history matching project. Therefore, it is very important to limit the number of the flow simulation runs during history matching. Secondly, the reservoir parameters have a non-linear impact on reservoir responses. Finally, the history matching is an ill-conditioned mathematical problem with many solutions like most inverse problems, and different combinations of model parameter values may match the observed production data.

The non-uniqueness and other factors lead to the uncertainty in reservoir performance prediction, which must be quantified to optimize reservoir management. Bayesian statistics offers a consistent framework to assess the uncertainty. Using the Bayes' rule, the uncertainty can be assessed by a posterior distribution of reservoir models as the product of prior information on the models and a likelihood function that measures the degree of fit between the production data and results from a forward simulator. The posterior distribution is the solution to the inverse problem, and history matched models can be regarded as samples from the distribution. However, it is practically impossible to obtain the entire distribution by exploring the whole of parameter space. In order to quantify the uncertainty, it is necessary to obtain multiple matched models that are sampled correctly and efficiently from the posterior distribution. By predicting future reservoir performance with each of the models and analyzing all the model outputs, we can estimate the uncertainty in the model forecast. However, the sampling is not an easy task because the posterior distribution is usually non-Gaussian, and defined on a high-dimensional reservoir model space with multiple modes. Moreover, the normalization constant of the posterior distribution is difficult to evaluate. Therefore, uncertainty quantification becomes how to efficiently sample from the posterior distribution.

1.1.1 Reservoir Data

Two types of data are often needed to build a reservoir model: static and dynamic data. Non-time varying static data include core, well log and seismic data. Core data provide porosity, permeability and relative permeability measurements, and has the smallest

scale of information. Well-log data indicate lithology, petro-physics and fluid. Seismic data provide large range of structure such as faults and surfaces. Although core and well-log data provide direct measurements on reservoir petrophysical properties, their scale of information is much smaller than the resolution of the grid on which we model the reservoir. Geostatistics (Deutsch and Journel 1998) such as cokriging method (Ma and Journel 1999) is a powerful tool to integrate all of the static data.

Dynamic data such as transient pressure, saturation and flow rates are usually generated from producing reservoir. The integration of dynamic data requires an iterative, trial and error process involving multiple runs of numerical flow simulations. The high resolution model (conditioned to seismic and hard data), would be CPU prohibitive for such flow simulations. An upscaling procedure to coarsen the high resolution model is necessary for making flow simulations feasible.

Bayesian statistics (Robert and Casella 1999) offers a consistent basis to integrate the static and dynamic data. In the framework, a prior distribution is used to express information about the reservoir parameters which is available before the dynamic data are observed. The likelihood function contains information about theoretical relations between the reservoir parameters and the dynamic data. Applying Bayesian theorem, a posterior distribution can integrate the static data and production naturally, which contains all information available about the reservoir parameters given the dynamic data.

1.1.2 History Matching and Uncertainty Quantification

Reconciling geologic models to the dynamic response of the reservoir is critical to building reliable reservoir models. This process is referred to as “history matching”. Traditionally, history matching is performed by manually adjusting a few reservoir model parameters through a trial-and-error procedure. Manual history matching runs the simulation model for the historical production period and then compares the results with known field performance. After the comparison is made, the reservoir engineer will adjust the simulation data in an effort to improve the match. The manual history matching might take months of effort and many reservoir flow simulations to achieve a

single history matched model. Moreover, the success of the method largely depends on the experience of reservoir engineer on the subject field.

Automatic history matching is similar to the manual history matching, except that computers and software tools are employed to adjust the reservoir parameters rather than direct intervention of reservoir engineers. Automatic history matching can be thought of as a minimization problem, whose objective function includes the sum of squared difference between observed data and computed data, as well as a model parameter regularization term arising from prior information about the reservoir under study. To minimize the objective function, an efficient minimization algorithm must be chosen. Two distinct methods to automatic history matching have been proposed, namely, gradient/sensitivity and stochastic method. Gradient-based methods such as the Gauss-Newton and Levenberg-Marquardt have been widely used for automatic history matching due to their faster convergence rates (Bissell et al. 1992; Lepine et al. 1999). Sensitivity coefficients are required for inputs of these methods, which are partial derivatives that define the change in production response because of a small change in reservoir parameters. Streamline derived sensitivity techniques have shown great potential (Vasco et al. 1999; Datta-Gupta and King 2007; Zhong et al. 2002) and they only require a single forward simulation to calculate the sensitivities analytically. Since the goal of the gradient-type methods is to seek a single history matched model, it is different for the methods to assess the uncertainty, and also do not guarantee that the solution is the global optimum.

The stochastic method such as simulated annealing or genetic algorithms assumes that the production data is a realization of a stochastic process (Halforsen et al. 1990; Sen et al. 1992). In these methods, the sensitivity is not needed, and only forward flow simulation runs are required. These methods can converge to the global minimum and can be used to assess the uncertainty. The primary disadvantage is that these methods require thousands of simulation runs to converge and can be computationally prohibitive for field-scale applications. The demanding computation needs always limits their applications in history matching and uncertainty quantification in practice.

As one of the stochastic methods, Markov Chain Monte Carlo (Robert et al. 1999; Oliver et al. 1997) provides the accurate sampling albeit at a high cost because of their high rejection rates and the need to run a full flow simulation for every proposed candidate. There is also additional cost associated with a burn-in time needed for the MCMC to assure that the starting state does not bias sampling. Approximate sampling methods, such as randomized maximum likelihood (RML) (Kitanidis 1995; Oliver et al. 1996) are commonly used to avoid the high cost associated with the MCMC methods. For linear problems (Gaussian posterior distributions), RML has an acceptance probability of unity; however, the assumptions made in RML may be too restrictive for nonlinear problems which is typically the case for reservoir history matching. The main appeal of RML is ease of implementation within the framework of traditional automatic history matching via minimization of an objective function that includes a production data misfit term and a model misfit term. There is also some evidence in the literature that the RML has favorable sampling properties for nonlinear problems (Liu et al. 2001), although it is likely to be problem specific. There is a need for an efficient and rigorous approach to uncertainty quantification for general non-linear problems related to history matching.

The Ensemble Kalman Filter (EnKF) is an alterative for generating a suite of plausible reservoir models, which has gained popularity in the history matching and uncertainty quantification in the recent past (Nævdal et al. 2003; Gu and Oliver 2004) because EnKF is suitable for any reservoir simulator and continuous model update. The ensemble of realizations is used to estimate covariance between model parameters and cross-covariance between data and model parameters. Then the EnKF uses the covariance to update the model parameters sequentially as more data become available.

1.2 Objectives

The objective of this research is to develop an efficient and rigorous sampling method to quantify the uncertainty in history matching geological models, and to adopt the MCMC

approach to rapidly generate multiple models via sampling from the posterior distribution with high acceptance rates. To reduce the number of simulation runs in the regular MCMC but also to exhaustively explore the parameter space, we employ several proxy model techniques based on streamline-derived sensitivity, response surface models, and upscaling and nonparametric regression to identify many good samples during the exploration by appropriate modification of the instrumental proposal distribution. The modification guarantees that the obtained Markov chain will converge to the target posterior distribution and will have a higher acceptance rate. After this, we collect reservoir models and identify representative samples for quantifying uncertainty. These techniques have been successfully applied in both synthetic and field cases.

Reservoir models are usually represented by discretized block values of reservoir properties. Parameterization tries to replace the reservoir model with a smaller group of parameters while preserving important geological features. Several parameterization approaches including Karhunen–Loève (*K-L*) expansion, gradual deformation and plurigaussian models for facies have been implemented for history matching and uncertainty assessment. We combine the parameterization methods with MCMC to provide efficient sampling from the posterior distribution.

The development of coarsened reservoir simulation models from high resolution geologic models is a critical step in a simulation study. Another objective of the research is to develop a new constrained optimization approach to the coarsening of 3D reservoir models for flow simulation. The optimization maximally preserves a statistical measure of the heterogeneity of a fine scale model. Constraints arise from the reservoir fluids, well locations, pay/non-pay juxtaposition, and large scale reservoir structure and stratigraphy. Our algorithm groups the layers in such a way that the heterogeneity measure of an appropriately defined static property is minimized within the layers and maximized between the layers. The optimal number of layers is then selected based on a statistical analysis resulting in the minimum loss of heterogeneity because of upgridding.

1.3 Dissertation Outline

In chapter II we describe a two-stage MCMC formulation with streamline-derived sensitivities. First, we present the theoretical background of the methodology including Bayesian framework and MCMC; then discuss three methods to generate the proposal in the Metropolis-Hastings algorithm. Secondly, we discuss two parameterization approaches, i.e. the gradual deformation method and Karhunen-Loeve expansion to replace a reservoir model with a smaller group of parameters. Finally, we present a 1D example to show that the two-stage MCMC method can correctly sample from a two-modal posterior distribution, and a 2D synthetic example and a field example to show the efficiency in uncertainty quantification compared to the traditional MCMC.

In chapter III we describe a two-stage MCMC formulation with response surface models. The formulation is sensitivity-free by building a response surface model. We apply the method to history matching three-phase flow including bottom hole pressure, water cut and GOR. Three numerical examples show the power of the method.

In Chapter IV we describe a two-stage MCMC formulation with upscaling and non-parametric regression. In the first stage we apply a cheap coarse model to guide the sampling procedure. Non-parametric regression is used to correct the reservoir responses of the coarse model. Two examples validate the efficiency of the method.

In Chapter V we describe an approach to optimal coarsening of 3D reservoir models for flow simulation. We plan to use the upgridding technique in our two-stage MCMC method in future. We mainly discuss the new statistical approach applied to layer coarsening. The approach has been validated for a number of oil and gas projects, where flow simulation through the coarsened model is shown to provide an excellent approximation to high resolution calculations performed in the original model.

CHAPTER II

TWO-STAGE MCMC WITH SENSITIVITY*

A Bayesian approach to history matching and uncertainty quantification is adopted here. In this approach a priori information on reservoir model parameter such as permeability or porosity is represented by a probability distribution over the parameter space. Using Baye's rule, the prior distribution is transformed into a posterior distribution by including the degree of fit between actual production data and data predicted from a reservoir flow simulator. The Bayesian approach offers a consistent framework to solve the history matching problems and to assess uncertainty. The solutions are a set of samples drawn correctly from the posterior distribution. By inputting the samples into a reservoir simulator to predict their performances, we calculate the statistics of the performance predictions, and perform the uncertainty quantification.

2.1 Introduction

Uncertainty exists inherently in dynamic reservoir modeling because of several factors, the primary ones being the modeling error, data noise, and the non-uniqueness of the inverse problems that causes several models to fit the dynamic data. Under a Bayesian framework, the uncertainty in the reservoir models can be evaluated by a posterior probability distribution, which is proportional to the product of a likelihood function and a prior probability distribution of the reservoir model. To quantify the uncertainty, it is necessary to generate a sequence of model realizations that are sampled appropriately from the posterior distribution. Rigorous sampling methods, such as Markov Chain

*Part of this chapter is reprinted with permission from "A Multistage Sampling Method for Rapid Quantification of Uncertainty in History Matching Geological Models" by Ma, X., Al-Harbi, M., Datta-Gupta, A., and Efendiev, Y., 2007. Paper SPE 102476 presented at Annual Technical Conference and Exhibition, San Antonio, TX

Monte Carlo (MCMC) (Oliver et al. 1997; Robert and Casella 1999), provide the accurate sampling albeit at a high cost because of their high rejection rates and the need to run a full flow simulation for every proposed candidate.

There are many methods proposed in literature. Caers et al. (2002) proposed to perturb jointly effective permeabilities along a set of streamline. The mapping of streamline effective permeability perturbations to each gridblock was carried out by MCMC. Agarwal and Blunt (2004) used streamlines to identify what parts of a reservoir impact the flow to each production well, and then estimated the modifications to reservoir properties that are needed to match production data based on rate comparison. Christie et al. (2002) applied the neighborhood algorithm (Sambridge 1999) to sample the lower data misfit regions of parameter space guided by the spatial properties of Voronoi cells. Generally, these methods either attempt to perform rigorous sampling of the posterior distribution, such as Markov Chain Monte Carlo (MCMC) methods and genetic algorithms or attempt to perform approximate sampling such as Randomized Maximum Likelihood (RML) (Oliver et al. 1996) method.

We propose a two-stage MCMC approach for quantifying uncertainty in history matching geological models. Our proposed sampling approach is computationally efficient with a significantly higher acceptance rate compared to traditional MCMC algorithms. In the first stage, we compute the acceptance probability for a proposed change in reservoir parameters based on a fast linearized approximation to flow simulation in a small neighborhood of the previously computed dynamic data. In this stage, no reservoir simulations are needed to explore the model parameter space. In the second stage, those proposals that passed a selected criterion of the first stage are assessed by running full flow simulations to assure the rigorousness in sampling. Then, these samples are either rejected or accepted using the MCMC selection criterion. The two-stage approach increases the acceptance rate, and reduces the computational cost required for the MCMC sampling. To propose MCMC samples, we consider two instrumental proposal distributions, the random walk sampler and the Langevin sampler (Robert and Casella 1999). In the chapter we first outline the major steps in the two-

stage MCMC method and illustrate the procedure using a 2D synthetic example. Next, we describe the mathematical formulation of the two-stage MCMC method. We then describe the proposal selection algorithms, including the Langevin sampling algorithm and its relationship to the commonly used RML approach. We also discuss the application of Langevin algorithms for nonlinear problems. Finally, we demonstrate the power and utility of our method, using a second synthetic waterflood example with repeated nine-spot patterns and a 3D field example that involves integration of over 20 years of water-cut history. In the appendix, we further explore the sampling properties of the Langevin and the RML methods.

2.2 Approach

An outline of the procedure in our proposed approach is given in the flow chart in **Fig. 2.1**. The loop ends when a predefined number of samples are collected or a maximum number of iterations are reached. Either streamline or finite-difference models can be used for fluid flow simulation, covering a wide range of applications. Briefly, the major steps are as follows:

Step 1: Define a suitable parameterization for the geologic model. We use two methods, the gradual deformation method (GDM) (Hu 2000) and the Karhunen–Loève (K-L) expansion (Loeve 1977).

Step 2: Generate geological models using geostatistical simulations based on the parameterization in Step 1.

Step 3: Run flow simulation for the initial model and calculate the reservoir response, and also streamline-based analytic sensitivities (Datta-Gupta et al. 2001). The sensitivity calculations do not require additional flow simulation.

Step 4: Perturb the parameterization coefficients to generate a new geologic model.

Step 5: Approximate the reservoir response for the new model using local linearization and the sensitivities.

Step 6: Check for the acceptance of the new model using the Metropolis-Hastings algorithm (Metropolis et al. 1953; Hastings 1970).

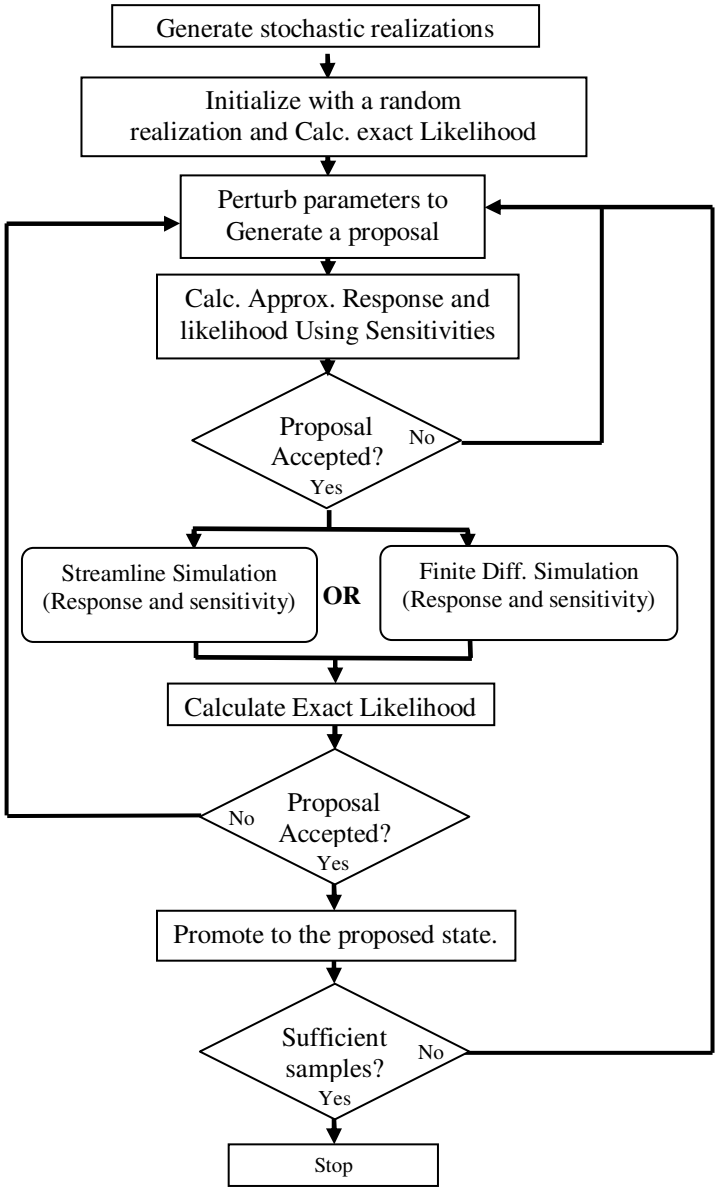

Fig. 2. 1—Two-stage MCMC flowchart.

Step 7: If the model is rejected, go to Step 4; otherwise, go to Step 8.

Step 8: Run the complete flow simulation for the new model and calculate streamline-based sensitivity.

Step 9: Check for the acceptance of the new model using the Metropolis-Hastings algorithm with updated acceptance probabilities.

Step 10: If the model is accepted, replace the current model with the new model. Go to Step 4.

Step 11: Check the Markov Chain convergence and collect samples.

2.2.1 Illustration of the Procedure: A Synthetic Example

Before discussing the detailed mathematical formulation, we will first illustrate our procedure using a simple nine-spot example. We would like to match the water-cut data. A 2D mesh of 47×47 was used with a total of 2,209 grid cells to study the performance of two-stage MCMC and compare with the conventional MCMC. The reference model is shown in **Fig. 2.2a.** We used the K-L expansion (described later) with 40 random parameters for the proposal generation. The starting model is shown in **Fig. 2.2b**.

In two-stage MCMC, the proposals are screened before running the fine-scale simulations. Therefore, unlike the full MCMC, the number of proposals is not equal to the number of simulations. **Fig. 2.3** shows the RMS error reduction for conventional and two-stage MCMC as a function of the number of simulations. The advantage of the two-stage MCMC is quite obvious in that it requires much less number of simulation runs to achieve the same level of misfit.

The two-stage MCMC will have the effect of filtering out the obvious rejections in the first stage without the cost of running a full simulation. Such filtering does not ensure automatic acceptance but will increase the probability of finding good proposals for the second stage, thus increasing MCMC efficiency.

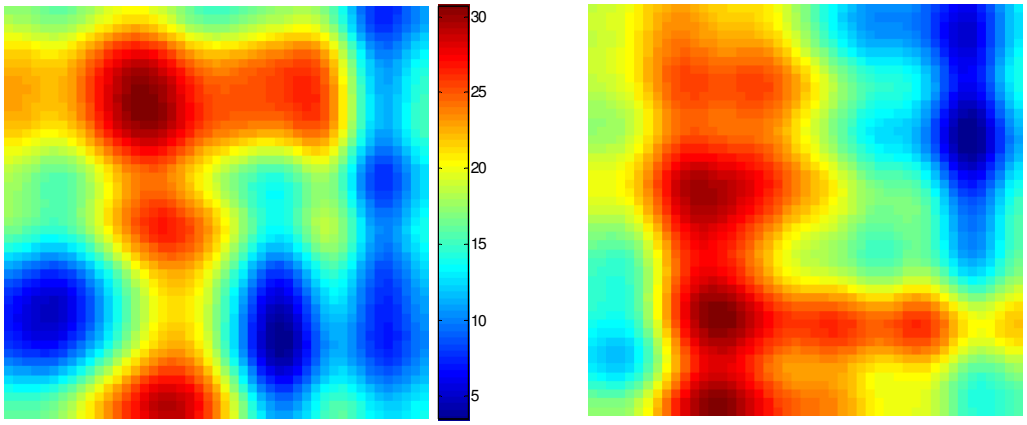

Fig. 2. 2— Nine-spot pattern example: reference and initial models.

Fig. 2.4 shows the acceptance rate for both conventional and two-stage MCMC methods, where we have computed the acceptance rate as the fraction of the final accepted proposals to the total proposals. The two-stage MCMC exhibits acceptance rate of around 60%, while the full MCMC fluctuates near 30%. Such doubling of the acceptance rate for a particular step size translates to a significant savings in computation time if the chains have similar convergence properties, as it is the case for our examples. In general, however, the high rate does not imply rapid convergence. For comparison purposes, we have also shown the acceptance rate as well as RMS error reduction for MCMC with Langevin sampling, which is discussed later in the paper. It shows improvement over the conventional MCMC while falling short of the two-stage method proposed here. For illustration purposes, five selected samples are shown in **Fig. 2.5,** indicating possible permeability distributions and displaying the uncertainty range to some extent. All these models honor the static data, share the same covariance model, and are conditioned to observed dynamic data. Risk analysis can be performed using multiple models to adequately describe the posterior distribution.

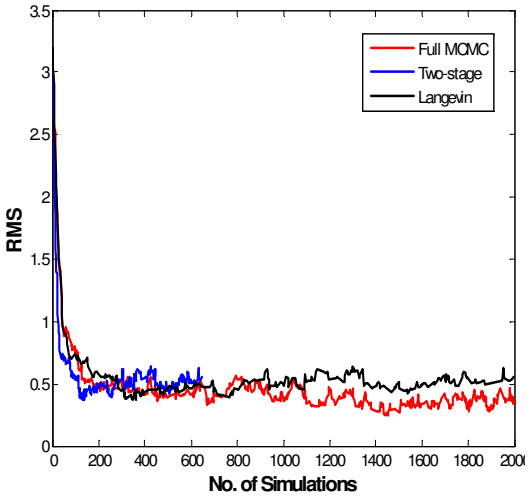

Fig. 2. 3— Reduction in RMS per simulation run.

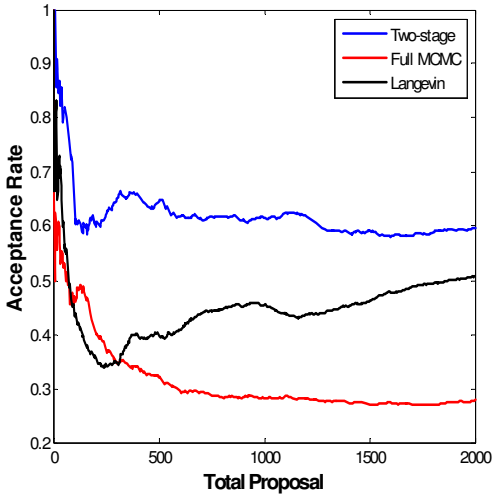

Fig. 2. 4—Comparison of acceptance rates for two-stage, full MCMC and Langevin algorithm.

2.3 Theoretical Background

In this session we briefly discuss the theoretical background which is related to two-stage MCMC method.

2.3.1 Bayesian Framework

The Bayesian framework for statistical inference provides a formal and systematic procedure for updating reservoir properties, for example permeability, based on the observed reservoir response, d_{obs}, such as the bottom-hole pressures (BHPs), the water cut, the gas-oil ratios (GORs). We start with a prior geological model that already integrates well logs, seismic and geologic data using geostatistical modeling or other methods. From Bayes' theorem, we have

$$P(k \mid d_{obs}) \propto P(d_{obs} \mid k) P(k) \quad \text{.....(2.1)}$$

where $P(k)$ denotes the prior probability distribution for permeability, $P(d_{obs}|k)$ is the likelihood function and $P(k|d_{obs})$ is the posterior probability distribution. In particular if we assume that the prior model and the data errors follow a Gaussian distribution, then $P(k|d_{obs})$ assumes the following form (Tarantola 1987):

$$P(k \mid d_{obs}) \propto \exp\left\{-\frac{1}{2}\left[(k-k_{prior})C_k^{-1}(k-k_{prior})^T + (g(k)-d_{obs})C_D^{-1}(g(k)-d_{obs})^T\right]\right\} \quad \text{.....(2.2)}$$

where k_{prior} is the prior model, $g(k)$ is the simulated reservoir response corresponding to the proposed k, C_k is the parameter covariance and C_D is the data covariance. Note that the likelihood function, which involves the forward simulation, $g(k)$ requires the solution of nonlinear partial differential equations related to reservoir flow and transport. Thus, the evaluation of the posterior distribution is time-consuming.

2.3.2 Markov Chain Monte Carlo

Markov Chain Monte Carlo (MCMC) (Robert and Casella 1999) is a strategy for drawing samples k while exploring the parameter space using a Markov chain mechanism. The mechanism is constructed so that the samples k mimic samples drawn from the target posterior distribution $P(k|d_{obs})$. The samples are drawn sequentially, with the distribution of the sampled draws depending on the last value drawn; hence, the draws form a Markov chain. The key to the method's success, however, is not the Markov property but rather that the approximate distributions are improved at each step in the simulation, in the sense of converging to the target distribution.

We use MCMC since we can not draw samples from the target distribution $P(k|d_{obs})$ directly; instead we build a set of samples using a Markov process to approximate the $P(k|d_{obs})$. The key to MCMC is to create the Markov process whose stationary distribution is the specified $P(k|d_{obs})$ and run the simulation long enough that the distribution of the current samples is significantly close to this stationary distribution.

Metropolis-Hastings (Metropolis et al. 1953; Hastings 1970) is a general term for a family of MCMC methods that are useful for drawing samples from the posterior distribution. The algorithm is described as follows.

Metropolis-Hastings Algorithm

This approach proceeds with the following steps.

- Step 1. At state k_n generate k from a specified proposal distribution $q(k|k_n)$
- Step 2. Accept k as a sample with the probability

$$\rho(k_n, k) = \min\left(1, \frac{q(k_n \mid k)\pi(k)}{q(k \mid k_n)\pi(k_n)}\right) \quad \text{.....(2.3)}$$

i.e. $k_{n+1} = k$ with probability $\rho(k_n, k)$, and $k_{n+1} = k_n$ with probability 1 - $\rho(k_n, k)$.

Direct (full) MCMC sampling can be prohibitively expensive, because the method usually requires thousands of iterations for the convergence to a steady state. More importantly, each of iteration involves the computation of the flow simulation over a large time interval. In addition, the acceptance rate of the direct MCMC is usually small, i.e., most proposals will be rejected and the associated flow simulation is simply wasted.

2.4 Proposal Generation

Various choices for the proposal distribution $q(k|k_n)$ can be used in the two-stage MCMC algorithm. In particular, the following choices and their modifications for the instrumental distributions have been used here for sampling.

2.4.1 Independent Sampler

This implies that a proposal that is independent of the current model. Usually, the proposal is sampled from a certain distribution such as a Gaussian distribution. The drawback of this method is that it generally has a very low acceptance rate. When used

in the two-stage MCMC, this method may yield very low acceptance probability because it does not ensure that the new proposal is in close proximity of the current model. Consequently, the linearized approximation used for estimating reservoir response may not be accurate.

2.4.2 Random Walk Sampler

A proposal is generated by perturbing the current model.

$$k = k_n + \sigma\varepsilon \quad \text{.....(2.4)}$$

where σ is a positive small number, ε is a random variable (at each location) sampled from a certain distribution, typically Gaussian with zero mean and unit variance. The random walk sampler will, in general, have a higher acceptance rate than the independent sampler.

2.4.3 Langevin Sampler

A proposal distribution is derived from the Langevin diffusion (Robert and Casella 1999). The Langevin diffusion is defined by the following stochastic differential equation

$$dk(\tau) = \frac{1}{2}\nabla \log \pi(k(\tau))d\tau + dW_\tau \quad \text{.....(2.5)}$$

where W_τ is the standard Brownian motion and τ is a time-like parameter. It can be shown that the diffusion process $k(\tau)$ has $\pi(k)$ as its stationary distribution ($\tau \to \infty$). The actual implementation of the Langevin diffusion requires a discretization of Eq. 2.5 as follows,

$$k_{n+1} = k_n + \frac{\Delta\tau}{2}\nabla \log \pi(k_n) + \sqrt{\Delta\tau}\varepsilon_n \quad \text{.....(2.6)}$$

where ε_n follows the standard normal distribution. The samples generated in this way are tested and corrected by the Metropolis-Hastings acceptance-rejection as given by Eq. 2.3. Therefore, we choose the proposal as

$$k = k_n + \frac{\Delta\tau}{2}\nabla \log \pi(k_n) + \sqrt{\Delta\tau}\varepsilon_n \quad \text{.....(2.7)}$$

and, the instrumental proposal distribution is given by

$$q(k \mid k_n) \propto \exp\left(-\| k - k_n - \frac{\Delta\tau\nabla \log \pi(k_n)}{2} \|^2 \Big/ 2\Delta\tau \right) \quad \text{.....(2.8)}$$

Unlike the random walk sampler, the Langevin algorithm uses the shape of the stationary distribution $\pi(k)$ to make better proposals, which have a higher chance of being accepted. However, it requires the calculation of the gradient as shown in Eq. 2.7.

We would like to note that one can apply the two-stage concept to speed-up the computations of the Langevin algorithm. In particular, the computations of the gradients in Eq. 2.8 can be performed using approximate models, which may speed-up the computations significantly (Dostert 2007). For example, fast but approximate gradients may be computed using the streamline approach for two-phase incompressible flow. However, for compressible flows, these approximations may not be accurate. In such situations, one can use the analytical approximations of gradients in the first stage of MCMC computations, which are then further corrected in the second stage using more accurate computation of gradients based on adjoint methods.

We would like to note that the Langevin algorithm actually bears some similarities with the RML method. The Langevin algorithm uses the gradient information for computing proposals, which is similar to RML. Unlike RML, the proposals of the

Langevin algorithm are not independent. However, by judicious choice of $\Delta\tau$, one can achieve the acceptance probability of unity for linear problems (as in RML). This is demonstrated in Appendix A. Moreover, MCMC with the Langevin proposal allows for rigorous sampling for nonlinear problems. In Appendix B, we give a geometrical description of RML, and provide partial computations of calibrated proposal distributions of RML which shows that RML can introduce a bias during sampling.

Finally, we note that the proposed algorithms are efficient when the proposals are close to the current model. This proximity makes the linearized analytical approximation more accurate and, consequently, improves the acceptance rate of MCMC. The proposals near the current models are also used in Langevin algorithms, which are often used in practice. Our approaches do not require a particular way of proposing new models and can use any proposal in the neighborhood of an accepted proposal. For general independent proposals, one can use single-phase flow upscaling (Efendiev et al. 2005) in the screening stage.

2.5 Parameterization

Reservoir models are usually represented by discretized block values of reservoir properties. Parameterization tries to replace the reservoir model with a smaller group of parameters while preserving important geological features.

2.5.1 Karhunen–Loève Expansion

The Karhunen–Loève (*K-L*) expansion allows us to describe permeability fields in terms of two-point statistics using few parameters (Loeve 1977). A key advantage of the *K-L* expansion is that these parameters can be varied continuously while the underlying two-point geostatistical structure is still maintained. By truncating the expansion, the permeability field can be represented by a small number of random parameters. Denote $Y(x)=log[k(x)]$, and the covariance function of $Y(x)$ as $C(x,y)$. The covariance, $C(x,y)$ can be represented by

$$C(x,y)=\sum_{k=1}^{\infty}\lambda_k\phi_k(x)\phi_k(y) \quad \text{.....(2.9)}$$

where ϕ_k and λ_k are eigenvectors and eigenvalues of *C(x, y)*.

$$Y(x)=\sum_{k=1}^{\infty}\sqrt{\lambda_k}\theta_k\phi_k(x) \quad \text{.....(2.10)}$$

Assume that the eigenvalues λ_k are ordered so that $\lambda_1 \geq \lambda_2 \ldots$, then the expansion in Eq. 2.10 is called the K-L expansion. In Eq. 2.10, the L^2 basis functions $\phi_k(x)$ are deterministic and resolve the spatial dependence of the permeability field. The randomness is represented by the random variable θ_k. Generally, the leading order terms (quantified by the magnitude of λ_k) only need to be retained and still capture most of the energy of the stochastic process *Y(x)*. For a $N-$term *K-L* expansion approximation $Y_N=\sum_{k=1}^{N}\sqrt{\lambda_k}\theta_k\phi_k$, we define the energy ratio of the approximation as

$$e(N):=\frac{E\,\|Y_N\|^2}{E\,\|Y\|^2}=\frac{\sum_{k=1}^{N}\lambda_k}{\sum_{k=1}^{\infty}\lambda_k} \quad \text{.....(2.11)}$$

If λ_k decay very fast, then the truncated KLE would be good approximations of the stochastic process in L^2 sense. To generate a realization, we only need to perturb the random variable. To honor hard data at well locations, we implemented conditional K-L expansion, which is described in the numerical example of the chapter.

The major drawback of K-L expansion is to requires a computationally expensive eigen-decomposition of a large covariance matrix, and this is exceedingly demanding for field applications. Jafarpour and McLaughlin (2007) proposed an efficient parameterization with discrete cosine transform (DCT). The DCT provides a robust

parameterization alternative that does not require specification of covariance and is computationally efficient.

2.5.2 Gradual Deformation Method

The gradual deformation method (GDM) (Hu 2000) was originally developed to gradually deform or change Gaussian related stochastic reservoir models while preserving their covariance structure. The method provides a good framework for performing global perturbation of reservoir models.

A gradually deformed model can be calculated as a weighed linear combination of *M+1* basis models. A general form for the combination of the models is given by

$$k(x,\alpha) = \bar{k}(x) + \sum_{i=0}^{M} \alpha_i \left(k_i(x) - \bar{k}(x)\right) \quad \text{.....(2.12)}$$

We deform the residuals around the mean $\bar{k}(x)$. The weights α_i satisfy the covariance constraint for any choice of random values t_i,

$$\begin{aligned} \alpha_0 &= \prod_{i=1}^{m} \cos(t_i) \\ \alpha_i &= \sin(t_i) \prod_{j=i+1}^{m} \cos(t_j) \qquad t_i \in (-\pi, \pi) \quad \text{.....(2.13)} \\ \alpha_m &= \sin(t_m) \end{aligned}$$

2.6 Description of Two-stage MCMC Method

One way to improve the performance of the direct MCMC is to increase the acceptance rate by modifying the proposal. We propose such an algorithm, where the proposal distribution is modified using analytical approximations of the flow simulation, *g(k)* based on streamline-derived sensitivities.

The main idea of the two-stage MCMC algorithm is to use an approximate method for the calculation of *g(k)* in the first stage (Christen et al. 2005; Efendiev et al. 2005; Ma et al. 2008) However, this approximation is used only to modify the instrumental proposal distribution of MCMC. Let us assume at state k_n, we propose $k = k_n + \delta k$, where δk is a small perturbation. For the small perturbation of the permeability field we can compute an inexpensive estimate of the reservoir response *g(k)* using a linearized approximation. For this purpose, we need to compute the first order approximation of *g(k)* using sensitivities which are simply the partial derivative of the reservoir response with respect to permeability. The streamline approach is particularly well-suited for this because computations are analytical and can be performed in a single flow simulation (He et al. 2002). Also, the streamline-derived sensitivities can be obtained from both finite-difference and streamline simulator. We denote the sensitivity matrix by *G*. Then the approximation of the reservoir response in the neighborhood of k_n is given by

$$g^*(k) = g(k_n) + G\delta k \quad \text{.....(2.14)}$$

The above approximation is clearly not adequate under all circumstances. In particular, its accuracy depends on the size of the perturbation δk. However, we use this approximation to modify the proposal distribution. Appropriate modification of the instrumental proposal distribution guarantees that the obtained Markov chain will converge to the correct posterior distribution and will have a higher acceptance rate.

To describe the use of approximate models in the MCMC computations, we denote by g^* the approximation of *g(k)* in Eq. 2.14 and the corresponding posterior distribution by

$$\pi^*(k) \propto \exp\left\{-\frac{1}{2}\left[(k-k_{prior})C_k^{-1}(k-k_{prior})^T + (g^*(k)-d_{obs})C_D^{-1}(g^*(k)-d_{obs})^T\right]\right\} \text{.....(2.15)}$$

We are now ready to describe the steps in our proposed two-stage MCMC algorithm.

2.6.1 Two-stage MCMC Algorithm

The two-stage MCMC sampling proceeds as follows.

- Step 1. At k_n generate k from the instrumental distribution $q(k|k_n)$.
- Step 2. Accept k as a sample with probability

$$\alpha(k_n, k) = \min\left(1, \frac{q(k_n \mid k)\pi^*(k)}{q(k \mid k_n)\pi^*(k_n)}\right) \quad \text{.....(2.16)}$$

i.e. pass k or k_n as a proposal to the model with probability $\alpha(k_n, k)$ or $1-\alpha(k_n, k)$ respectively. Therefore, the final proposal to the model is generated from the effective instrumental distribution

$$Q(k \mid k_n) = \alpha(k_n, k)q(k \mid k_n) + \left(1 - \int \alpha(k_n, k)q(k \mid k_n)dk\right)\delta_{k_n}(k) \quad \text{.....(2.17)}$$

- Step 3. Accept k as a sample with probability

$$\rho(k_n, k) = \min\left(1, \frac{Q(k_n \mid k)\pi(k)}{Q(k \mid k_n)\pi(k_n)}\right) \quad \text{.....(2.18)}$$

i.e. $k_{n+1} = k$ with probability $\rho(k_n, k)$, and $k_{n+1} = k_n$ with probability $1-\rho(k_n, k)$.

In the above algorithm, if the trial proposal k is rejected at Step 2, the chain stays at k_n and we return to Step 1. No further flow simulation for k is needed. Thus, the expensive direct flow computations can be avoided for those proposals that are unlikely to be accepted. In comparison, the regular MCMC method requires a direct simulation for every proposal k.

Although the two-stage algorithm looks complicated, it is actually fairly straightforward to implement in practice. First of all, we note that there is no need to

compute the modified proposal distribution $Q(k_n|k)$ and $Q(k|k_n)$ separately in Eq. 2.18. In fact, the acceptance probability in Eq. 2.18 can be simplified as follows

$$\rho(k_n, k) = \min\left(1, \frac{\pi(k)\pi^*(k_n)}{\pi(k_n)\pi^*(k)}\right) \quad \text{.....(2.19)}$$

To elaborate on Eq. 2.19, it is obviously true for $k=k_n$ because $\rho(k_n, k_n) = 1$. For $k \neq k_n$,

$$\begin{aligned} Q(k_n \mid k) &= \alpha(k, k_n) q(k_n \mid k) \\ &= \frac{1}{\pi^*(k)} \min\left(q(k_n \mid k)\pi^*(k), q(k \mid k_n)\pi^*(k_n)\right) \quad \text{.....(2.20)} \\ &= \frac{q(k \mid k_n)\pi^*(k_n)}{\pi^*(k)} \alpha(k_n, k) = \frac{\pi^*(k_n)}{\pi^*(k)} Q(k \mid k_n) \end{aligned}$$

In the appendix A (Efendiev et al. 2008 (In press)), we proved the irreducibility and aperiodicity of the modified Markov chain, and therefore the modified Markov chain converges to the correct posterior distribution. One of the necessary conditions for this convergence is that the support of π^* contains the support of π. Next, we discuss this necessary condition. From numerical point of view, we need to show that if $\pi(k) > 0$ implies that $\pi^*(k) > 0$. Given the formulations of $\pi(k)$ and $\pi^*(k)$ it is clear that they both are greater than zero. However, from numerical point of view, we need to show that if the probability of $\pi^*(k)$ is small, then the probability of $\pi(k)$ is also small. This is equivalent to the fact that if $-\frac{1}{2}(k-k_{prior})C_k^{-1}(k-k_{prior}) - \frac{1}{2}(g(k)-d_{obs})C_D^{-1}(g(k)-d_{obs})$ is not large then $-\frac{1}{2}(k-k_{prior})C_k^{-1}(k-k_{prior}) - \frac{1}{2}(g^*(k)-d_{obs})C_D^{-1}(g^*(k)-d_{obs})$ is also not large. Clearly, this will hold provided that $g^*(k)$ is an approximation of $g(k)$. This condition may not hold only when $g^*(k)$ significantly deviates from $g(k)$. However, it is known that streamline approach provides a consistent approximation of $g(k)$ for small perturbations of the permeability field.

Next, we attempt to understand the acceptance rate of the modified MCMC. Here, we define the acceptance rate as the total number of flow simulations that is performed divided by the total number of accepted samples at last stage of MCMC. Clearly, if $g^*(k)$ is very close to $g(k)$, then the acceptance rate is close 1.

$$\rho(k_n,k)=\min\left(1,\frac{\exp\left(-\frac{1}{2}\left((g(k)-d_{obs})C_D^{-1}(g(k)-d_{obs})+(g^*(k_n)-d_{obs})C_D^{-1}(g^*(k_n)-d_{obs})\right)\right)}{\exp\left(-\frac{1}{2}\left((g^*(k)-d_{obs})C_D^{-1}(g^*(k)-d_{obs})+(g(k_n)-d_{obs})C_D^{-1}(g(k_n)-d_{obs})\right)\right)}\right) \quad \text{……..(2.21)}$$

If we write

$$\begin{aligned} g^*(k) &= g(k)+\varepsilon_k \\ g^*(k_n) &= g(k_n)+\varepsilon_{k_n}, \end{aligned} \quad \text{……..(2.22)}$$

where ε_k and ε_{k_n} are the approximation errors, then

$$\rho(k_n,k)=\min\left(1,\exp\left(-\frac{1}{2}\left(2\varepsilon C_D^{-1}(g^*(k)-d_{obs})+2\varepsilon_{k_n}C_D^{-1}(g^*(k_n)-d_{obs})\right)\right)\right) \quad \text{……..(2.23)}$$

up to a first order. Clearly, $\rho(k_n,k)$ exponentially is close to one, depending on the approximation errors.

2.7 Illustrative Example

We use the same example from Oliver et al. (1996) to show that the proposed method can actually sample from the posterior distribution. The univariate posterior distribution is given as follows.

$$\pi(k) = a \exp\left(-\frac{(k-k_0)^2}{2\sigma_k^2} - \frac{(g(k)-d)^2}{2\sigma_d^2} \right) \text{.....(2.24)}$$

Where k_0=*1.9, d= 0.8,* $\sigma_k^2 = 0.1$, $\sigma_d^2 = 0.01$, *g(k) = 1 – 9(k-2π/3)*^{2}*/2*, and *a = 4.567*. In Eq. 2.24, the first term represents a prior distribution, and the second is the likelihood term which includes nonlinear function *g(k)*. To sample from the posterior distribution using two-stage MCMC, we calculate the first derivative of *g(k)*, which is

$$G = \frac{dg(k)}{dk} = -9k + 6\pi \text{ .....(2.25)}$$

Based on Eq. 2.25, the local linearization of $g(k^*)$ is $g^*(k^*) = g(k)+G\delta k$.

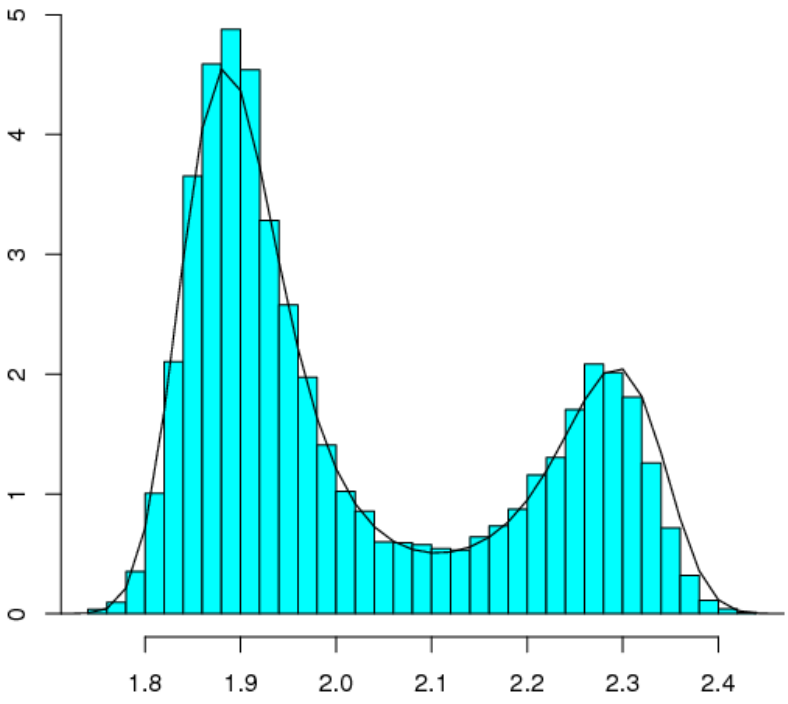

Fig. 2. 5—Histogram generated by two-stage MCMC matches to the posterior distribution that was to be sampled from.

Using the stage MCMC, we generated a histogram of occurrences of values which is given in **Fig. 2.5**. Clearly, the histogram generated by the two-stage MCMC method matches the true distribution quite well without undersampling in the region between two peaks.

2.8 Synthetic Example

We consider a synthetic example that involves waterflooding in two adjacent 9-spot patterns. The 2-D permeability field is generated using the *K-L* expansion with an exponential variogram and dimensionless correlation lengths of 0.2 and 0.4 in the *x* and *y* directions, respectively. The log permeability variance was set at 2. In the *K-L* expansion, we calculate the dominant eigenvalues which provide 93 percent of the sum of all eigenvalues. For the field we consider 40 dominant eigenvalues. We assume that the permeability field is known at the well locations. This condition is imposed by setting

$$\sum_{k=1}^{40} \sqrt{\lambda_k}\,\theta_k \phi_k(x_j) = \alpha_j \quad \text{.....(2.26)}$$

where α_j ($j=1,\ldots 15$) are prescribed constants and x_j are well locations. In our simulations we propose 25 θ_i and calculate the rest of θ_i from Eq. 2.26.

The reference permeability field (50x50 mesh) is plotted in **Fig. 2.6a**. The full MCMC, two-stage MCMC and the Langevin algorithm are run starting with the same initial model as shown in **Fig. 2.6b**, and carried out for 1000 iterations. The random walk sampler with step size 0.2 is used in the MCMC. The same step size is also used for Langevin sampler. It is important to note that for the two-stage MCMC the number of iterations is not the same as the number of flow simulations like other two methods. This is because of the inherent filtering mechanism that can reject a substantial number of

poor proposals without conducting any flow simulation. **Fig. 2.7** shows the RMS error reduction vs. the number of flow runs for the three sampling algorithms. The two-stage MCMC converges faster than the full MCMC, requiring only about half the number of flow simulations compared to the full MCMC to reach the same level of misfit.

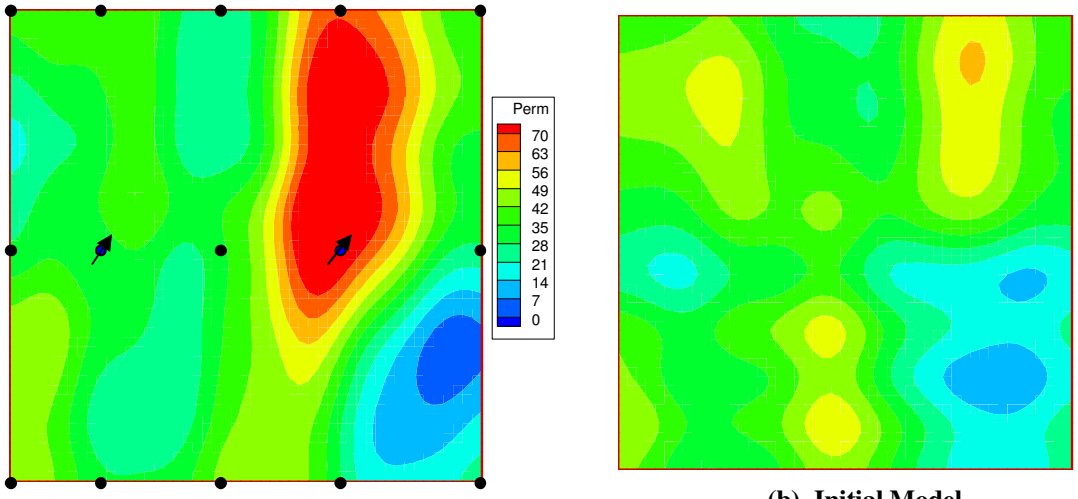

(a) Reference Model **(b) Initial Model**

Fig. 2. 6—Reference (a) and initial (b) models of adjacent nine-spot example.

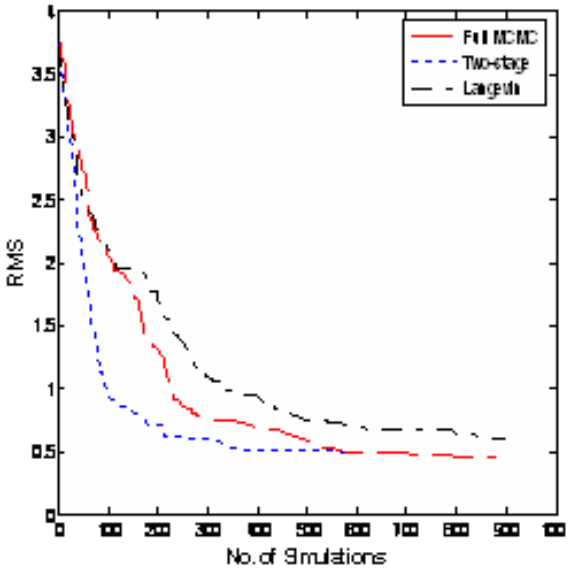

Fig. 2. 7—Reduction in RMS per simulation run.

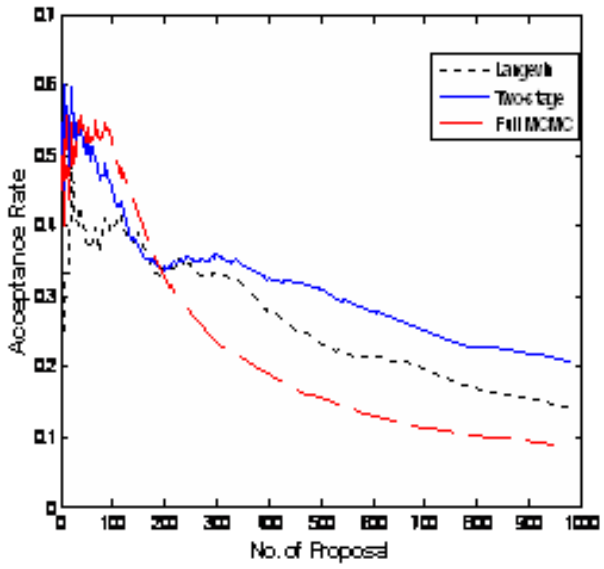

Fig. 2. 8—Comparison of acceptance rates for two-stage, full MCMC and Langevin algorithm.

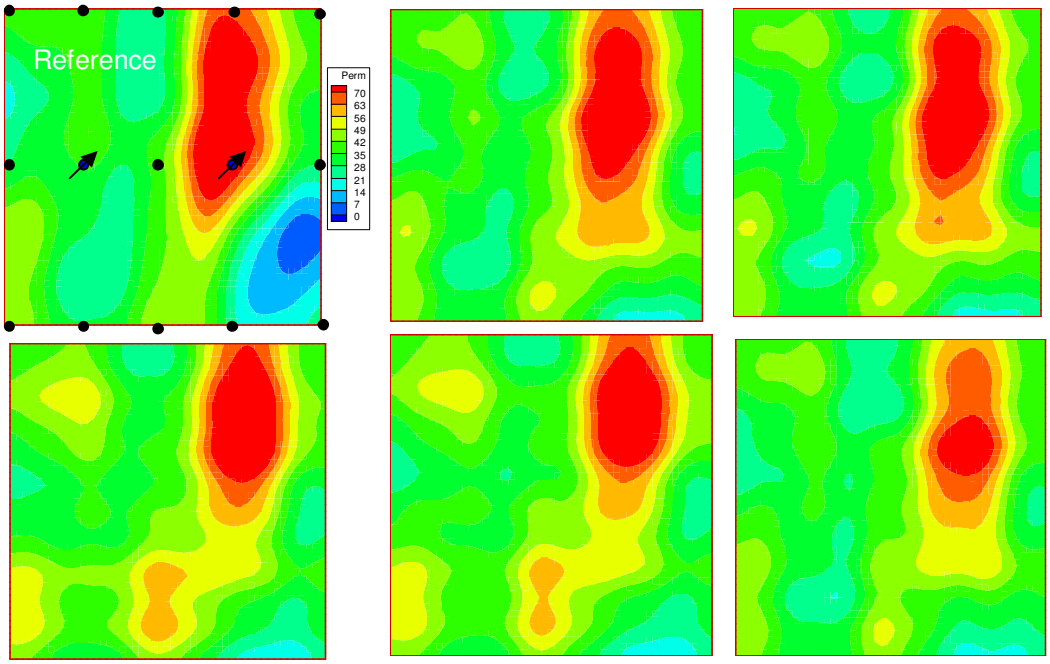

Fig. 2. 9—Collected samples using two-stage MCMC in the adjacent example.

Fig. 2.8 gives the acceptance rate for the three methods. Again, the two-stage MCMC has the highest acceptance rate, almost twice than that of the full MCMC and also higher than the Langevin algorithm. After the Markov chain converged, 5 samples are collected which are shown in **Fig. 2.9**. These numerical results clearly demonstrate that the two-stage MCMC can be used for efficient sampling of the posterior distribution during reservoir history matching.

2.9 Field Example

This 3D example is for the Goldsmith field case, a carbonate reservoir in West Texas (He et al. 2002). The study area is discretized using a 58x53x10 mesh with a total of 30,740 grid cells. There are nine inverted 5-spot patterns covering 320 acres with average thickness of 100 ft. The model has 11 injectors and 31 producers but only 9 producers showed significant water cut in the first 20 years of waterflooding and will be used for history matching purposes. **Fig. 2.10a** shows the well configuration of the study area and **Fig. 2.10b** shows the well schedule with infill drilling and pattern conversions.
To generate proposals for the two-stage MCMC for the field application, we used the Gradual Deformation Method (GDM). To start with, 100 basis geologic models were generated using the Sequential Gaussian Simulation after incorporating core data, well log data and the seismic data as a secondary variable.

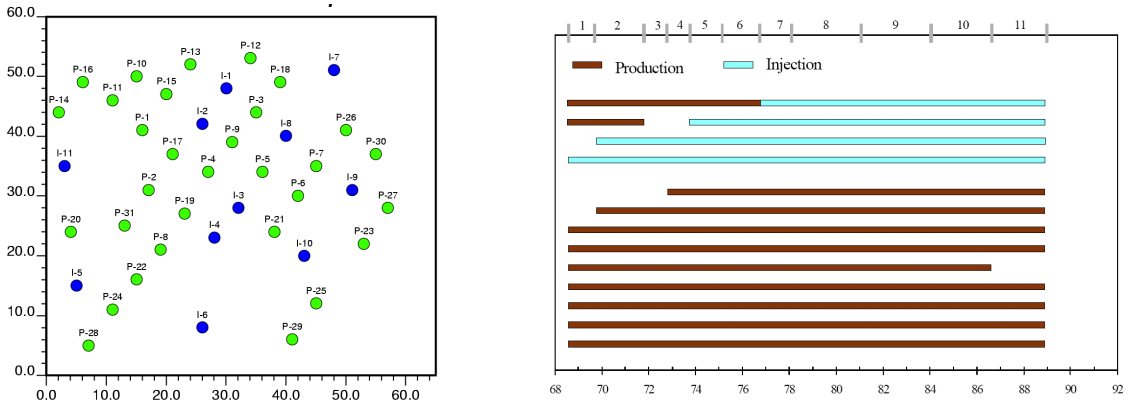

(a) Well configuration **(b) Well schedule**

Fig. 2. 10— Well configuration (a) and schedule (b) of the Goldsmith field case.

The 100 basis models exhibit a wide range of variability and connectivity patterns which will enable the GDM to generate proposals with a wide range of permeability distributions. **Fig. 2.11** shows four samples generated by the GDM by perturbing 100 random deformation parameters.

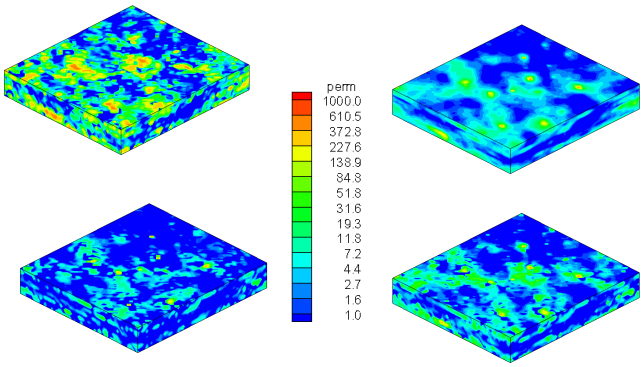

Fig. 2. 11— 3D Realizations generated by gradual deformation method.

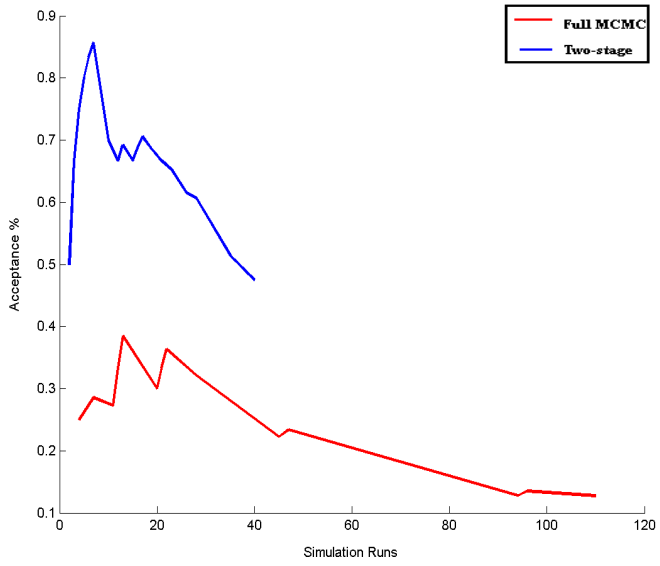

Fig. 2. 12—Acceptance rate for the full and two-stage MCMC.

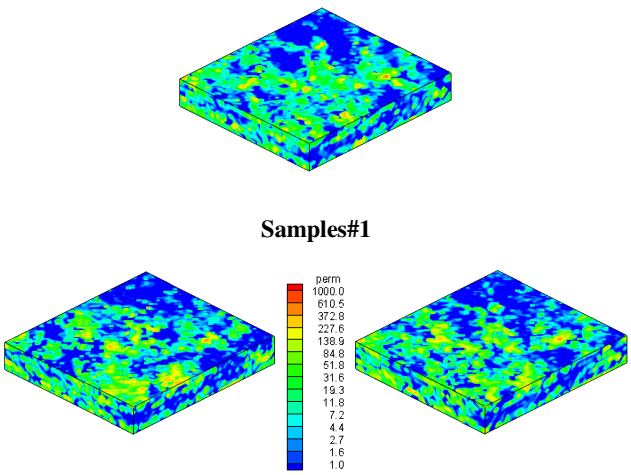

Samples#1

Samples#6 **Samples#11**

Fig. 2. 13—Two-stage MCMC: three collected samples.

These models range from the highly heterogeneous to the relatively smooth and from the highly connected to somewhat patchy. All the models, however, honor the same static data and can be gradually deformed to a new state through perturbation of the GDM parameters. We ran the two-stage MCMC using a commercial finite difference simulator. A maximum limit of 150 total simulation runs was used and the target RMS error was set to 2.7. The improved acceptance rate for the two-stage MCMC compared to the conventional (full) MCMC with the random walk sampler can be clearly seen in **Fig. 2.12**. The two-stage MCMC maintained a high acceptance rate during the 40 simulations runs needed to converge to an RMS error of 2.7. It is important to note that the same step size (0.3) is used in both full and two-stage MCMC. The full MCMC, however, required 110 simulation runs to lower the RMS to the same level. The speed up gained by the two-stage MCMC will lead to a shorter burn-in time and a higher convergence rate.

When considering the total number of iterations, both methods evaluated a comparable number of proposals. The two-stage MCMC, however, required only 40 simulation runs compared to 110 runs for the full MCMC which translates to 64% reduction in computational cost. A total of 13 samples were collected via the two-stage MCMC out of which three are shown in **Fig. 2.13** for illustration purposes.

The integration of dynamic data should reduce the uncertainty observed in unconditioned models. In **Fig. 2.14**, the variances for five selected layers are shown for both the GDM basis models and the two-stage MCMC samples. The reduction in uncertainty is clear where the variance has been reduced significantly when compared to the original basis models that were used to generate the proposals.

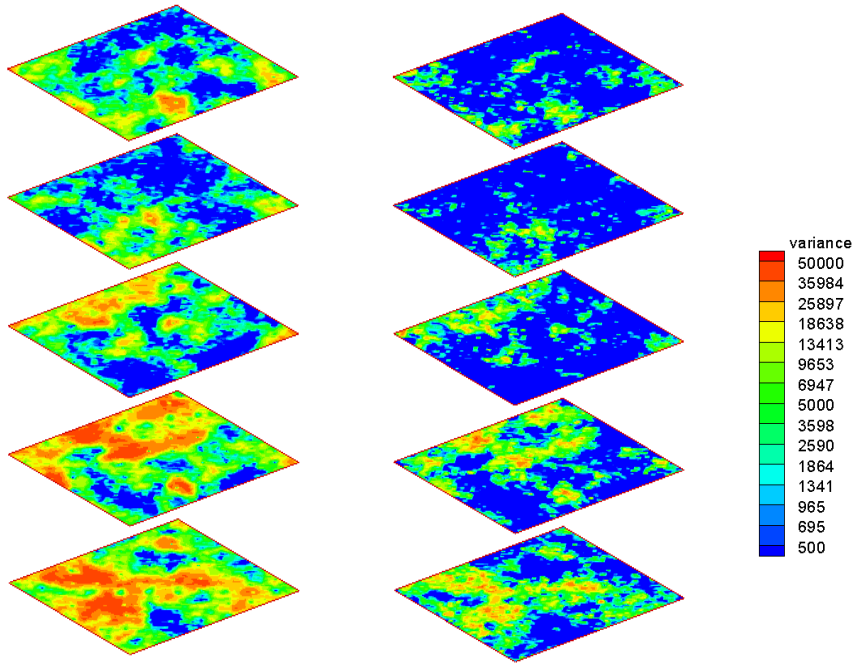

(a) Starting realizations **(b) Two-Stage MCMC samples**

Fig. 2. 14—Permeability variance reduction.

The reduction in uncertainty is also reflected in the water cut response as shown in **Fig. 2.15**. The initial water cut responses shown in **Fig. 2.15a** are for the initial 13 realizations that are conditioned to static data. The final matches shown in **Fig. 2.15b** for the two-stage MCMC samples show a significant reduction in the spread of the reservoir responses from these models.

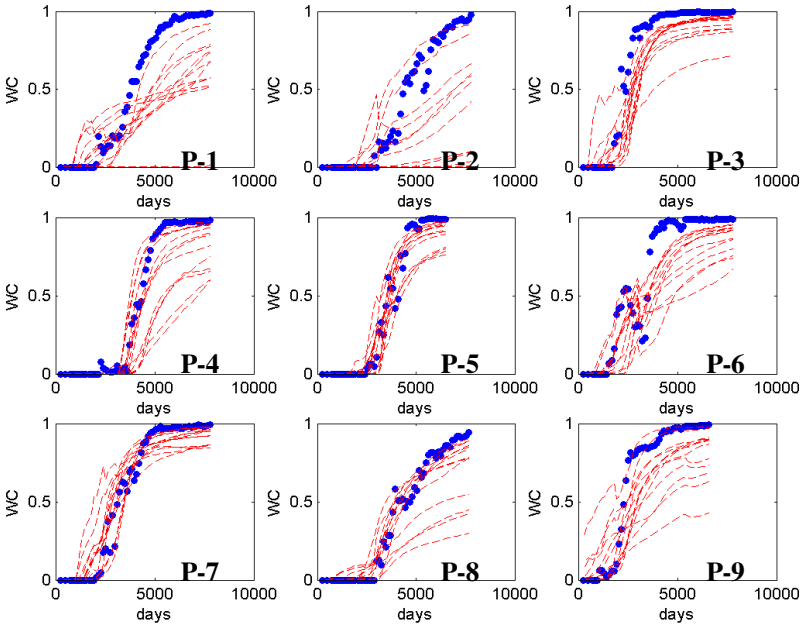

(a) Initial match

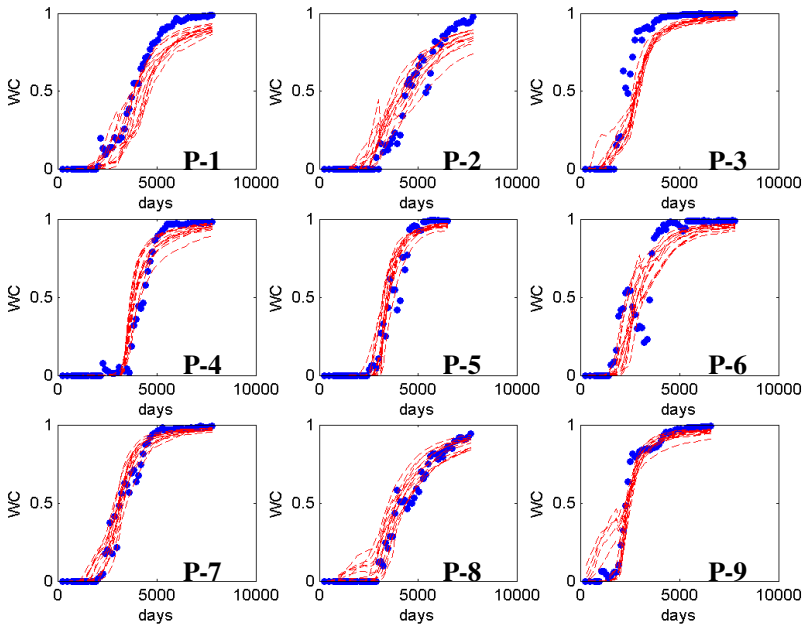

(b) Final match

Fig. 2. 15—Initial and final water cut responses.

CHAPTER III

TWO-STAGE MCMC WITH RESPONSE SURFACE MODELS

In the sensitivity-based two-stage MCMC method, the derivatives of the production response with respect to changes in the reservoir parameters are needed to approximate the reservoir response in the first stage. However, the calculation of the derivatives of some production responses such as bottom hole pressure is not an easy task even for the streamline-derived method. Moreover, for many discrete reservoir parameters such as facies type, sensitivities are simply inappropriate because they are non-differentiable. In addition, the previous method relies on the linearized approximation to flow simulation in a small neighborhood, which implies that the proposed permeability should lie in a close neighborhood of the previously accepted permeability field using the small step size in the random walk sampler. This limitation may lead to inefficiency in the exploring the sampling space. The two-stage MCMC based on response surface models was proposed to address the issues. In the first stage, the response surfaces as surrogate models take the place of expensive multiphase flow simulations to guide the sampling. Moreover, surrogate models exist independently of the expensive flow simulation, and can provide new information about reservoirs without requiring additional runs of the flow simulations.

3.1 Introduction

The two-stage MCMC based on response surface models is non-gradient based iterative application of the stochastic search of MCMC and the surrogate model method for sampling. The MCMC probes the search space to find optimal regions. Then the response surface model maps local regions of search, produces computationally inexpensive estimates to the reservoir responses, therefore accelerating the sampling.

The method is similar to surrogate-model assisted global optimization algorithms, where the surrogate models are applied to optimization problems to limit the number of computationally expensive simulations. Jones (2001) provided a detail review of the optimization methods based on approximation models.

The new formulation of two-stage MCMC allows us to try different strategies to where to put next points to be sampled, i.e. infill samples. There are two methods to select the infill samples based on the response surface. The first one is to optimize the current response surface and to sample at the optimum found. The second is to find the point where estimated error of the predictor such as kriging variance is at a maximum, i.e. where we are least certain about the predicted value. As pointed out by Sobester et al. (2005), the first strategy may work very well on simple and single modal functions. It may easily get trapped in a local optimum for multimodal problems. The second one is to always choose the point where the uncertainty associated with the predictor is highest. The method may reach global convergence, but it requires a very large number of simulations to achieve this.

Here we propose a new strategy which combines the response surface model into the random search, which is similar to the procedure given by Brigham and Aquino (2007). To keep the size of initial sample to a minimum, we choose the infill points that are sampled from a normal distribution centered on the current point. The mean of the normal distribution is the value of the current sample, and the standard deviation is set to 10% of the current sample values.

The response surface is often constructed on pre-sampled data $(\boldsymbol{\theta}_i, G(\boldsymbol{\theta}_i))$, $i=1,\ldots,N$, where $\boldsymbol{\theta}_i$ are perturbation parameters, called design points, and $G(\boldsymbol{\theta}_i)$, defined in Eq. 3.1, are the sum of the data misfits in water cut, GOR and BHP. The flow simulation runs are first performed on the design points to evaluate the data misfits in order to fit the response surface models.

$$G(\theta_i) = (g^{wcut}(k_i) - d_{obs}^{wcut})C_{wcut}^{-1}(g^{wcut}(k_i) - d_{obs}^{wcut}) + (g^{bhp}(k_i) - d_{obs}^{bhp})C_{bhp}^{-1}(g^{bhp}(k_i) - d_{obs}^{bhp}) \quad \text{.....(3.1)}$$
$$+ (g^{gor}(k_i) - d_{obs}^{gor})C_{gor}^{-1}(g^{gor}(k_i) - d_{obs}^{gor})$$

In Eq. 3.1, k_i is a reservoir model which depends on parameter $\boldsymbol{\theta}_i$, and $g(k_i)$ represents the reservoir response of the corresponding model.

To construct the response surface, Design of Experiment (DoE) methods are available to determine where to place the design points in the parameter space. Factorial, fractional factorial, central composite (Montgomery 2000), Latin hypercube (Mackay et al. 1979) designs are commonly used methods. Since we do not have a prior knowledge where to fill, uniformity of the sample points throughout the parameter space is favorable. To date there is no clear theory to determine the optimum size of the initial sample. Some researcher (Jones et al. 1998) use rules of thumb, such as the number should be ten times the number of dimensions.

Since these response surfaces are algebraic summaries obtained from previous runs of the flow simulation, they are cheap to evaluate. The response surfaces can be differentiated based on whether they are interpolating (pass through all points) or non-interpolating. The methods we will deal with Kriging (interpolating) and Bayesian partition modeling (non-interpolating).

3.2 Bayesian Partition Modeling

The new Bayesian approach, Bayesian partition modeling (BPM), to fitting surface was suggested by Denison et al. (2002). BPM constructs arbitrarily complex regression surface by splitting the space into an unknown number of disjoint regions. The motivation behind the BPM is that points nearby in the parameter space have similar values in the response space. We construct a number of disjoint regions in parameter space using Voronoi tessellation and the data within regions are assumed to be exchangeable.

The Voronoi tessellation is determined by a number of sites $S = (s_1,\ldots,s_M), s_j \in R^\eta$, which split the parameter space into M disjoint regions such that points within R_i are

closer to s_i than any other center s_j, $j \neq i$. i.e. $R_i = \{k : \| k - s_i \| < \| k - s_j \| \text{ for all } j \neq i\}$ *where* $\| (k_1,\ldots,k_\eta) \|^2 = \sum_{i=1}^{\eta} \omega_i^2 k_i^2$. The parameter $w = (\omega_1,\ldots,\omega_\eta)$ is a normalized weighting vector that places different emphasis on different directions, although generally we could adopt any distance metric. **Fig 3.1** demonstrated a 2D Voronoi tessellation.

We now define some notation to ease the following exposition. We take the number of disjoint sets to be M and define g_{ij} to denote the j^{th} observation of $G(\boldsymbol{\theta}_i)$, which is in region R_i , $i = 1,\ldots,M$, $j = 1,\ldots,n_i$ where n_i is the number of points in R_i . Let $G_i = (g_{i,1},\ldots,g_{i,n_i})'$ ($'$ denotes transpose) and K_i denote the $n_i \times \eta$ design matrix of points, including the intercept term, found in the i^{th} partition. And let T denote number and location of the region centers and the weighting vector that define the tessellation, $T = \{S, w, M\}$, and $\theta = \{\beta_1,\ldots,\beta_M, \sigma^2\}$ denotes the set of all other model parameters. By assigning conjugate prior distributions over the parameters, we are able to integrating out most of the parameters in the model and obtain analytic expressions for the marginal likelihood $P(G|T)$ of any partition structure defined by the generating centers.

We resort to the reversible jump sampler to explore the parameter space of variable dimensions in MCMC. Within each dimension, the posterior distribution of T is analytically intractable and approximate sampling methods based on MCMC techniques are used. We propose one of the following moves, each with probability 1/4 .

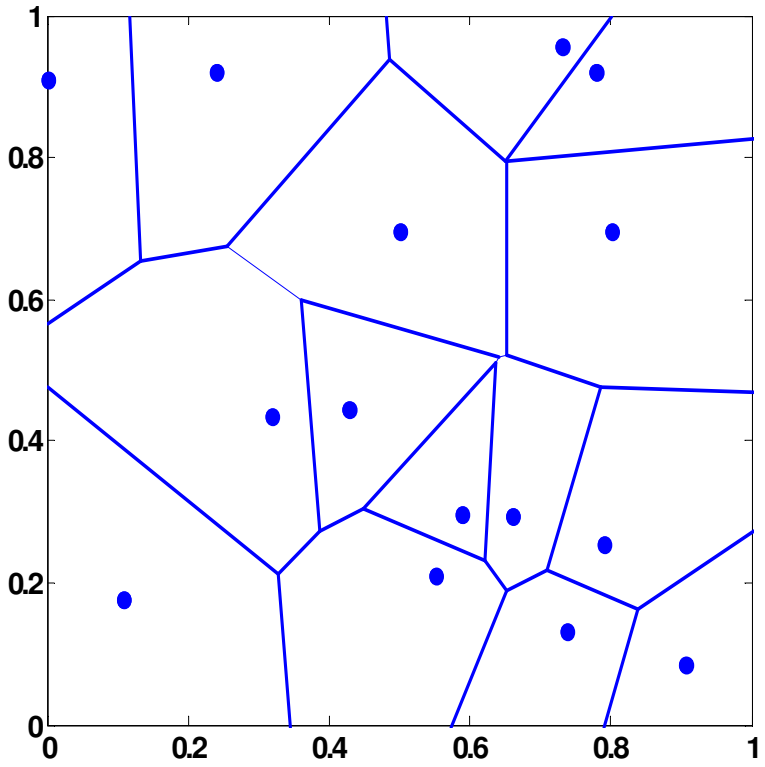

Fig. 3. 1—2D Voronoi diagram.

Birth. Construct a new region by splitting one of the regions in two.

Death. The exact opposite of the Birth step; remove a region by deleting one center.

Update. Move a center by redrawing its position uniformly from the marginal predictor points.

Alter. The distance weighting w using proposal density is tuned during a burn-in phase to give an acceptable rate of approximately 30% . The proposed change is accepted with probability

$$\alpha = \min\left(1, \frac{P(G \mid T_p)}{P(G \mid T_c)}\right) \quad \text{.....(3.2)}$$

where the subscripts *c* and *p* refer to the current and proposed tessellation *T*, respectively.

3.3 Kriging

Kriging (Deutsch and Journel 1992) is a minimum error-variance estimation algorithm in Geostatistics using known values and a semivariogram or covariance to determine unknown values. The kriging estimator at a unobserved location u is given by a linear combination of observations at nearby locations $u_1, \ldots u_n$ as given by:

$$\hat{y}(u) = \sum_{i=1}^{n} \lambda_i y(u_i) \quad \text{.....(3.3)}$$

Where λ are weights, and chosen by minimizing the variance

$$\sigma^2(u) = Var\left[\hat{y}(u) - y(u)\right] \quad \text{.....(3.4)}$$

The kriging estimator is unbiased: $E\left[\hat{y}(u) - y(u)\right] = 0$, and honors the actually observed value. In the conventional kriging, u represents a 3D spatial location. However, the design points are usually defined in more than three dimensional spaces in this work. Design and Analysis of Computer Experiments (DACE) by Sacks et al. (1989) extends the kriging estimation to the high-dimensional space. The DACE framework has gained wide applications in mechanical, electrical engineering as a method for approximating expensive functions (Jones et al. 1998; Sacks et al. 1989). A DACE software package was implemented in a Matlab toolbox (Lophaven et al. 2002). In the DACE framework the kriging correlation model is often presented as products of one-dimensional correlations.

$$R(\beta, w, x) = \prod_{j=1}^{n} R_j(\beta, | w_j - x_j |) \quad \text{.....(3.5)}$$

Where R_j is a correlation function between points w_j and x_j with the parameters β.

The Matlab toolbox contains seven common correlation models, e.g., exponential, Gaussian and spherical.

3.4 Two-stage MCMC Algorithm

To apply the algorithm, we first need to build a response surface model, which is given in the following steps.

- Select a finite initial set of design points $S_1=\{k(\theta_1),....,k(\theta_n)\}$ for flow simulation
- Run reservoir simulations at the points in S_1
- Fit a response model denoted by $G^*(\theta_i)$ using the data points $D_i=\{(k(\theta_i), G(\theta_i): k(\theta_i) \in S_1)\}$

Once the response surface is approximated, we can use two-stage MCMC, the corresponding probability distribution in the first stage is given by Eq. (3.6).

$$\pi^*(k) \propto \exp\left\{-\frac{1}{2}\left[(k - k_{prior}) C_k^{-1} (k - k_{prior})^T + G^*(\theta_i)\right]\right\} \quad \text{.....(3.6)}$$

- Step 1. At k_n generate k from instrumental distribution $q(k|k_n)$.
- Step 2. Accept k as a sample with probability

$$g(k_n, k) = \min\left(1, \frac{q(k_n \mid k)\pi^*(k)}{q(k \mid k_n)\pi^*(k_n)}\right) \text{.....(3.7)}$$

i.e. $k_{n+1}=k$ (conditionally) with probability $g(k, k_n)$, and $k_{n+1}=k_n$ (conditionally) with probability $1- g(k, k_n)$. If rejected go to step 1. If accepted, run flow simulation for k, and update information $S_2=S_1\cup\{k(\theta_{n+1})\}$, $D_{i+1}= D_i\cup\{(k(\theta_{n+1}), G(\theta_{n+1})\}$. Update the response model $G^*(\theta_i)$ using the data points D_{i+1} if necessary.

- Step 3. Accept k with probability

$$\rho(k_n, k) = \min\left(1, \frac{\pi(k)\pi^*(k_n)}{\pi(k_n)\pi^*(k)}\right) \quad \text{.....(3.8)}$$

3.5 Illustrative Example

The minimization of the Rastrgin's function was considered first to show the benefits of the two-stage MCMC algorithm.

The Rastrgin's function is a well known non-convex error surface with many local minima and on global minimum (Brigham and Aquino 2007).

The function to be minimized was given by

$$R(x, y) = 20 + (x-100)^2 + (y-900)^2 - 10\{\cos[2\pi(x-100)] + \cos[2\pi(y-900)]\} \quad \text{.....(3.9)}$$

The minimum value of R(x, y) is 0 at (100, 9000), and x and y are the optimization parameters. **Fig. 3.2** shows a graphical representation of the function. The number of sample points to construct a response surface is 200. The response surfaces are shown in **Fig. 3.3 and Fig. 3.4**. The response surface using the BPM is much smoother than that using kriging.

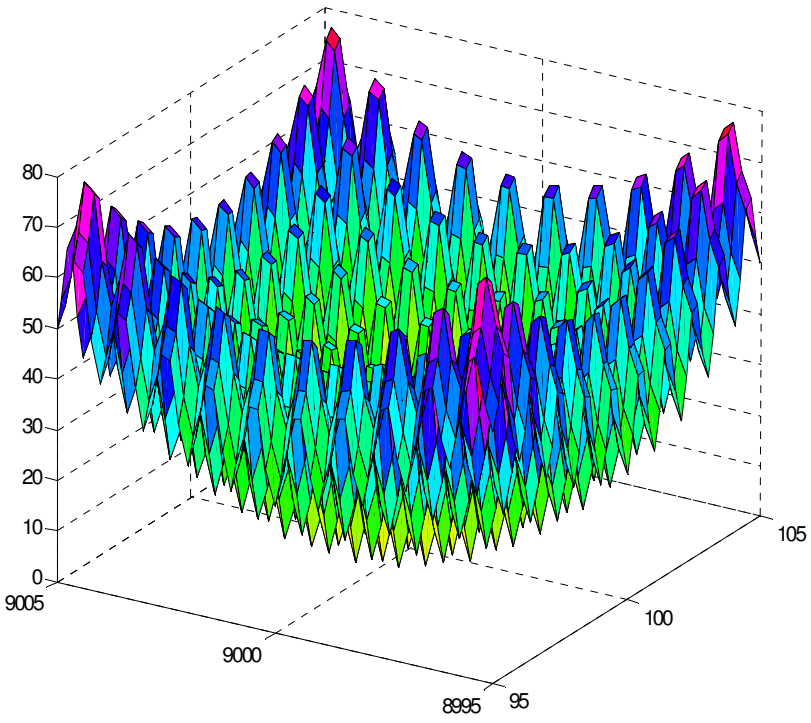

Fig. 3. 2—Graphical representation of Rastrigin's function.

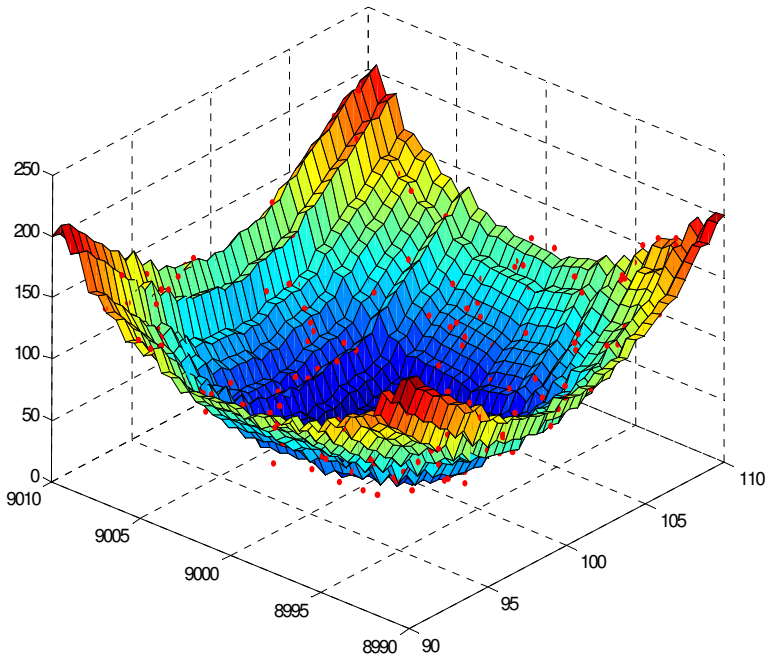

Fig. 3. 3—Response surface built using Kriging.

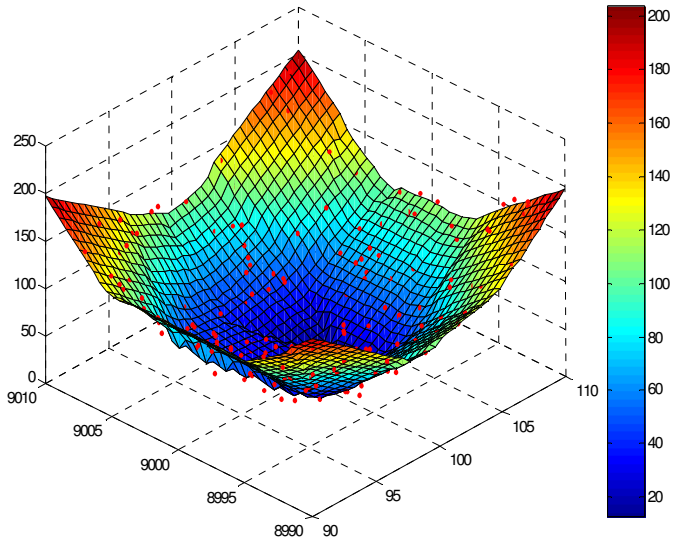

Fig. 3. 4—Response surface built using BPM.

Fig. 3.5 shows the functional value at each iteration using two-stage MCMC with kriging and BPM.

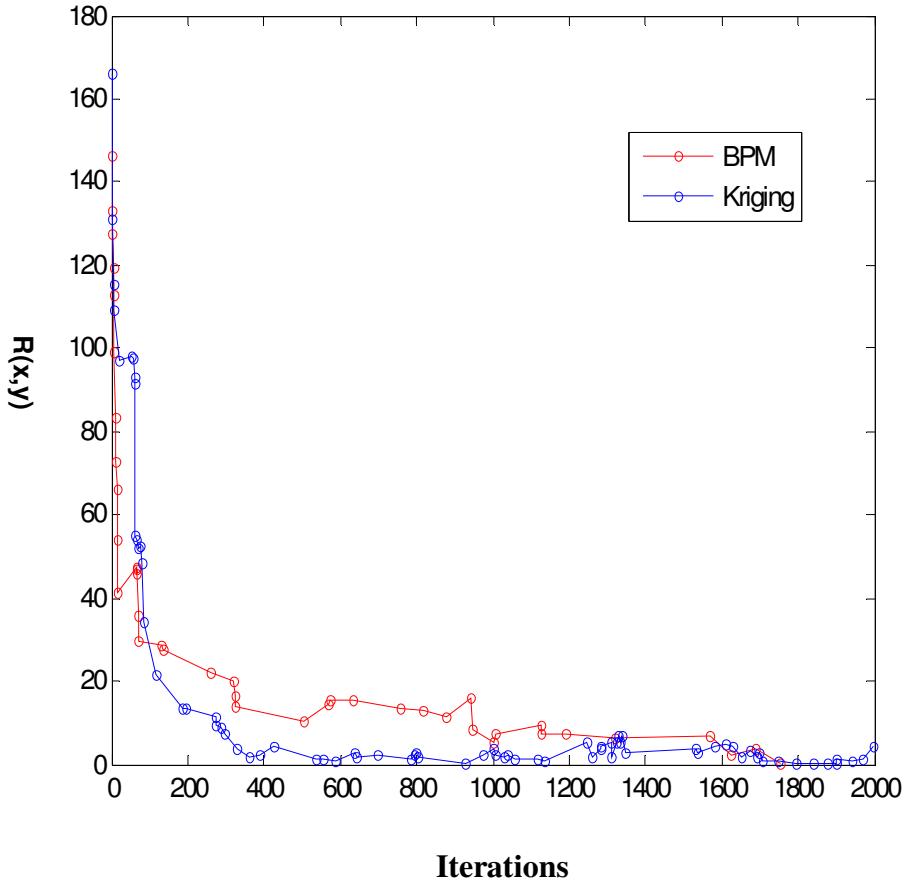

Fig. 3. 5—Functional value versus the number of iterations.

Among 2000 iterations, the acceptance rate for two-stage MCMC using kriging is 18%, and 11% using BPM. **Fig. 3.5** also shows the two-stage MCMC using kriging converges to the global minimum faster.

3.6 2D Synthetic Example

The synthetic case involves three-phase flow and includes matching water-cut, bottom hole pressure, and GOR from a 9-spot pattern. The mesh size used is 21×21×1. The reference and initial permeability distributions are given in **Fig. 3.6**. The water-cut, BHP and GOR simulation responses from the two permeability fields are shown in **Figs. 3.7**, **3.8** and **3.9**. Starting from the initial permeability model, we applied conditional K-L expansion for the model update. This allows us to describe permeability field in terms of two-point statistics by truncating the expansion. A key advantage of the K-L expansion is that these parameters can be varied continuously while maintaining the underlying geostatistical structure. In the example, we maintain 15 terms in the K-L expansion.

To apply the two-stage MCMC, we first used a random latin hypercube design of experiments to generate 200 sample points, then run flow simulations of the samples to calculate the corresponding water cut, BHP and GOR data misfits. Next, two-stage MCMC with Kriging and BPM are applied to sample from the posterior distribution. The comparison of initial and sampled water-cut matches is shown in **Fig. 3.7**, that of BHP is given in **Fig. 3.8** and that of GOR is in **Fig. 3.9**. **Fig. 3.10** shows the RMS error reduction vs. the number of iterations using Kriging and BPM. Among 1000 iterations, there are 62 proposals that pass the first stage, and 27 pass the second stage among 62 proposals if we use kriging in the first stage. Similarly if the BPM was used, there are 33 proposals that are accepted from 89 proposals that pass the first stage. **Fig. 3.11** gives some collected samples after the Markov chain converges.

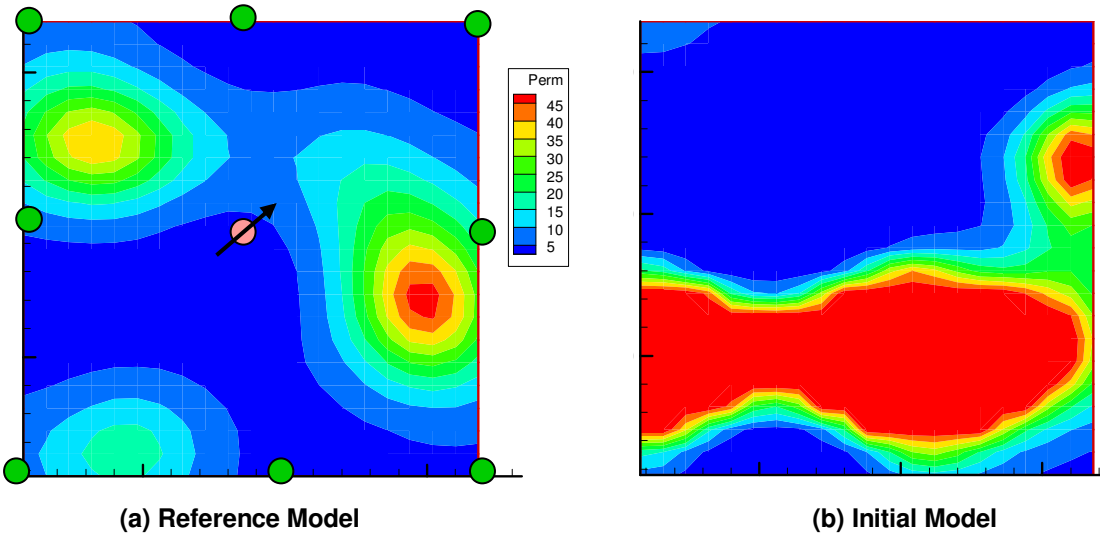

Fig. 3. 6—History matching 3-phase model for a nine-spot heterogeneous case (a) reference and (b) initial model.

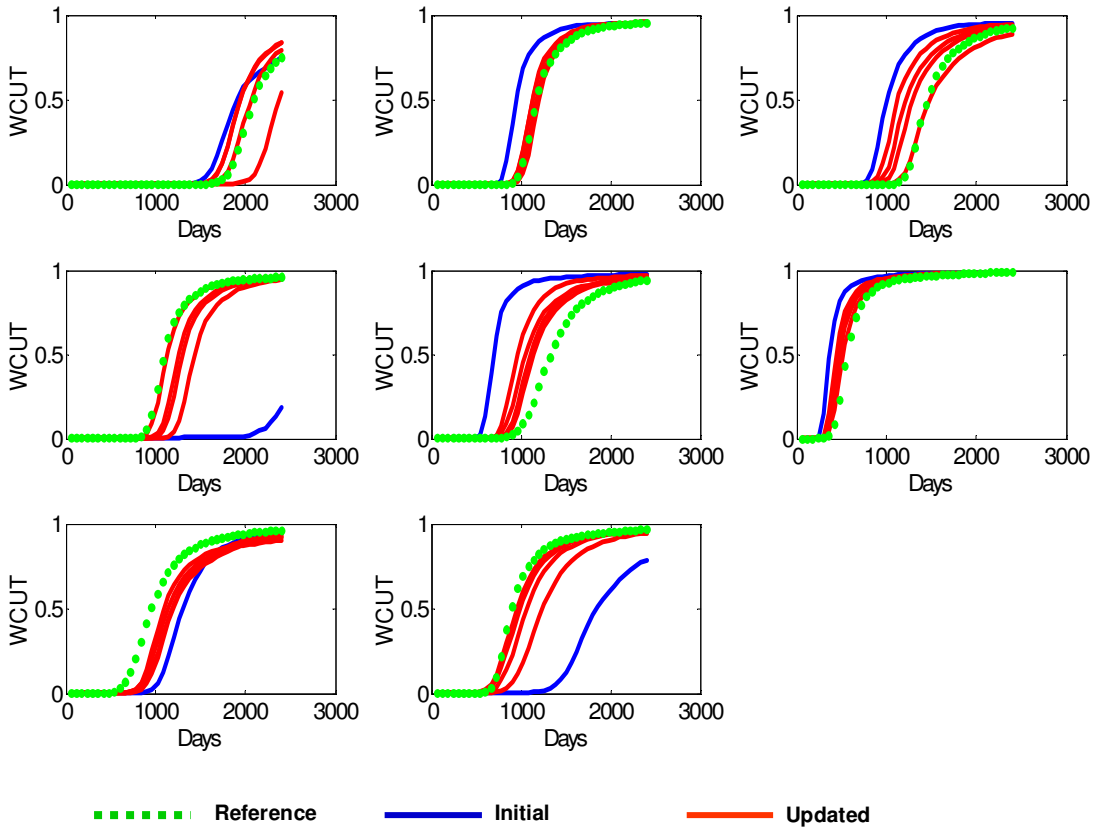

Fig. 3. 7—Water cut match and uncertainty assessment.

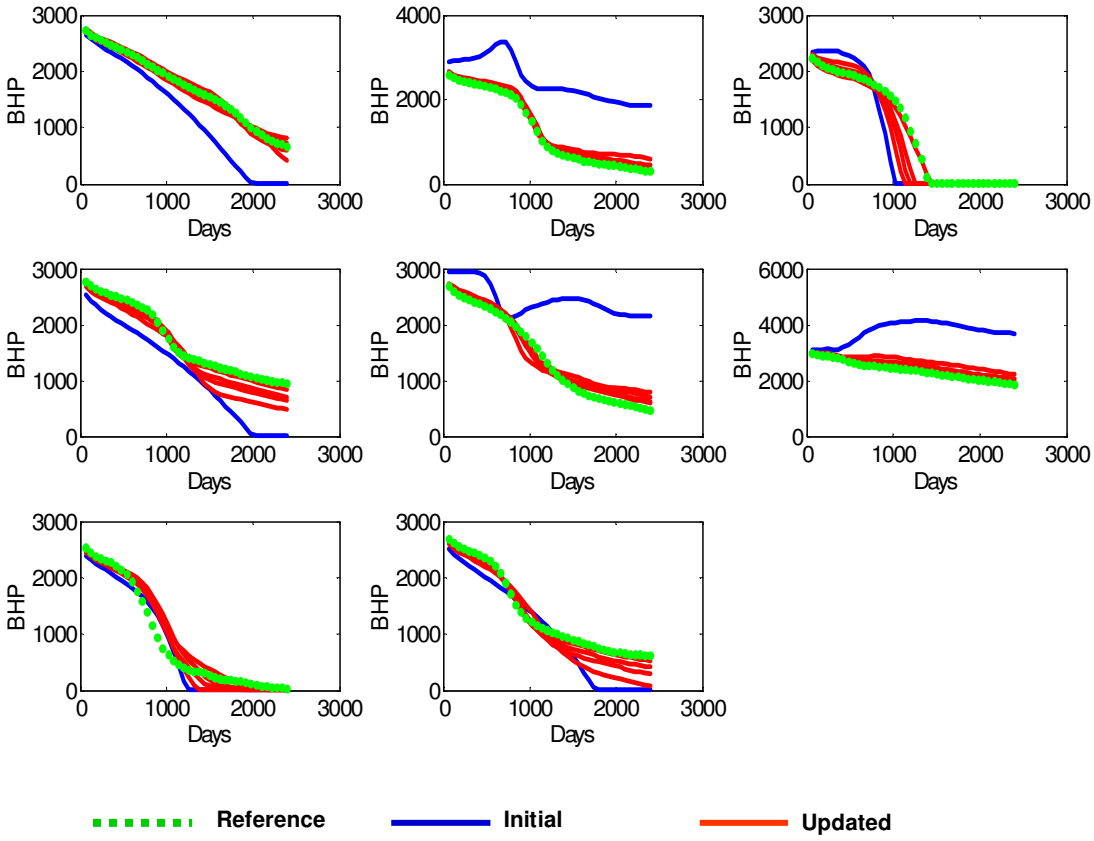

Fig. 3. 8—BHP match and uncertainty assessment.

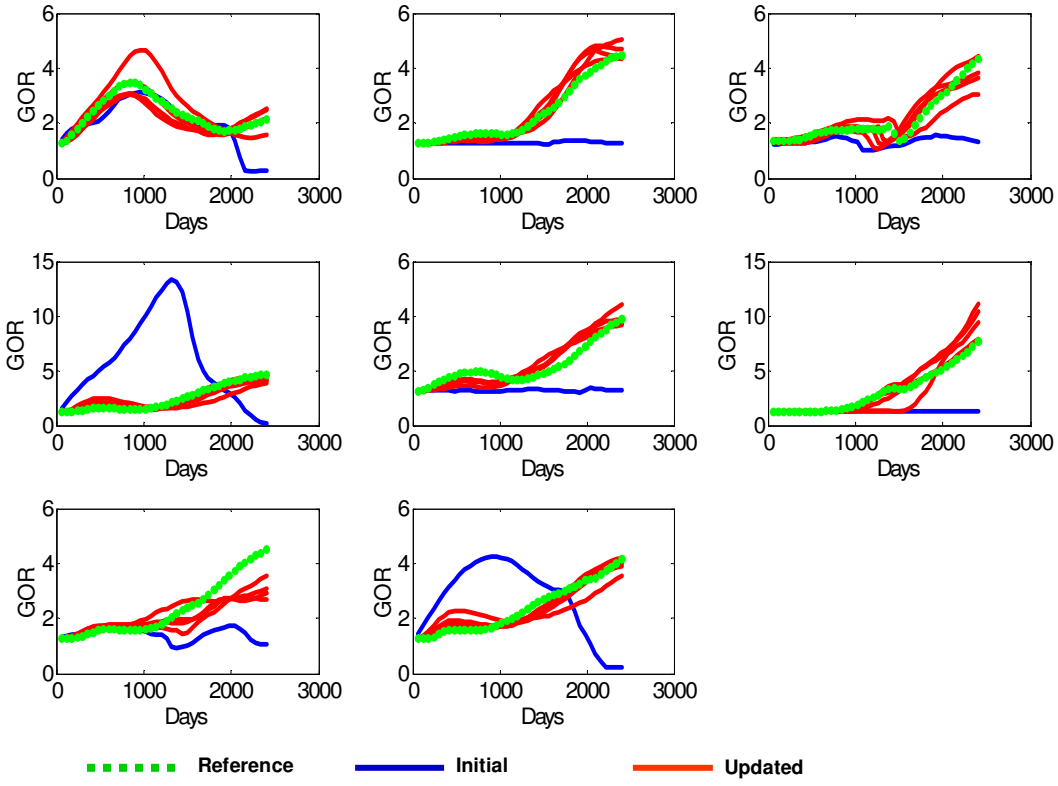

Fig. 3. 9—GOR match and uncertainty assessment.

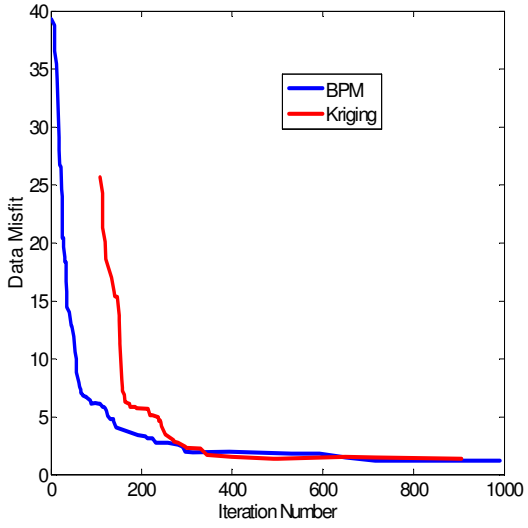

Fig. 3. 10— History matching 3-phase model for a nine-spot heterogeneous case: data misfit reduction.

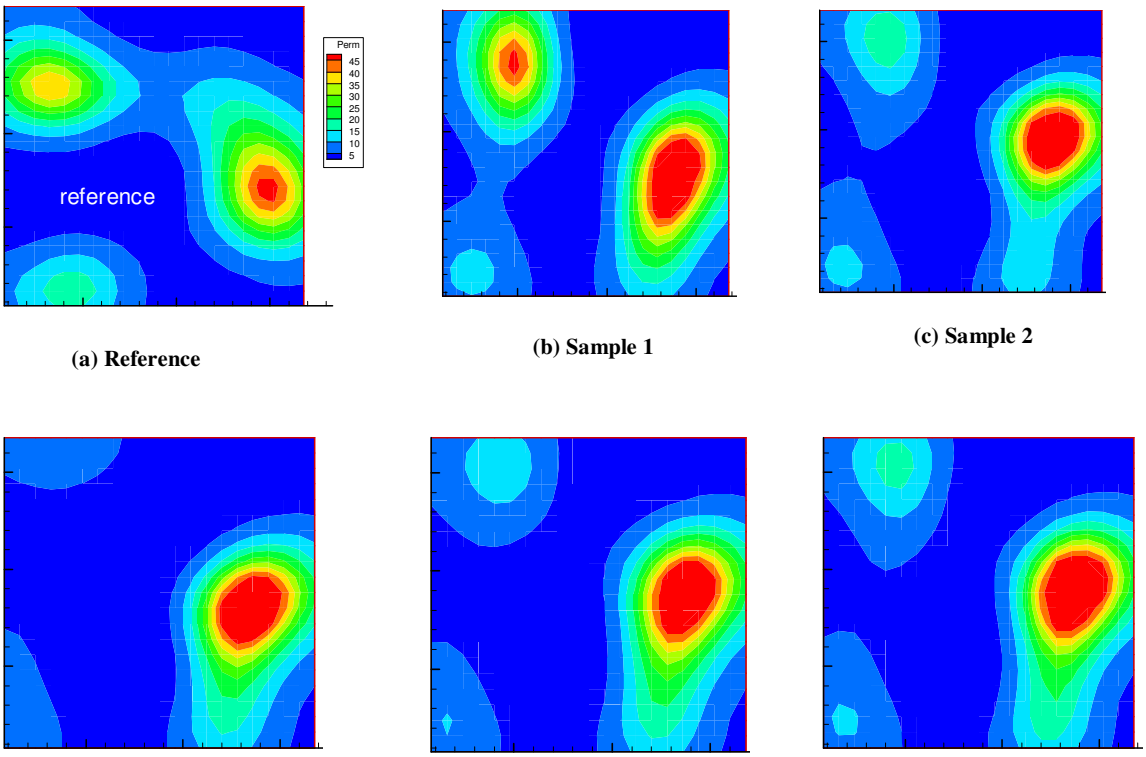

(a) Reference

(b) Sample 1

(c) Sample 2

(d) Sample 3

(e) Sample 4

(f) Sample 5

Fig. 3. 11— Collected samples of history matching 3-phase model for a nine-spot heterogeneous case.

3.7 Facies Type Example

Until now we demonstrated the application of the two-stage MCMC method to continuous reservoir properties, where the reservoir properties are randomly distributed. We can describe the randomness by the mean and the spatial covariance of the property, so called two-point statistics. However, the proposed method is not limited to the continuous type of reservoir properties. Here we show an application to a two-dimensional facies distribution in a reservoir, where the facies type is a discreet variable.

3.7.1 Plurigaussian Simulation

The plurigaussian model (Armstrong et al. 2003) is a useful method of simulating lithofacies in a reservoir. The basic idea is to represent facies by indicators, which are simulated via one or more Gaussian variables that are truncated to yield the indicators. Consider two independent spatial random variables $\boldsymbol{Y_1(x)}$ and $\boldsymbol{Y_2(x)}$ that are sampled from standard Gaussian distribution ($\boldsymbol{x}$ is a 3D spatial location), and define a random field $\boldsymbol{Y(x)=[Y_1(x),\ Y_2(x)]}$. Suppose we have n facies $F_1, F_2, \ldots, F_n$. The i^{th} facies is defined at the location x such that the value of Y(x) is between specified threshold t_{i-1} and t_i:

$$F_i = \{\forall x, t_{i-1} < Y(x) \le t_i\} \quad \text{.....(3.10)}$$

The threholds can be evaluated from the proportions of each of the facies. Armstrong et al. 2003 gave the detail steps including choosing the model type, estimating the parameter values, generating Gaussian values at wells and simulating values at grid nodes given values at wells when we apply the plurigaussian simulation. **Fig. 3.12** is an example illustrating the plurigaussian procedure using two normally distributed Gaussian variables. At the top we have two Gaussian images. The variable Y_1 has an exponential-type variogram, and Y_2 has a Gaussian-type variogram. The three facies, one, two and three are determined using the relationship among the facies as shown in

Fig. 3.12c and the truncation of the two random variables. **Fig. 3.12d** shows the simulated facies map.

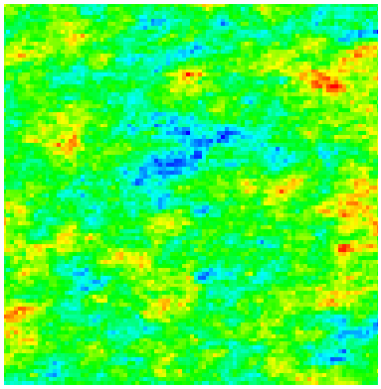

(a) Exponential type random field (Y_1)

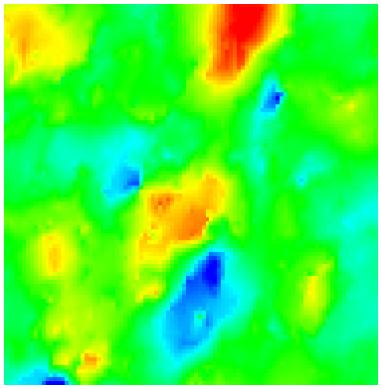

(b) Gaussian type random field (Y_2)

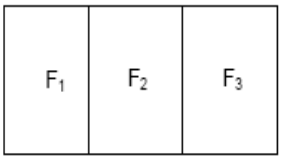

(c) Rock type rule

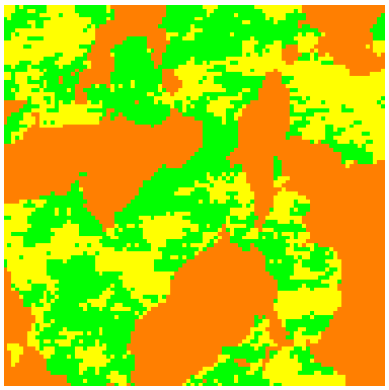

(d) Simulated facies map

Fig. 3. 12— Simulation of lithofacies distribution using random Gaussian fields (Y_1 and Y_2) and rock type rule (a) exponential type random field; (b) Gaussian type field; (c) rock type rule (d) simulated facies map.

Emery (2007) provides a set of MATLAB programs to perform conditional plurigaussian simulation to honor hard data at well locations. We have used the programs in the two-stage MCMC codes.

3.7.2 Production Data Matching and Uncertainty Quantification

The synthetic case involves three-phase flow and includes matching water-cut, bottom hole pressure, and GOR from a 9-spot pattern. The mesh size used is 99×99×1. The reference and initial lithofacies are given in **Fig. 3.13**. The water-cut, BHP and GOR simulation responses from the two permeability fields are shown in Figs. 3.2, 3.3 and 3.4. Three lithofacies (sand, dolomite and shale) are distributed in the field and have very distinct properties. **Table 3.1** lists the permeability and the porosity values for each of the facies types.

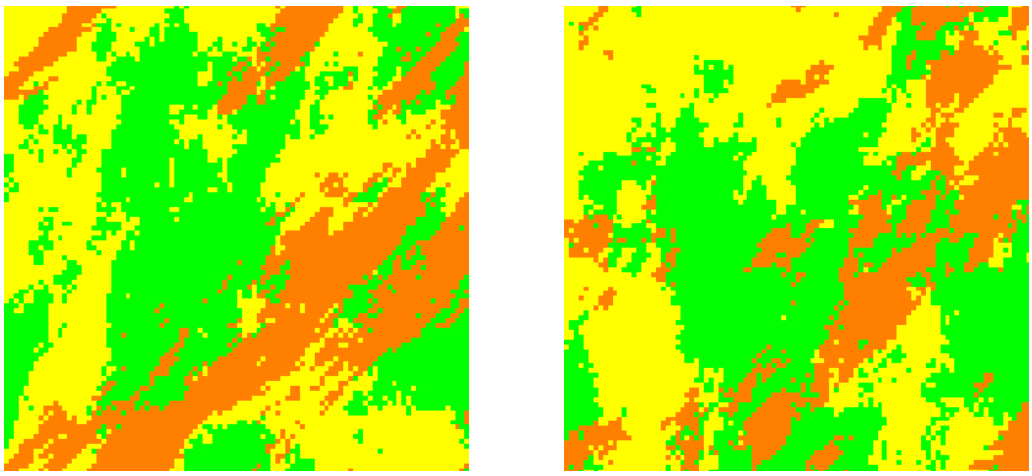

(a) Reference facies map **(b) Initial facies map**

Fig. 3. 13— Reference and initial facies map.

Table 3.1—Properties for each of the lithofacies in the synthetic example

Index	Facies 1	Facies 2	Facies 3
Lithotype	Sand	Dolomite	Shale
Permeability (md)	300	75	5
Porosity	0.25	0.15	0.1

In the example, if we assume that the variogram models for both Gaussian variables (Y1 and Y2) are known, only six parameters are needed to define the two Gaussian random fields. The six parameters are

{a11, a12, angl1} Ranges and principal anisotropy for Y_1

{a21, a22, angl2} Ranges and principal anisotropy for Y_2

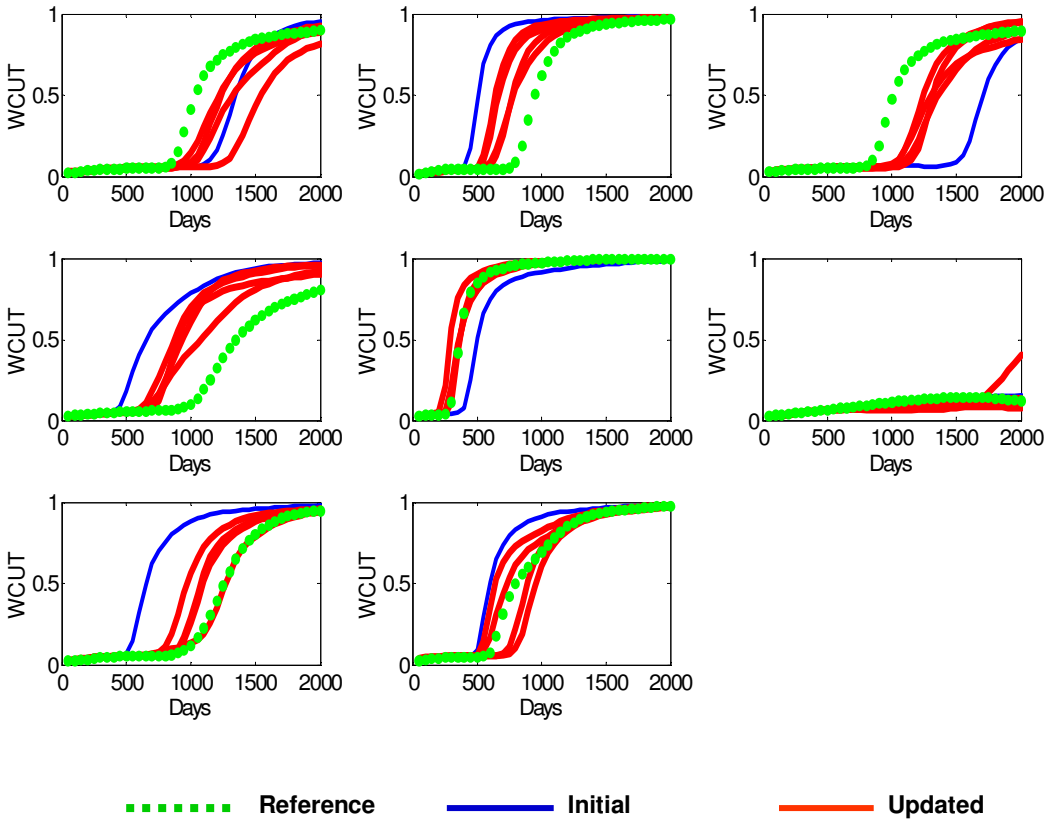

Fig. 3. 14— Water cut match and uncertainty quantification.

Therefore, the response surface models are built between the data misfits and the six parameters. All of the six parameters follow the triangular distributions with different minimum, maximum and mode values. 200 initial sample points are generated using the Latin hypercube method. Kriging is used to fit the samples points between the data misfits and the six parameters. The two-stage MCMC method was applied to history matching the three-phase flow. **Figs. 3.14, 3.15** and **3.16** show the matches and

uncertainty quantification of water cut, BHP and GOR. **Fig. 3.17** gives some collected samples.

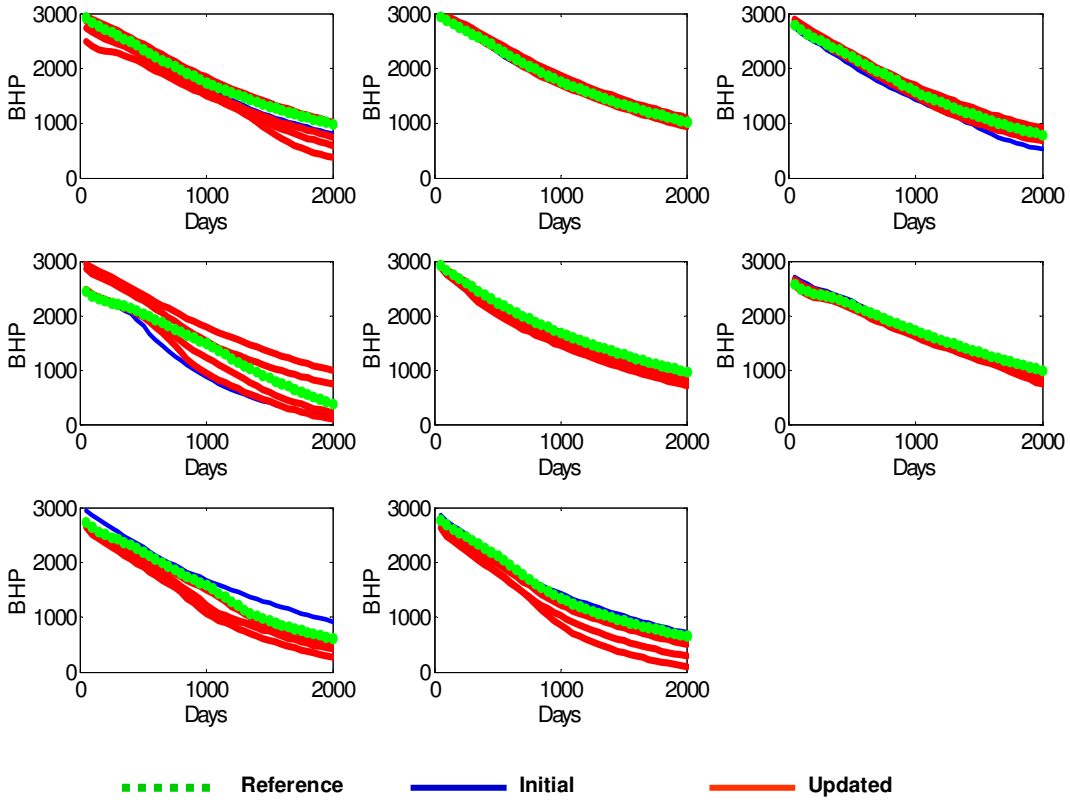

Fig. 3. 15—BHP match and uncertainty quantification.

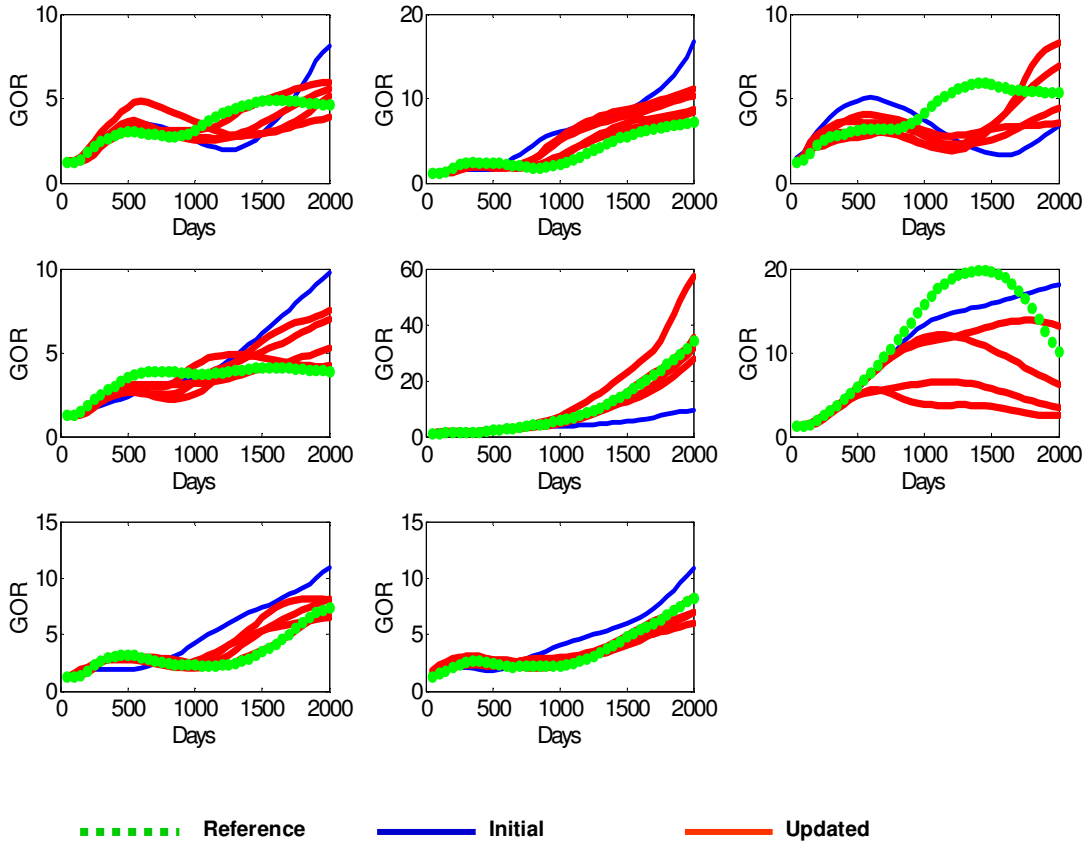

Fig. 3. 16—GOR match and uncertainty quantification.

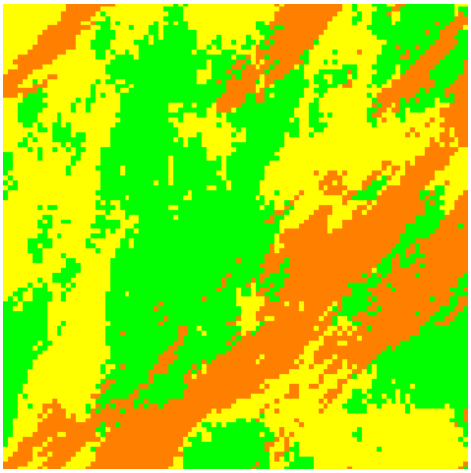

(a) Reference

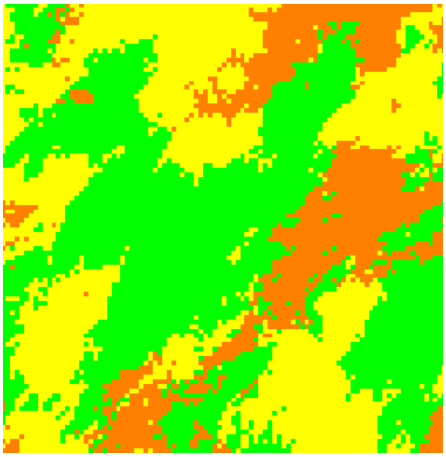

(b) Sample 1

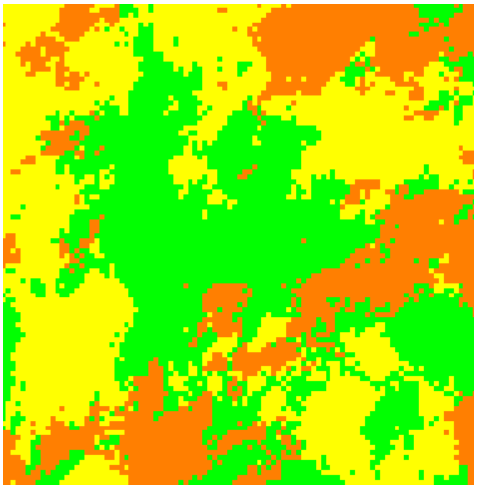

(c) Sample 2

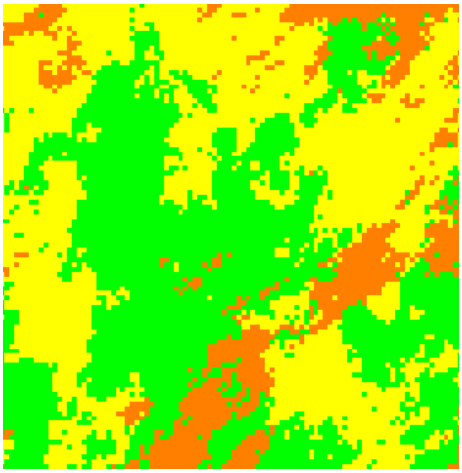

(d) Sample 3

Fig. 3. 17—Collected samples of facies type example.

3.8 Field-scale Example

3.8.1 Reservoir Model Description

The ninth SPE benchmark problem (Killough 1995; Cheng et al. 2007) was used to validate the methodology. The SPE9 problem studies a bottom waterflooding in a dipping reservoir with natural water encroachment from an aquifer. The reservoir (**Fig. 3.18**) is represented by a *24×25×15* mesh system with conventional rectangular coordinates. The dimensions of the grid blocks are 300 feet in both the X- and Y-directions. Cell (1, 1, 1) is at a depth of *9000* feet subsea at the center of the cell top. The remaining cells dip in the X-direction at an angle of 10 degrees. Values of porosity and thickness can be found in Ref. 64. The total thickness from Layers 1 to 13 is 209 feet (16 feet per layer in average), and Layer 14 and 15 has a thickness of 50 and 100 feet respectively.

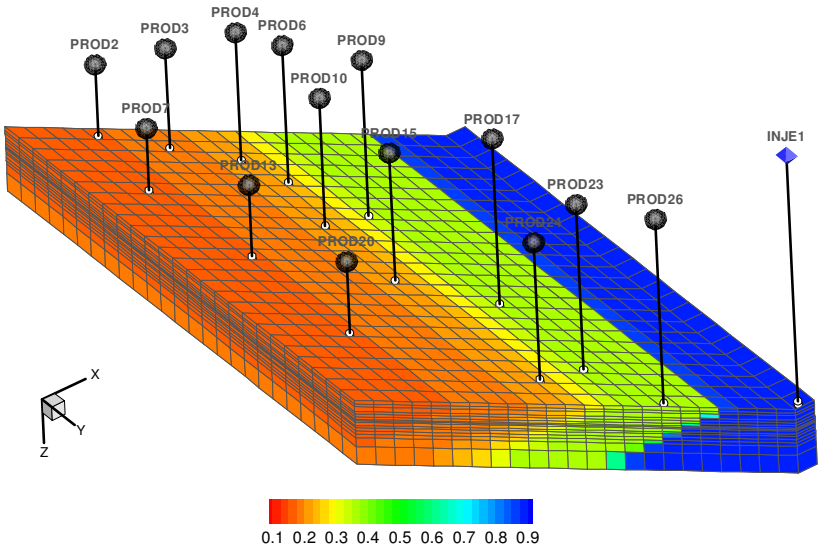

Fig. 3. 18—Initial water saturation for SPE 9.

Solution gas/oil ratio and gas formation volume factor are shown in **Fig. 3.19**. Relative permeabilities are shown in **Fig. 3.20**. Modified Stone's second model was used to compute oil relative permeability.

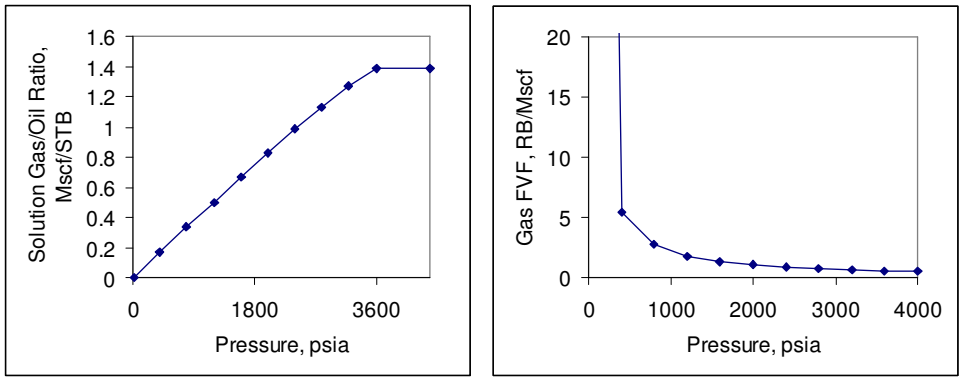

Fig. 3. 19— Solution gas/oil ratio and gas formation volume factor curves.

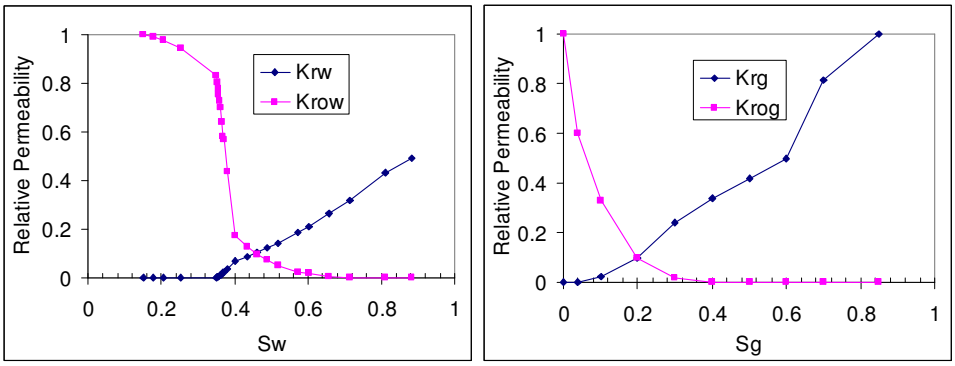

Fig. 3. 20— Relative permeability curves.

The initial oil phase pressure at 9035 feet subsea is 3600 psia which is the bubble-point pressure. The oil/water contact is 9950 feet subsea. There is no free gas initially in the reservoir. After 900 days of production, there is plenty of free gas as shown in **Fig. 3.21**.

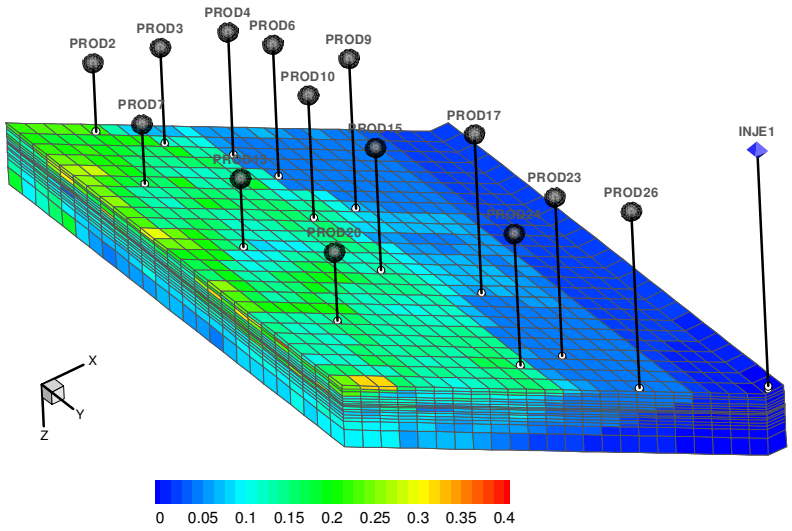

Fig. 3. 21—Gas saturation distribution at the end of simulation time (900 days).

The permeability field used by the original SPE9 problem was generated geostatistically on a cell by cell basis. The permeability is log-normally distributed with a mean of 108 md, a minimum of 0.003 md and a maximum of 10054 md. The correlation length in the X-direction is about 6 grid blocks, and there is no correlation in the Y- and Z- directions. For validation purpose, this permeability field was used as a true or reference model to generate production history by running flow simulation (Cheng et al. 2007).

A total of 1 water injector (I1) and 25 producers (named as PROD 2 to PROD 26) were included in the reservoir. The injector was completed from layers 11 through 15. In the original SPE9 problem, all producers were completed in layers 2, 3, and 4 only. For validation purpose, all producers except produces 9, 17, 23, and 26 were changed to be completed in layers 1 to 13. Producers 9, 17, 23, and 26 are completed in layers 1 to 5 so that wells will not be perforated in the water leg. The water injector was injecting at a maximum bottomhole pressure of 4500 psia at a reference depth of 9110 feet subsea, and the producers were producing with a constant reservoir volume rate of 1800 RB/D and minimum flowing bottomhole pressure of 1000 psia.

3.8.2 Uncertainty Assessment

To generate an initial permeability model to start with, the permeability values at the well blocks are regarded as known hard data. Analysis of the variogram indicated a correlation length of about 2100 feet (7 grids) in the X-direction and about 2 grids in the Y-direction. No correlation in the Z-direction was found. Using these variogram parameters and the conditioned data at well locations, sequential Gaussian simulation was used to generate 15 realizations of the permeability model for the gradual deformation method. **Fig. 3.22** shows the RMS error reduction vs. the number of iterations for both Kriging and BPM in the first stage.

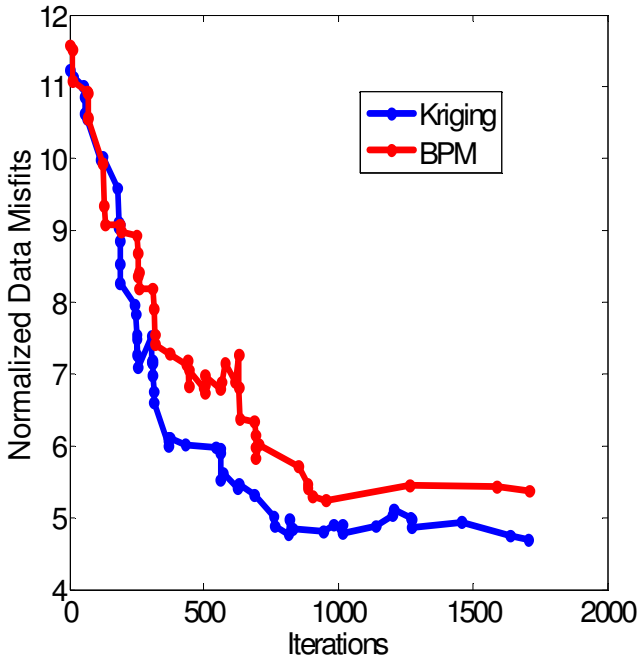

Fig. 3. 22— Two stage for SPE9: data misfit reduction.

Among 2000 iterations, when kriging was used in the first stage, there are 381 proposals that pass the first stage and 61 accepted in the second stage. When the BPM was used, there are 51 proposals accepted in the second stage among 385 proposals that pass the first stage. After the Markov chain converged, several samples were collected.

Figs. 3.23-3.27 show the reservoir responses of the models compared with the observed data.

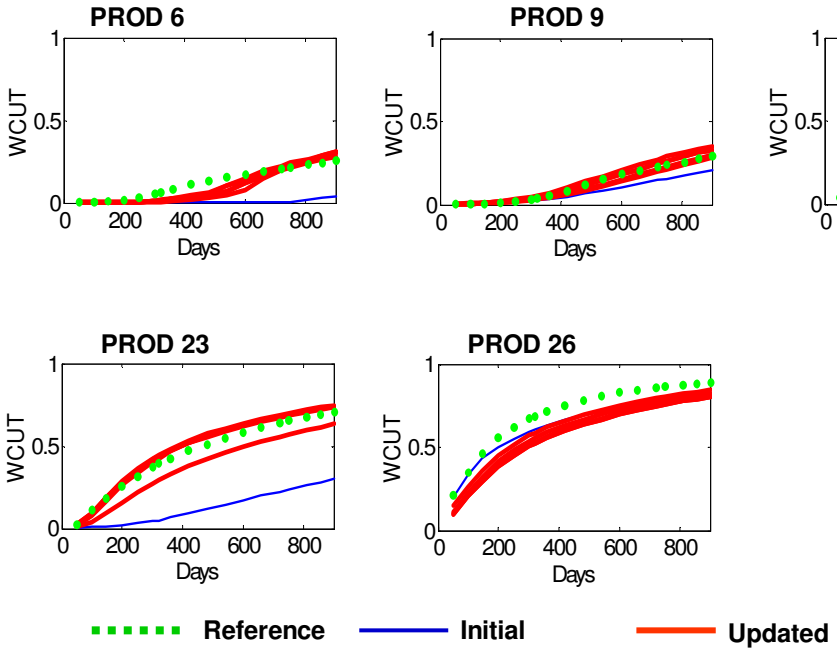

Fig. 3. 23— Two stage for SPE9: water cut match.

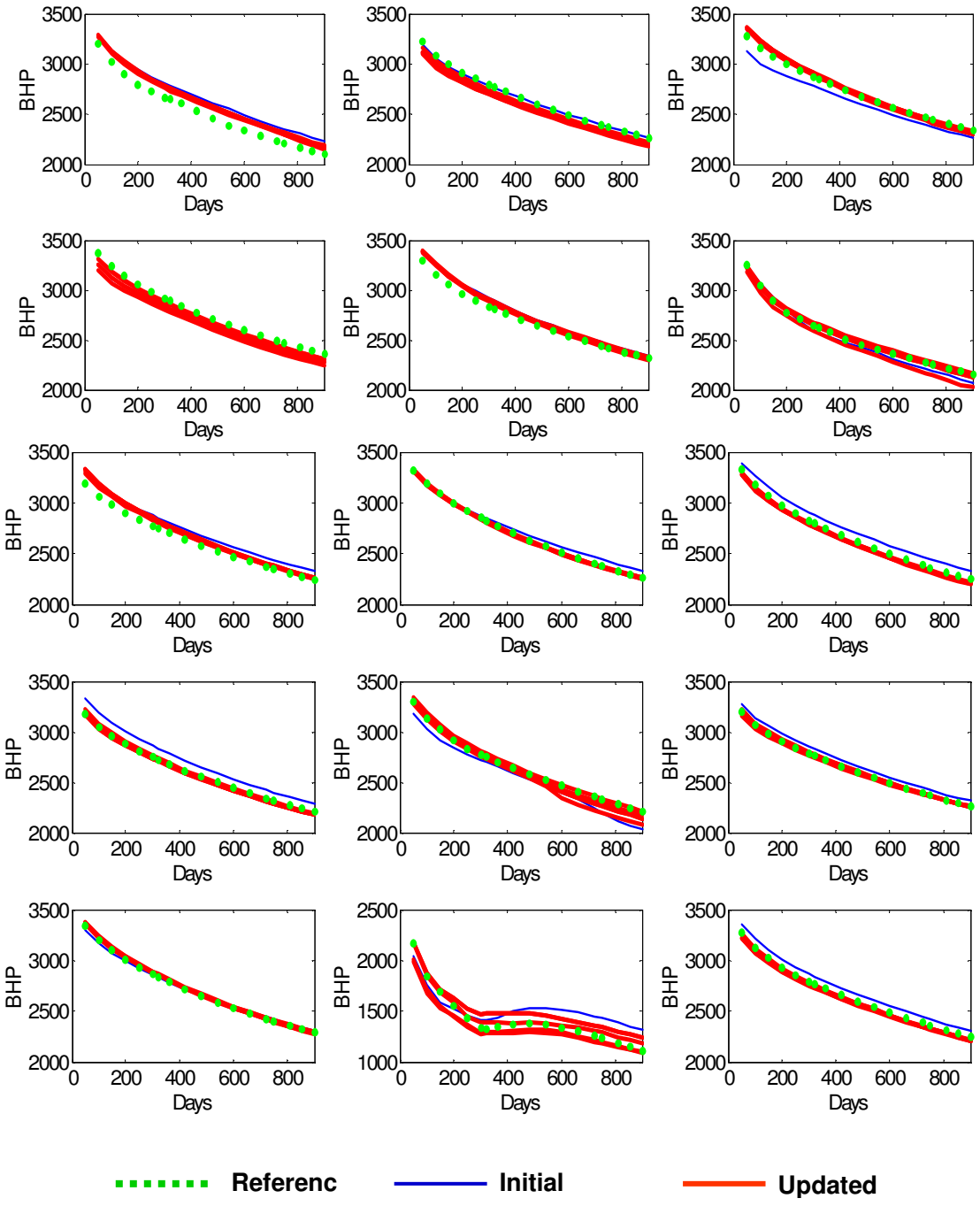

Fig. 3. 24— Two stage for SPE9: BHP match (PROD 2 ~ PROD 16).

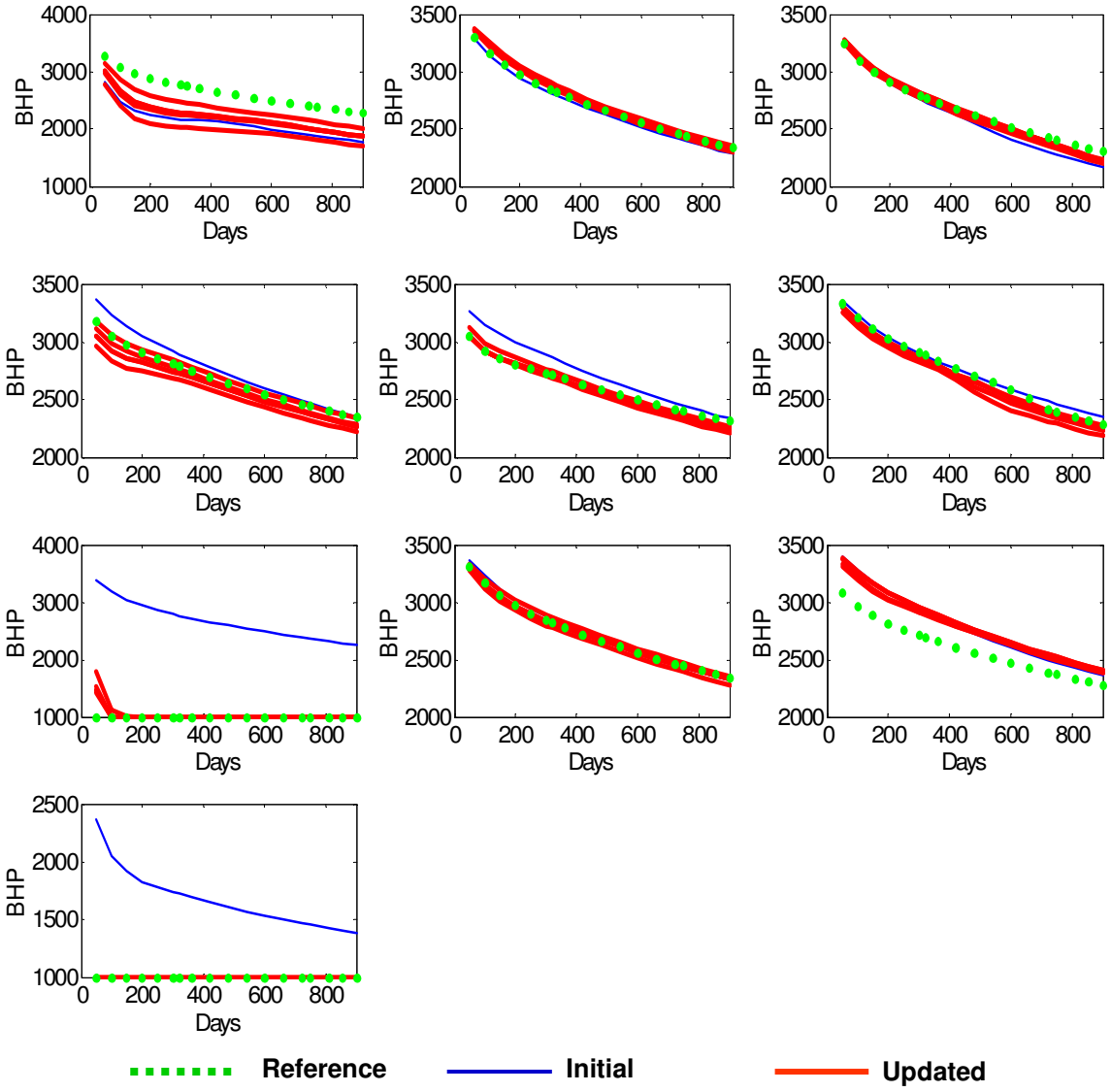

Fig. 3. 25— Two stage for SPE9: BHP match (PROD 17 ~ PROD 26).

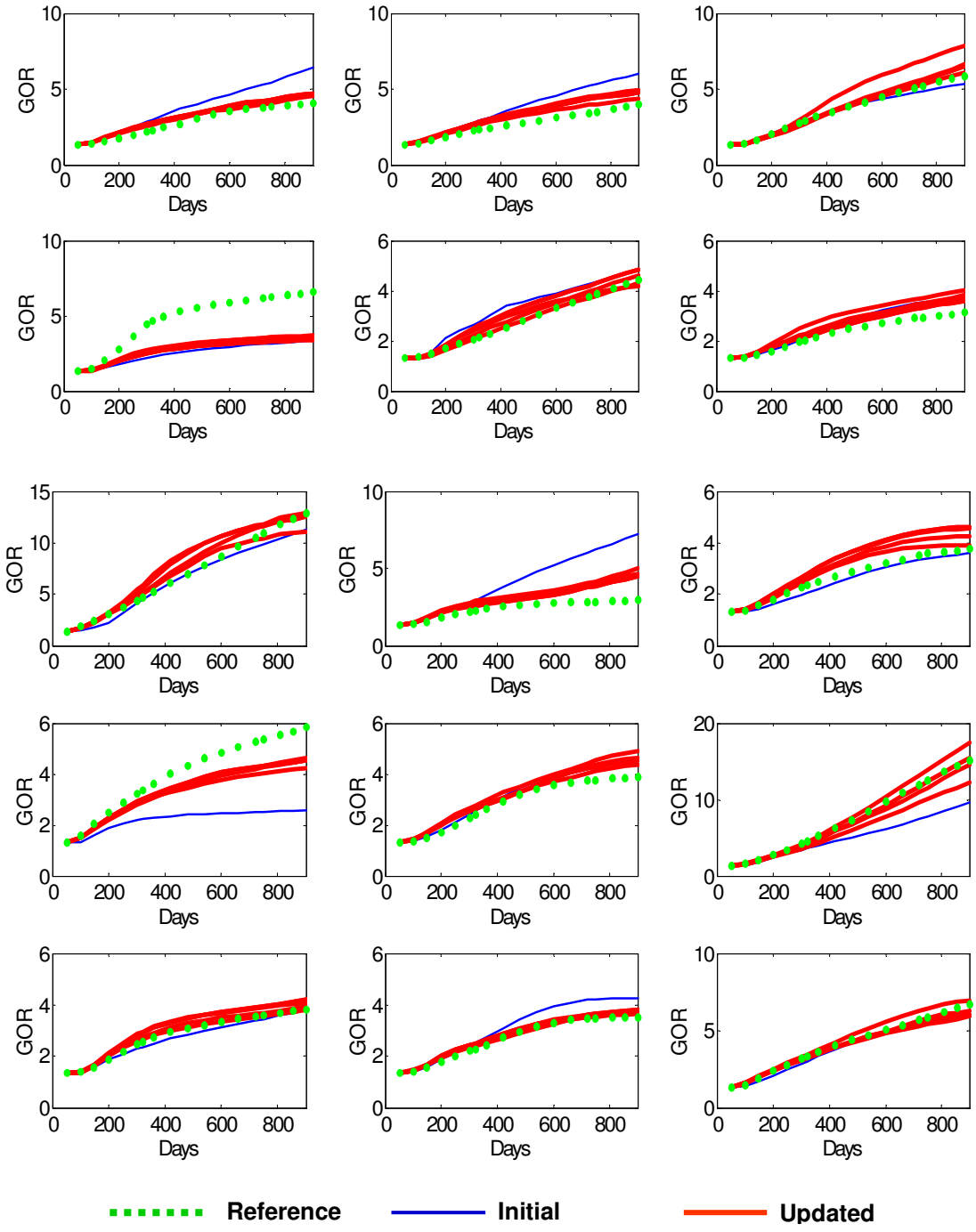

Fig. 3. 26— Two stage for SPE9: GOR match (PROD 2 ~ PROD 16).

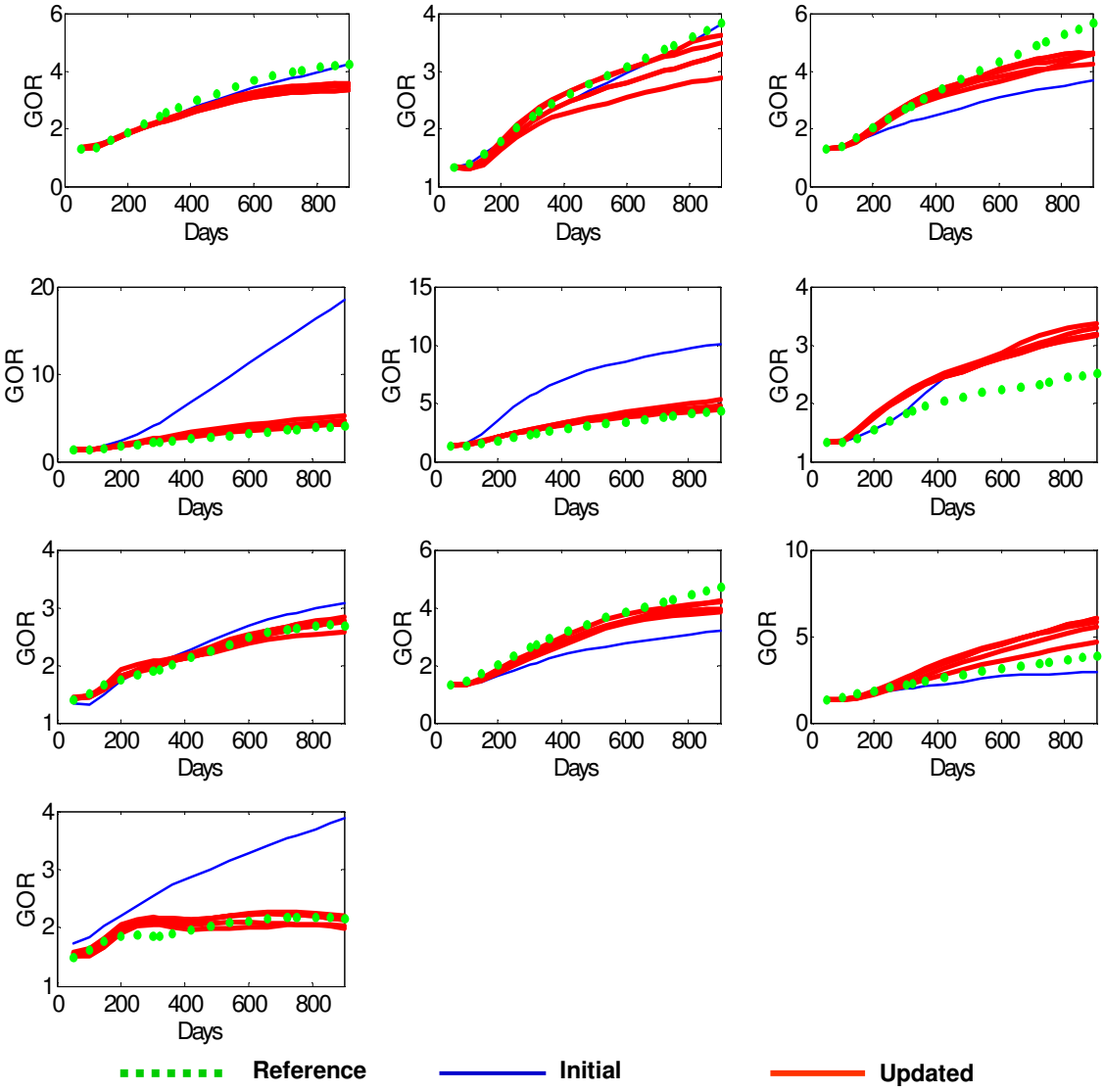

Fig. 3. 27— Two stage for SPE9: GOR match (PROD 17 ~ PROD 26).

CHAPTER IV

TWO-STAGE MCMC WITH UPSCALING AND NONPARAMETRIC REGRESSION

The response surface models are purely algebraic constructs without knowledge of actual governing equations related to reservoir flow and transport. They only embody the behavior of the function it is approximating based on the sampled data. In addition, the application of the method relies on efficiently constructing accurate response surfaces. If the response surfaces can accurately predict the reservoir responses, i.e. they are linearly correlated, the acceptance probability in the second stage is close to 1. However, most response surfaces tend to smooth out non-linear effect caused by parameters. Therefore, it is a difficult task to generate accurate response surfaces.

In this chapter we extend previous two-stage MCMC methods by constructing a surrogate model based on a physical model governed by multiphase flow equations. The surrogate model is a cheap coarse scale model by upscaling an expensive fine scale model. In the first stage, the inexpensive coarse-scale simulations are performed to determine whether or not to run the fine-scale expensive flow simulations. Since the evaluation of the data misfits are based on the flow simulation of the coarse model, the misfits are different from these on the fine scale model. We would apply a response correction to obtain the data misfits on the fine scale model. The response correction could be a simple linear function or very sophisticated nonlinear function. Nonparametric regressions are employed for this purpose.

4.1 Two-stage MCMC with Upscaling and Nonparametric Regression

We extend two-stage MCMC methods considered before. The proposed method employs offline computations for modeling the relation between coarse- and fine-scale error

responses (Efendiev et al. 2008 (submitted)). This relation is modeled using nonlinear statistical maps. The resulting statistical models are used in efficient sampling within MCMC framework. We propose two-stage MCMC where inexpensive coarse-scale simulations based on single-phase upscaling are performed to determine whether or not to run the fine-scale simulations. The latter is determined based on the statistical model developed offline. The proposed method improves the existing two-stage MCMC methods which use coarse-scale or other approximate models. The new method does not rely on the proximity of approximate and resolved models and can employ much coarser and inexpensive models to guide the fine-scale simulations.

To formulate the algorithm, we assume that the likelihood function is given by.

$$P(d_{obs} \mid k) \propto \exp\left(-\frac{\| d_{obs} - d_k \|^2}{\sigma_f^2}\right) \quad \text{.....(4.1)}$$

where ||…|| is a norm, d_{obs} is the observed history data, and d_k is calculated reservoir responses from reservoir simulator for fine-scale permeability k, and σ is main diagonal of data covariance matrix. After the fine-scale permeability k is upscaled to k^*, we can obtain the reservoir responses d_{k*} of the coarse-scale from the simulator. Therefore, we have two data misfits: $\| d_{obs} - d_k \|$ and $\| d_{obs} - d_{k*} \|$. Based on a limited number of permeability realizations we can construct nonlinear relation between these quantities using known statistical methods.

$$\| d_{obs} - d_k \| = G(\| d_{obs} - d_{k^*} \| \quad \text{.....(4.2)}$$

where G is a nonlinear function which is estimated based on a limited number of realizations of permeability field. G can be assumed to be random as it is done in our simulations. In the study, we use piece-wise Gaussian processes to fit the relation G. In this case, the surrogate likelihood function is

$$\pi^*(k) = P(d_{obs} \mid k) \propto \exp\left(-\frac{1}{\sigma_f^2} \frac{G_0\left(\| d_{obs} - d_{k^*} \|\right)}{\sigma^*} \right) \ldots\ldots\ldots\ldots\ldots\ldots\ldots\ldots(4.3)$$

where G_0 and σ_{k^*} are the mean and the variance of the piece-wise Gaussian for a given k^*

4.1.1 Algorithm

Start with offline computations of GOR cross-plot by computing $\| d_{obs} - d_k \|$ and $\| d_{obs} - d_{k*} \|$. Estimate the function G, such that $\| d_{obs} - d_k \| = G(\| d_{obs} - d_{k*} \|)$.

- Step 1. At k_n generate k from $q(k|k_n)$.
- Step 2. Accept k for the fine-scale run with probability

$$g(k_n, k) = \min\left(1, \frac{q(k_n \mid k) P(k^* \mid d_{obs})}{q(k \mid k_n) P(k_n^* \mid d_{obs})} \right) \ldots\ldots\ldots\ldots\ldots\ldots\ldots\ldots\ldots\ldots(4.4)$$

- i.e. $k_{n+1}=k$ (conditionally) with probability $g(k, k_n)$, and $k_{n+1}=k_n$ (conditionally) with probability $1- g(k, k_n)$. If rejected go to step 1.
- Step 3. Accept k with probability

$$\rho(k_n, k) = \min\left(1, \frac{\pi(k)\pi^*(k_n)}{\pi(k_n)\pi^*(k)} \right) \ldots\ldots\ldots\ldots\ldots\ldots\ldots\ldots\ldots\ldots\ldots\ldots(4.5)$$

4.1.2 Single Phase Upscaling

We will briefly describe single-phase flow upscaling procedure used in the two-stage MCMC method. This type of upscaling is discussed by many authors (Durlofsky et al. 1996; Efendiev et al. 2000). The main idea of this approach is to upscale the absolute permeability field k on the coarse-grid (see **Fig. 4.1**), then solve the original system on the coarse-grid with upscaled permeability field. Below, we will discuss briefly the upscaling of absolute permeability used in our simulations.

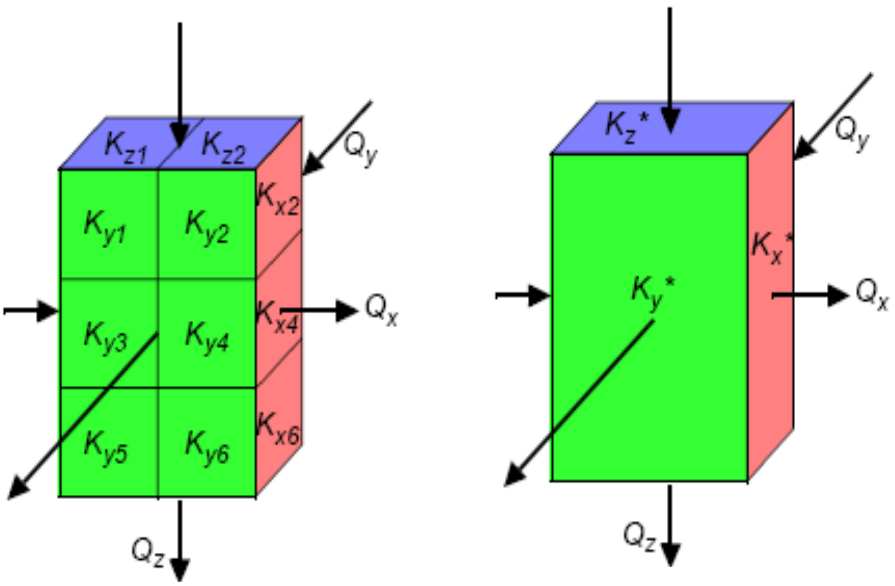

(a) Fine scale cells **(b) Coarse scale cell**

Fig. 4. 1 —Fine scale cells and coarse scale cell.

Consider the fine-scale permeability that is defined in the domain with underlying fine grid as shown in **Fig. 4.1**. On the same graph we illustrate a coarse-scale partition of the domain. To calculate the upscaled permeability field at the coarse-level, we use the solutions of local pressure equations. The main idea of the calculation of a coarse-scale permeability is that it delivers the same average response as that of the underlying fine-scale problem locally. For each coarse domain *D*, we solve the local problems

$$div(k(x)\nabla\phi_j) = 0, \quad \text{.....(4.6)}$$

with some coarse-scale boundary conditions. Here $k(x)$ denotes the fine-scale permeability field. We will use the boundary conditions which are given by $\phi_j = 1$ and $\phi_j = 0$ on the opposite sides along the direction e_j and no flow boundary conditions on

all other sides. For these boundary conditions, the coarse-scale permeability tensor is given by

$$(k^*(x)e_j, e_l) = \frac{1}{|D|}\int_D \left(k(x)\nabla\phi_j(x), e_l\right)dx \quad \text{.....(4.7)}$$

where ϕ_j is the solution of Eq. 4.7 with prescribed boundary conditions. Various boundary conditions can have some influence on the accuracy of the calculations, including periodic, Dirichlet and etc. Wu et al. (2002) have discussed the issues. In particular, for determining the coarse-scale permeability field one can choose the local domains that are larger than the target coarse block, *D*, for Eq. 4.7. We have also tested the two-stage MCMC with ensemble level upscaling methods (Efendiev et al. 2008).

4.2 Convergence Diagnostics

A critical issue of MCMC methods in applications is how to decide when it is safe to stop the Markov chain, which is the topic of current research MCMC methods (Gelman and Rubin 1992; Raftery and Lewis 1992; Geweke 1992). After all, the main purpose of using MCMC is to get a sample from the target distribution and estimate its characteristics. If the resulting chain has not converged to the target distribution, the estimates we get from it are suspect.

Most of the methods that have been proposed in the literature are really diagnostic in nature and have the goal of monitoring convergence. Here we briefly discuss one of the most popular methods proposed by Gelman and Rubin (1992) amongst the statistical community.

4.2.1 Gelman and Rubin Method

The Gelman-Rubin method convergence diagnostic is based on running multiple chains, each with different stating values which are over-dispersed with respect to the target

distribution. The Gelman and Rubin diagnostic was first proposed as a univariate statistic, referred to as the potential scale reduction factor (PSRF), for assessing convergence of individual model parameters. Calculation of this statistic is based on the last *n* samples in each of *m* parallel chains. In particular, the PSRF is calculated as

$$PSRF = \sqrt{\frac{n-1}{n} + \frac{m+1}{mn}\frac{B}{W}} \quad \text{.....(4.8)}$$

where *B/n* is the between-chain variance and *W* is the within-chain variance. The between-chain variance and within-chain variance for a scalar summary *v* is defined by

$$B/n = \frac{1}{m-1}\sum_{j=1}^{m}(\bar{v}_{j.} - \bar{v}_{..})^2 \quad \text{.....(4.9)}$$

$$w = \frac{1}{m(n-1)}\sum_{j=1}^{m}\sum_{t=1}^{n}(v_{jt} - \bar{v}_{j.})^2 \quad \text{.....(4.10)}$$

where the subscript *j* denotes from which chain it was calculated, and *t* represents the position in the chain.

As chains converge to a common target distribution, the between-chain variability should become small relative to the within-chain variability and yield a PSRF that is close to 1. Conversely, PSRF values larger than 1 indicate non-convergence.

Brooks and Gelman (1998) extended the diagnostic in the form of a multivariate potential scale reduction factor (MPSRF) that can be used assess simultaneous convergence of a set of parameters. The MPSPF is calculated as

$$MPSRF = \frac{n-1}{n} + \frac{m+1}{m}\lambda \quad \text{.....(4.11)}$$

where λ is largest eigenvalue of the positive definite matrix $W^{-1}B/n$. The MPSRF has property that

$$\max_i \{PSRF_i\} \leq MPSRF \quad \text{.....(4.12)}$$

where i indexes the parameters being examined.

The R package **boa** was designed by Smith (2007) for convergence assessment and posterior inference of MCMC output. We apply the diagnostics implemented in the package to the project.

4.2.2 Maximum Entropy Test

The test was applied by Maucec et al. (2007) to summarize the MCMC convergence using a single chain. The negative entropy is defined as the expected value of the logrithms of un-normalized posterior terms $p(k|d)$.

$$-s = \frac{1}{I}\sum_{j=1}^{J}\sum_{i}^{I}\log(p(k\,|\,d)_i^j \quad \text{.....(4.13)}$$

The variance of entropy s is defined as

$$Var(s) = \frac{1}{I}\sum_{j=1}^{J}\sum_{i}^{I}\left[\log(p(k\,|\,d)_i^j\right]^2 - \left[\frac{1}{I}\sum_{j=1}^{J}\sum_{i}^{I}\log(p(k\,|\,d)_i^j\right]^2 \quad \text{.....(4.14)}$$

Index i runs over the number of new realizations of reservoir models and index j runs over the number of Markov chain iterations.

The Gelman-Rubin method is very expensive for our applications as it requires multiple chains. Therefore we limit its usage to the following 2D synthetic example, for the following 3D example we apply use maximum entropy test.

4.3 2D Synthetic Example

The synthetic and anisotropic case involves three-phase flow and includes matching GOR from a 9-spot pattern. The initial solution GOR is 1.27 Mscf/STB. The reservoir was produced starting at bubblepoint pressure. As the pressure drops, solution gas comes out from the oil phase and accumulates as mobile free gas. The fine grid size is 50×50. The coarse grid size is 5×5. The reference and initial permeability distributions are given in **Fig. 4.2**. The reference permeability field is generated by *sgsim* (Deutsch and Journel 1998) using 30 and 2 as maximum and minimum horizontal ranges while initial permeability field was generated using 18 and 3 as maximum and minimum horizontal correlation lengths. The KLE expansion was performed in the initial permeability and 50 dominant eigenvalues are kept. To implement the two-stage MCMC, we first perturb the 41 random variables (9 variables are used to condition the values at 9 well ocations) and generate 200 fine grid permeability fields, which are upscaled into corresponding 5×5 coarse grid. The GOR misfits for the fine and coarse grid are presented in **Fig. 4.3**. In the figure we also plot both mean as well as mean plus/minus standard deviation. We have used piecewise linear relation to model the mean behavior and constant variation within each segment. Furthermore, Gaussian distribution is assumed in each segment.

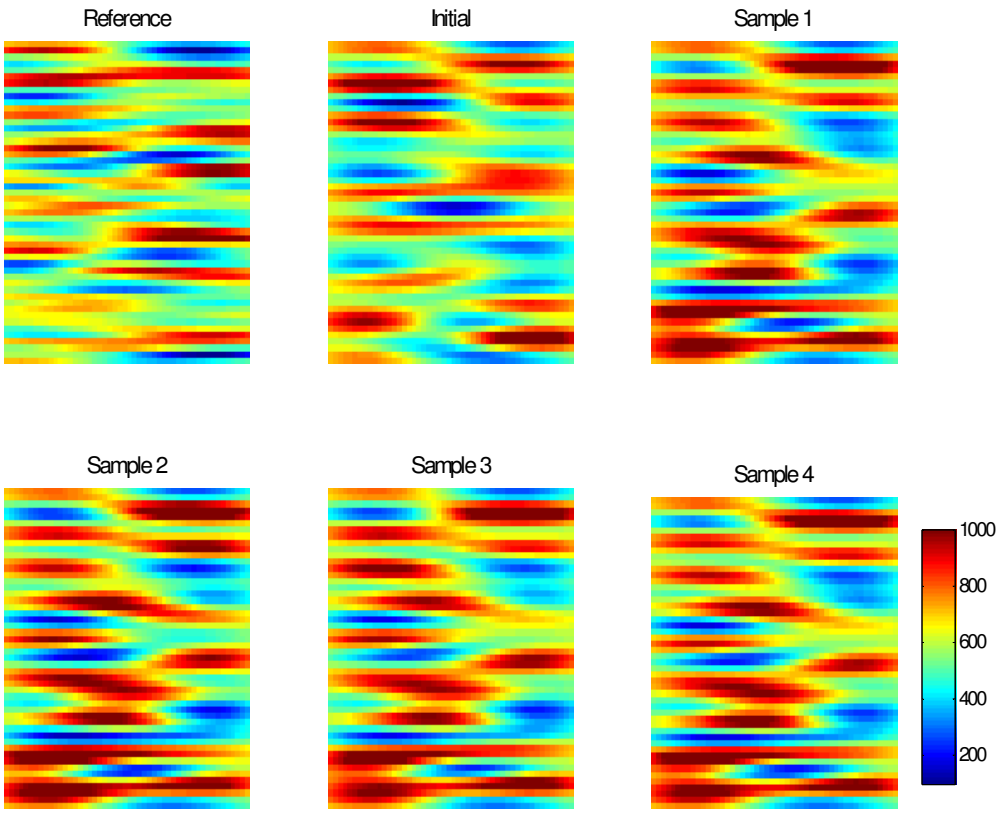

Fig. 4. 2—Reference, initial models and collected samples.

In **Fig. 4.4**, GOR misfit vs. iterations are plotted using two-stage MCMC and full MCMC. The two curves show that two-stage MCMC has similar convergence as the MCMC. However, the acceptance for the full MCMC is 8.8% and 33% for two-stage MCMC with upscaling. **Fig. 4.5** shows the GOR matches.

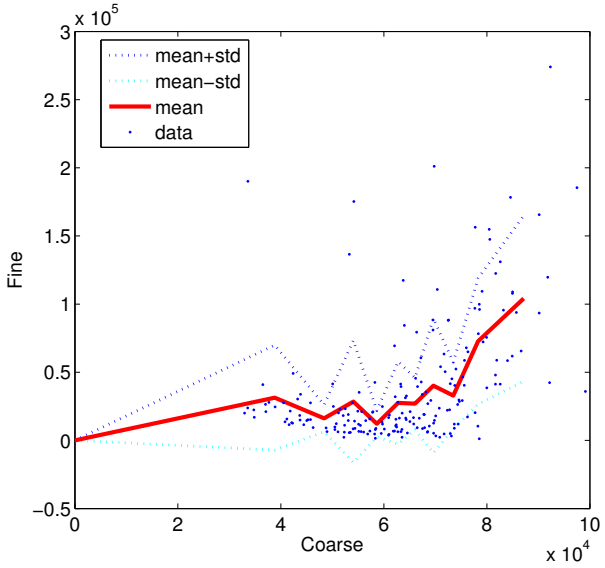

Fig. 4. 3—Error model of 2D synthetic example.

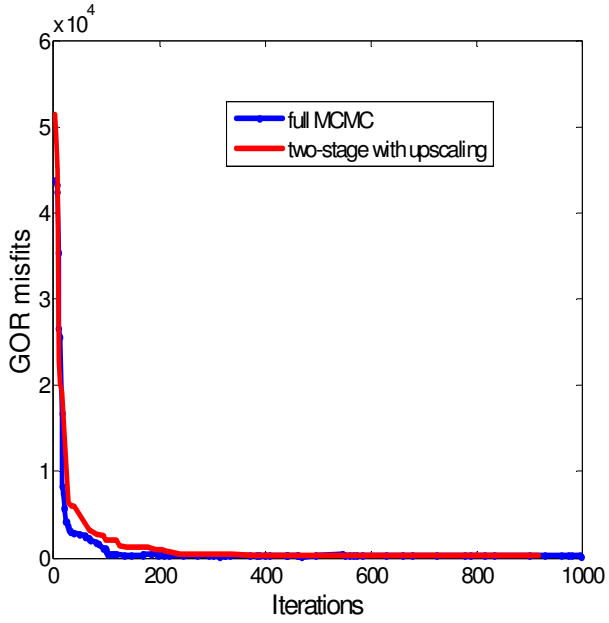

Fig. 4. 4—GOR misfits reduction of 2D synthetic example.

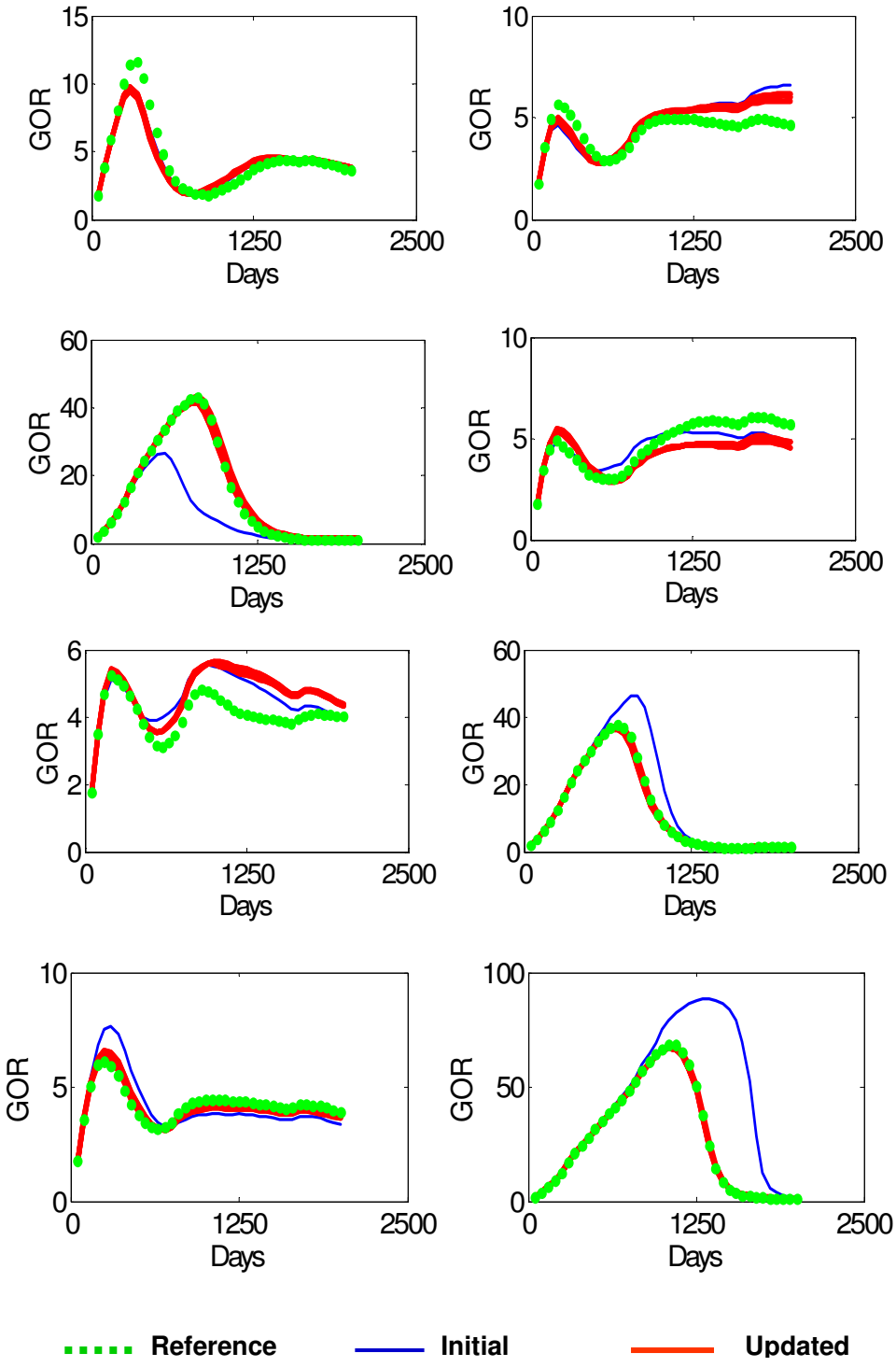

Fig. 4. 5 —GOR match of 2D synthetic example.

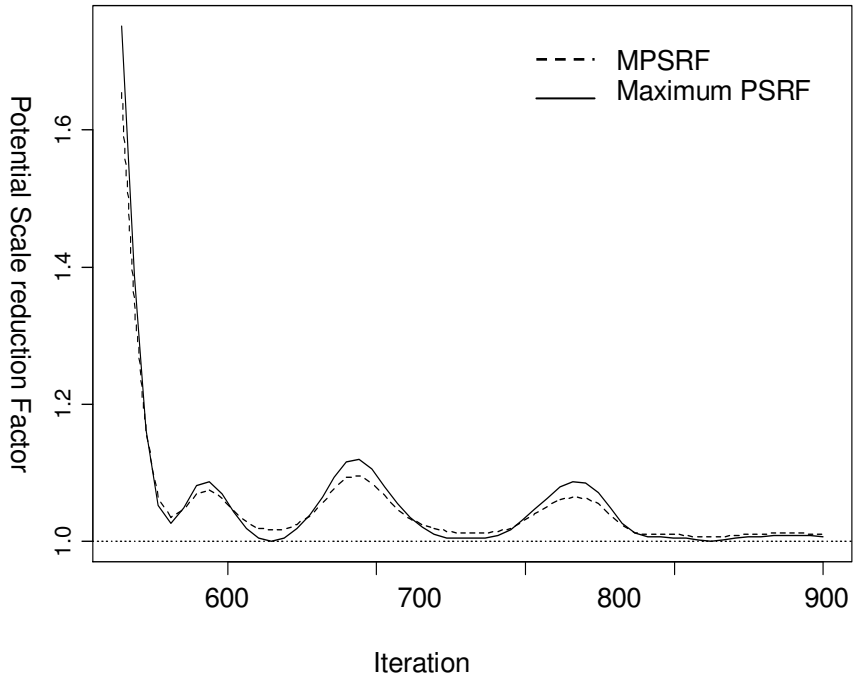

Fig. 4. 6—Brooks and Gelman diagnostic plot for 2D synthetic example.

The Gelman–Rubin convergence diagnostic was applied to the 10 chains. The value of the Brooks–Gelman MPSRF is 1.01. **Fig. 4.6** shows a plot of the Brooks–Gelman MPSRF along with the maximum PSRF for successively larger segments of the chains. The plot shows that the MPSRF has settled down close to 1.0 after 600 iterations, suggesting that the chains have mixed together, and that it is probably safe to assume convergence.

4.4 3D Synthetic Example

The synthetic case involves two-phase flow and includes matching water cut. There are 8 producers and 4 water injectors as shown in **Fig. 4.7**. The fine grid size is 80×80×12. The coarse grid size is 8×8×3. The reference and initial logarithmic permeability distributions are given in **Fig. 4.7**. The reference permeability field is generated by *sgsim* (Deutsch and Journel 1998) using 40, 5 maximum and minimum horizontal ranges, 2 as the vertical range. Initial permeability field was generated using 35 and 10 as maximum and minimum horizontal ranges, 4 as as the vertical range. The gradual deformation method is used to combine 11 realizations. To implement the two-stage MCMC, we first perturb 11 gradual deformation parameters and generate 200 fine grid permeability fields, which are upscaled into corresponding 8×8×3 coarse grid. The water cut misfits for the fine and coarse grid are presented in **Fig. 4.8**. In **Fig. 4.9**, water cut misfit vs. iterations is plotted using two-stage MCMC and full MCMC.

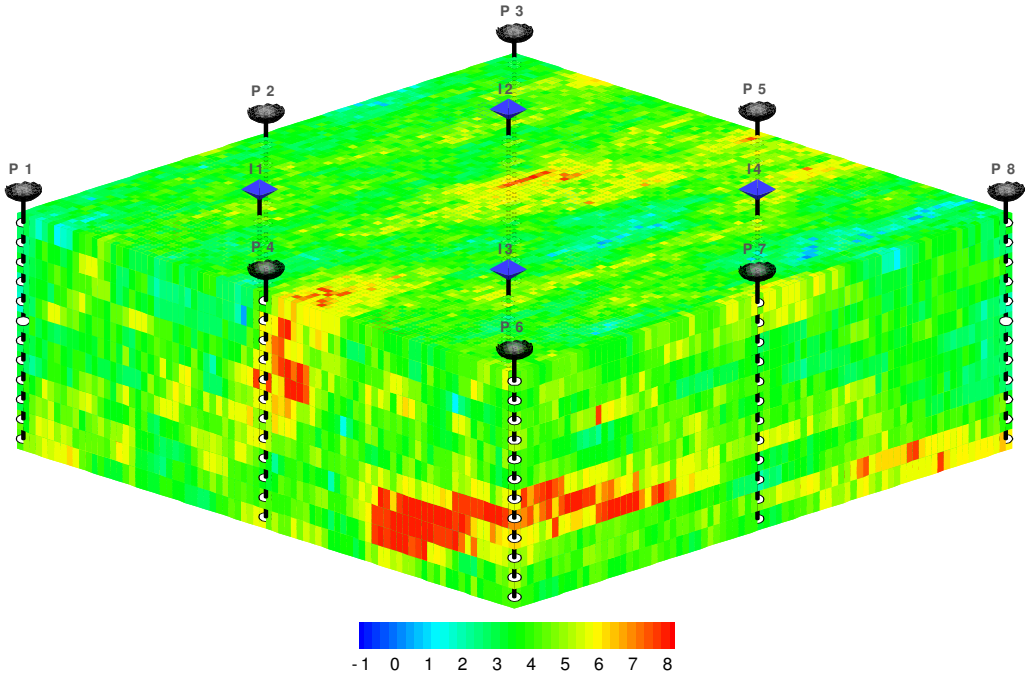

(a) Reference log permeability field

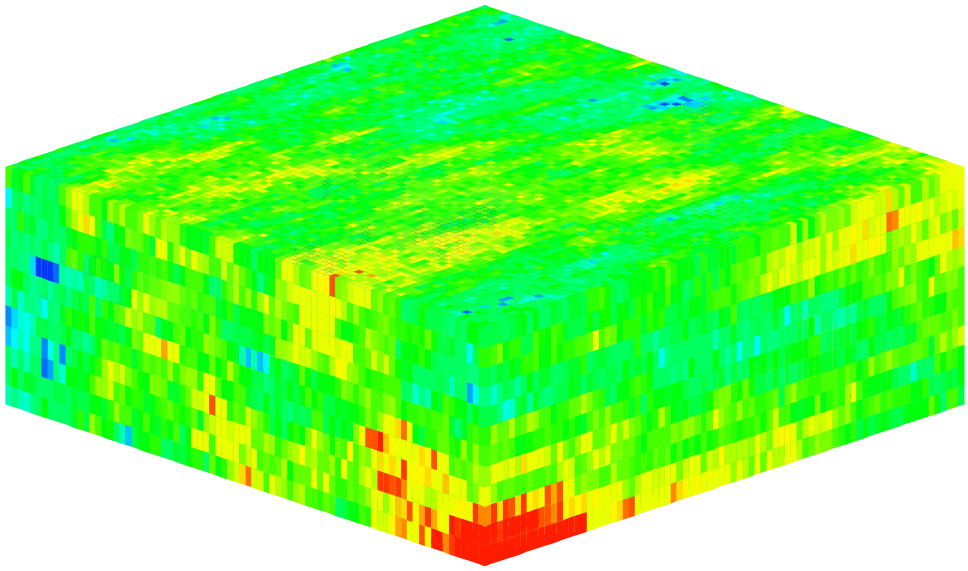

(b) Initial log permeability fields

Fig. 4. 7—Reference and initial log permeability fields.

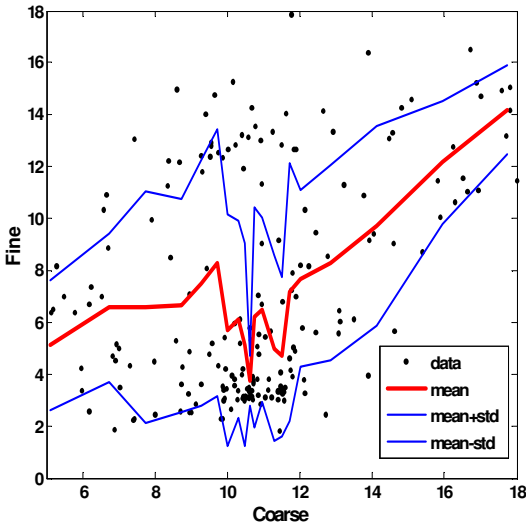

Fig. 4. 8—Error model of 3D example.

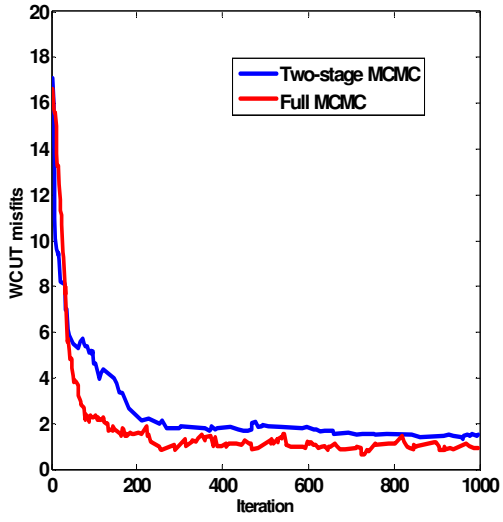

Fig. 4. 9— Water cut misfits reduction of 3D example.

The acceptance rate for two-stage MCMC is 26% and 19% for the full MCMC. **Fig. 4.10** shows the water cut matches from collected samples. **Fig. 4.11** shows the permeability histogram for (i) initial model (ii) the updated models via two-stage sampling from the initial geologic model. We can see from **Fig. 4.11** that collected samples leads to a similar permeability statistics of the initial models. We can see that the low permeability at the initial geological model have been removed, indicating the need to increase permeability at the low permeability regions to match the production data. **Fig. 4.12** shows the convergence diagnostics using entropy and variance of entropy.

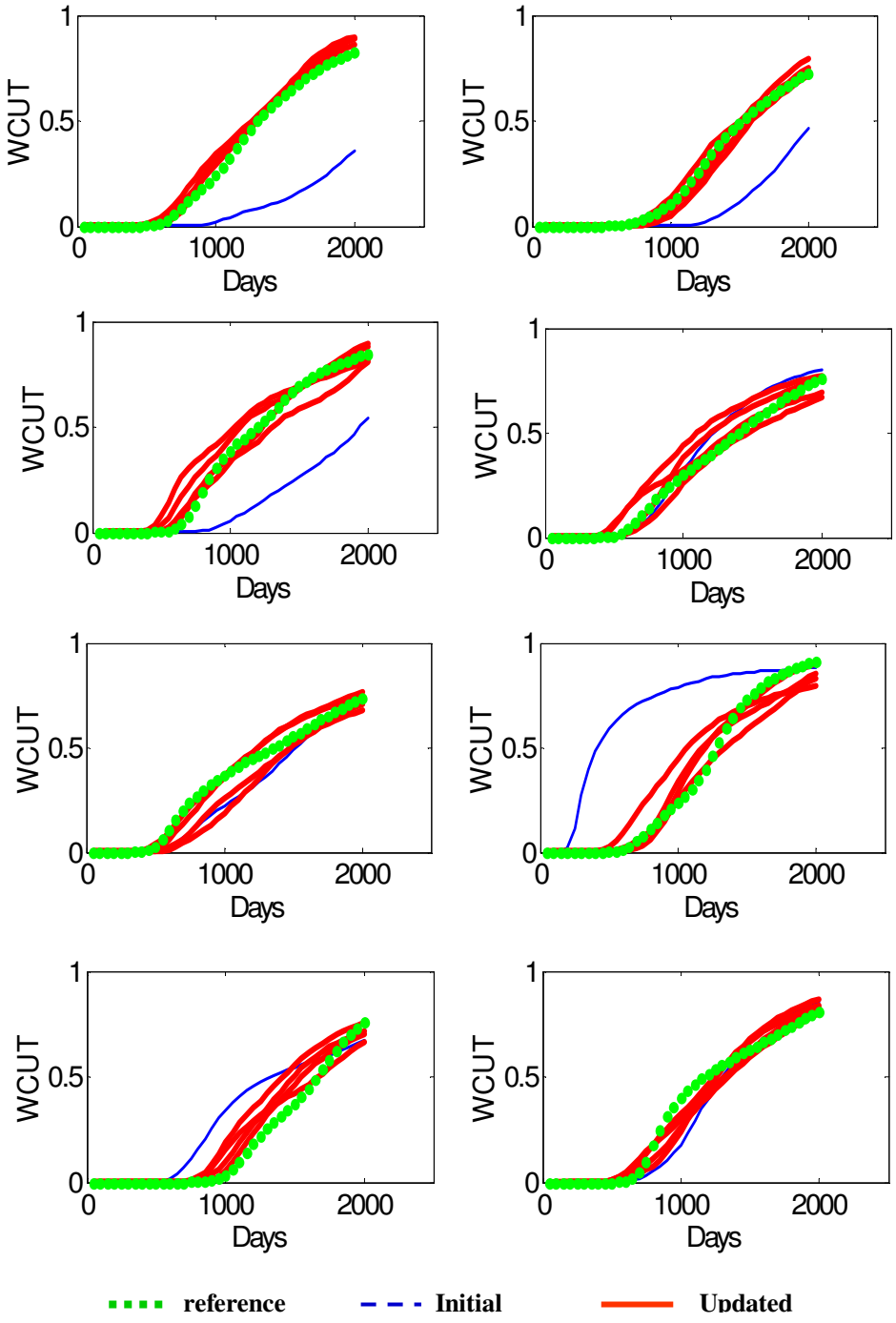

Fig. 4. 10—Watercut match of 3D example.

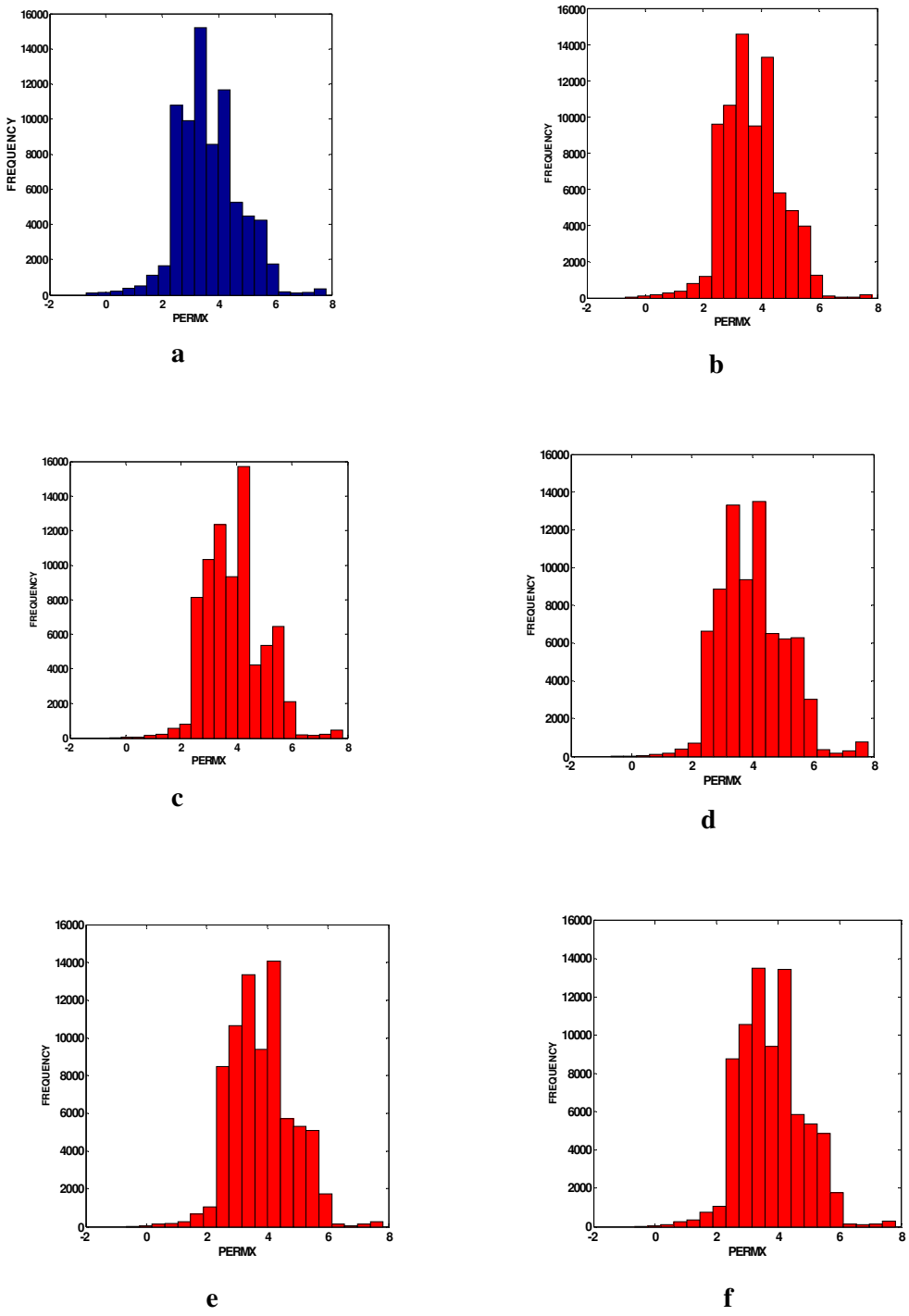

Fig. 4. 11—Horizontal permeability histogram for (a) inital model, (b)-(f) sampled inverted model starting from initial model.

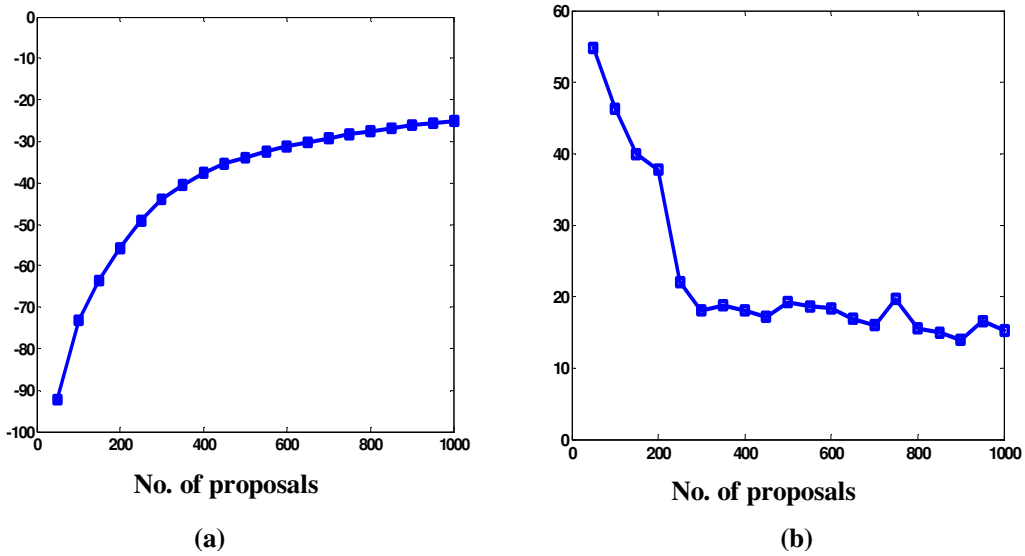

Fig. 4. 12 —Convergence parameters for two-stage MCMC on 1000 proposals (a) entropy (b) variance of entropy.

CHAPTER V

OPTIMAL COARSENING OF 3D RESERVOIR MODELS*

We have developed a new constrained optimization approach to the coarsening of 3D reservoir models for flow simulation. The optimization maximally preserves a statistical measure of the heterogeneity of a fine scale model. Constraints arise from the reservoir fluids, well locations, pay/non-pay juxtaposition, and large scale reservoir structure and stratigraphy. The approach has been validated for a number of oil and gas projects, where flow simulation through the coarsened model is shown to provide an excellent approximation to high resolution calculations performed in the original model.

The optimal layer coarsening is related to the analyses of Li and Beckner (2000), Li et al. (1995), and Testerman (1962). It differs by utilizing a more accurate measure of reservoir heterogeneity and by being based on recursive sequential coarsening, instead of sequential refinement. Recursive coarsening is shown to be significantly faster than refinement: the cost of the calculation scales as $(NX \cdot NY \cdot NZ)$ instead of $(NX \cdot NY \cdot NZ)^2$. The more accurate measure of reservoir heterogeneity is very important; it provides a more conservative estimate of the optimal number of layers than the analysis of Li et al. (1995). The latter is shown to be too aggressive and does not preserve important aspects of the reservoir heterogeneity. Our approach also differs from the global methods of Stern and Dawson (1999) and Durlofsky et al. (1996). It does not require the calculation of a global pressure solution and it does not require the imposition of large scale flow

* Part of this chapter is reprinted with permission from "Optimal Coarsening of 3D Reservoir Models for Flow Simulation", by King, M., Burn, K., Wang, P., Muralidharan, V., Alvarado, F., Ma., X., and Datta-Gupta, A., 2005. Paper SPE 95759 presented at the SPE Annual Technical Conference and Exhibition, Dallas, TX. Part of this chapter is reprinted with permission from "Upgridding 3-D Geologic Models in a Channel-type Environment", by Talbert, M., Ma., X., and Datta-Gupta, A., 2008. Paper SPE 113245 presented at the Indian Oil and Gas Technical Conference and Exhibition, Mumbai, India.

fields, which may bias the analysis (see Fincham et al. 2004). Instead, global flow calculations are retained only to validate the reservoir coarsening.

Our approach can generate highly unstructured, variable resolution, computational grids. The layering scheme for these grids follows from the statistical analysis of the reservoir heterogeneity. Locally variable resolution follows from the constraints (reservoir structure, faults, well locations, fluids, pay/non-pay juxtaposition). Our reservoir simulator has been modified to allow a fine scale model to be initialized and further coarsened at run time. This has many advantages in that it provides both simplified and powerful workflows, which allow engineers and geoscientists to work with identical shared models.

5.1 Introduction

The development of (coarsened) reservoir simulation models from high resolution geologic models remains an active field of research (Li and Beckner 2000; Stern and Dawson 1999; Fincham et al. 2004; Durlofsky et al. 1996). In the current study we will report upon our success in the use of coarsening algorithms to determine a 'best' reservoir simulation grid obtained by grouping fine scale geologic model cells into effective simulation cells (King et al. 2006). Our results differ from previous studies in that we have found a statistical analysis of the static properties of the model that appears to identify the best grid for dynamic reservoir simulation. Coarsening beyond the degree indicated by our analysis discards too much of the underlying heterogeneity. It will overly homogenize the properties on the simulation grid. Finer models will, of course, retain at least as much reservoir heterogeneity, but are more costly.

We will not address property upscaling algorithms. Instead we will emphasize the grouping of fine cells into logical coarse cells: the problem of coarsening. In an areal sense we have found this problem to be heavily constrained by requirements of resolution: number of cells between wells, resolution of flow near wells, resolution of fluid contacts, and representation of fault block boundaries.

The bulk of the chapter is the discussion of the new statistical approach applied to layer coarsening. Before describing the new technique, we will briefly review those papers from which we have learned the most, as a precursor to this work.

The earliest application of statistical techniques to zonation was by Testerman (1962), who looked at the problem of how to zone individual wells and how to build up a reservation zonation scheme from multiple wells. Our layer coarsening problem is simpler, as the reservoir zonation has already been developed within the geologic model. However, the logic of zonation for individual wells has immediate utility for us. Simply put, Testerman (1962) looked at the permeability data at a vertical well and grouped the permeabilities in such a way to minimize the variance within each group and to maximize the variance between groups. We will apply the logic of 'Within' and 'Between' variance (or variation) repeatedly in our work. This general decomposition problem is computationally expensive, but Testerman (1962) demonstrated an effective sequential refinement approach. In his analysis, the reservoir is first blocked to a single layer. All possible refinements into two layers are considered, and the split that maximizes 'Between' variance and minimizes 'Within' variance is selected. With this split maintained, the two layer model is analyzed for refinement into a three layer model, and so on. These refinements proceed sequentially until the change in the ratio of 'Within' to 'Between' variance drops below an empirically chosen threshold.

The work by Li and Beckner (2000) on layer coarsening is related to the earlier work by Li et al. (1995) on volumetric coarsening and to the work of Testerman (1962). It is specifically applied to the problem of grouping the layers of a geologic model to develop a simulation model. Following Testerman (1962), it applies sequential refinement to a measure of heterogeneity. This measure is deriving by averaging the properties within each layer of the geologic model to build a 1D pseudo-well, which is then analyzed using Testerman's approach. There is a correction within the heterogeneity measure for the amount of variance within each layer, but other than this, most of the information on the 3D reservoir heterogeneity is lost.

In a static statistical study there is a question of what property should be used for analysis, and how that property should be averaged. Li and Beckner (2000) argued that we should use a local dynamic error measure. Specifically, when a column of cells is replaced by one cell, the different horizontal flow velocities in each layer are replaced by a single average value as shown in **Fig. 5.1**. In detail, when upscaling a geologic model, we will upscale porosity to preserve pore volume and directional permeabilities to preserve volumetric flux per unit pressure drop. However, neither of those calculations minimizes the variance in transit time across the column of cells; the latter is the dominant error in upscaling. Within each layer this velocity is given by $f'k/\phi$, where k/ϕ is the interstitial velocity and the Buckley-Leverett speed f' includes the facies and saturation dependent relative permeability terms. During the statistical analysis, arithmetic averaging of the velocity will be used, as it provides an unbiased estimator of the mean. This works well for the statistical analysis, although the genuine upscaling error will be somewhat greater since the independent upscaling of porosity and permeability will provide a biased estimate of the average velocity.

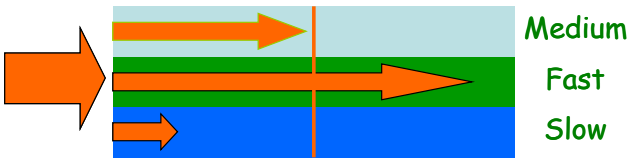

Fig. 5. 1—Error in velocity is introduced while upscaling; different fluid velocities are replaced by a single value.

Li and Beckner (2000) utilized sequential refinement, as did Testerman (1962). Unlike Testerman (1962), they provided a complete analysis of the reservoir heterogeneity, starting with a one layer simulation model, and eventually recovering the vertical resolution of the geologic model.

Finally, it is worth mentioning two layer grouping schemes based upon global flow calculations. In the layer grouping work of Durlofsky et. al. (1996), a global pressure field is introduced to the geologic model, and flow is calculated numerically. The flow field is used to guide the groupings, with regions of high flow rates retaining more resolution and regions of slow flow having fewer layers. This approach is not restricted to layer grouping, as the simulation layers may follow the flow lines as they cut across geologic layers. This approach is not sequential.

An interesting variation was provided by Stern and Dawson (1999) who utilized a sequential coarsening approach based on tracer breakthrough time and swept volume calculations. As with the work of Li and Beckner (2000), the engineer was able to assess the fidelity of the representation as a function of the number of layers. As with the work of Durlofsky et al. (1996), this information was obtained using a global pressure and (steady state) velocity field. The approach appears to provide a more predictive approach to simulator performance than the analysis of Li and Beckner (2000).

5.2 Approach and Mathematical Formulation

The advantages and disadvantages of the methods we have described were examined in some detail in the recent work of Fincham et al. (2004). The static methods have the advantage of being fast. Unfortunately, they do not predict the appropriate number of layers for a dynamic model. The latter must be tested by simulation, and the appropriate number of layers determined by trial and error. We will see this as well, when we demonstrate that a different measure of heterogeneity can provide such a prediction.

The global dynamic methods have the advantage of providing a more accurate representation of how a simulator will perform. However, their application becomes more problematic as the reservoir geometry becomes more complex. As a reservoir looks less and less like a shoebox, the use of pre-determined global boundary conditions becomes less and less informative. In addition, when these methods do work, these grids are, in some sense, too good. They are optimized to a specific flow field, with potentially

highly variable spatial resolution. During the life of a field, as the reservoir is actively managed, the flow fields will be changing dramatically: the flow during primary depletion will look nothing like the pattern floods within an infill program late in field life. Revising a simulation grid as the flow field changes is a difficult and problematic activity.

As with Testerman (1962), and with Li and Beckner (2000), we will utilize a static analysis and a sequential approach. However, our will use a sequential recursive coarsening algorithm which is significantly faster than sequential refinement. If N is the total number of cells in the geologic model, then the cost of our calculation scales as N. In contrast, sequential refinement scales as N^2, which is significantly more expensive for a multi-million cell geologic model. This allows us to use a more informative measure of heterogeneity than Li and Beckner (2000). They examined a measure similar to the one that we will use and discarded it because of the cost of the calculation.

Our algorithm relies on a sequential coarsening of the fine-scale geologic model. To start with, we determine which two adjacent layers may be merged. This is based on an analysis of the total variation of a defined static property denoted as *p*. Following Li and Beckner (2000), we choose the property given by $p = kf'/\phi$ as our coarsening parameter. However, in contrast to the work of Durlofsky et al. (1996) and of Stern and Dawson (1999), we will not design our layering scheme using global dynamic information. Because of the choice of parameter we believe that the Li and Beckner (2000) approach and our current analysis should both be characterized as a local dynamic method. However, these methods have been called static and we will retain that usage to minimize confusion. We retain the use of dynamic simulation and/or tracer time of flight to test the results of our static analysis.

The 'total variation', as a measure of heterogeneity during coarsening, is decomposed into 'within cell variation (W)' and 'between cell variation (B)'. These quantities are discussed below.

At any stage of coarsening, the quantity 'W' is given by

$$W = \sum_{i,j,k=1}^{NX,NY,NZ} n_{i,j,k}\left(p_{i,j,k} - p^{C}_{i,j,k}\right)^2 \quad \text{..... (5.1)}$$

Eq. 5.1 is a summation over the entire reservoir model and quantifies the variation removed from the model after upgridding. The summation is weighted by $n_{i,j,k}$, which is the bulk rock volume of the cell. This ensures that W does not change under numerical refinement of the grid. Also, $p_{i,j,k}$ refers to the static property at the fine-scale and $p^{C}_{i,j,k}$ is the transitional static property that is calculated after every merging of adjacent layers as follows

$$p^{C}_{i,j,k} = \sum_{k} n_{i,j,k} \cdot p_{i,j,k} \Big/ \sum_{k} n_{i,j,k} \quad \text{.....(5.2)}$$

The quantity B, 'the between cell variation' quantifies the amount of heterogeneity preserved during upgridding. At any stage of coarsening it is given by

$$B = \sum_{i,j,k=1}^{NX,NY,NZ} n_{i,j,k}\left(p^{C}_{i,j,k} - \overline{p}_{i,j}\right)^2 \quad \text{..... (5.3)}$$

Where $\overline{P}_{i,j}$ is the column based average of our static property given by the following

$$\overline{p}_{i,j} = \sum_{k=1}^{NZ} n_{i,j,k} \cdot p_{i,j,k} \Big/ \sum_{k=1}^{NZ} n_{i,j,k} \quad \text{..... (5.4)}$$

The goal of our algorithm is to minimize the amount of variation removed from our model and maximize the variation preserved while honoring geological markers during upgridding. The total variation of the model which is preserved during upgridding is given by the sum of 'within cell variation' and 'between cell variation' as follows

$$H = W + B \qquad (5.5)$$

Fig. 5.2 shows the trends of *W* and *B* as a function of number of layers. The optimal number of layers will be decided by minimizing W (that is minimizing the loss of heterogeneity) or alternately maximizing *B* (that is preserving the geologic heterogeneity to the maximum possible extent).

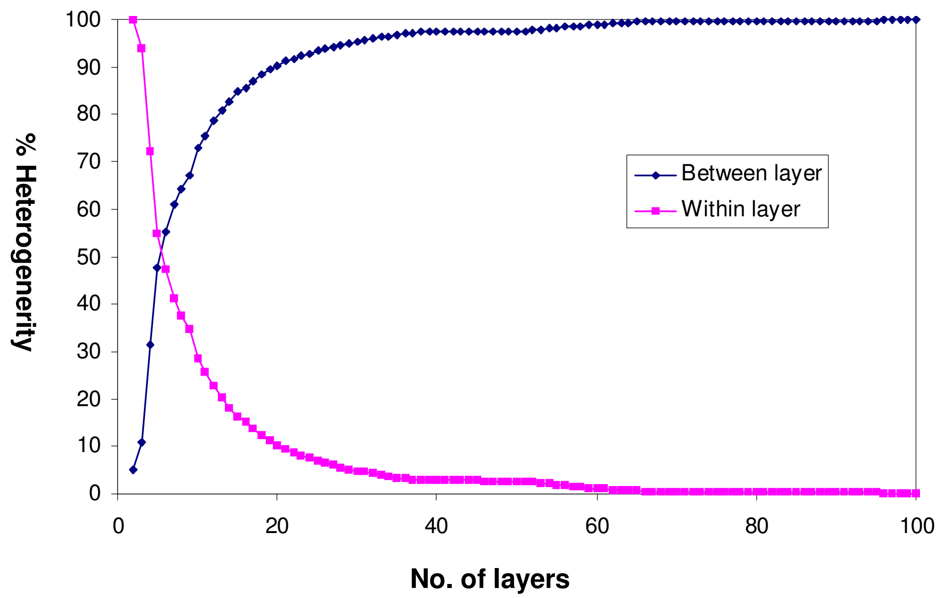

Fig. 5. 2—Between-variation heterogeneity analysis; the heterogeneity has been normalized to 100%.

In **Fig. 5.2** the within cell variation (*W*) shows three distinct heterogeneity regimes: a slow increase for large number of layers, a rapid increase for few layers, and a moderate increase between two. Intuitively, the optimal number of layers should be in the intermediate regime. An algorithm for this will be described later. The major steps of the upgridding approach are as follows:

Step 1: Calculate the values of the property $p_{i,j,k}$ based on permeability, porosity and relative permeability at each grid cell

Step 2: Group two adjacent layers sequentially and calculate the 'within the cell variation (*W*)' to quantify the loss of heterogeneity from the merging

Step 3: Merge those two layers that result in minimal loss in heterogeneity based on the calculations in step 2

Step 4: Repeat steps 2 and 3 and continue merging layers until the model is reduced to a single layer

Step 5: Determine the optimal number of layers from the plot of *W* vs. number of layers

5.2.1 Illustration of the Procedure: A Synthetic Example

We will now illustrate our procedure using a simple example. A 2D channel on a 100x100 cross section is used to demonstrate our approach and compare the results with the uniform coarsening method. To simplify the problem, the property upscaling is performed by arithmetic averaging. The fine scale model is shown in **Fig. 5.3**. In **Fig. 5.4** we have shown the percentage of heterogeneity as quantified by 'between the cell variation (B)' vs. the number of layers. Also superimposed is a curve that shows the optimal number of layers as given by the point of inflection in the 'B' curve. The results show 18 layers as the optimal, which preserves 88% of the heterogeneity. The same results can also be arrived at by using the 'within the cell variation (W)' as outlined in the step-by-step procedure above. **Fig. 5.5** shows the channels described by 18 layers using the optimal upgridding algorithm, and **Fig. 5.6** gives the channels described by 20 layers using a uniform upgridding. Compared to the fine scale, the first channel is clearly smeared and distorted by the uniform upgridding. However, our upgridding method appeared to have preserved the channel geometry. Next, we analyze the layer models using tracer travel time or the time of flight along streamlines (Datta-Gupta and King 2007). An injector is introduced on the left of the cross-section and a producer on the right. The minimum values in time of flight characterize the channels. The inverse time of flight is shown in **Fig. 5.7**. There are two peaks which correspond to the two channels. It is clear that the 18 layer optimal solution is better than the 20 layer solution using uniform upgridding.

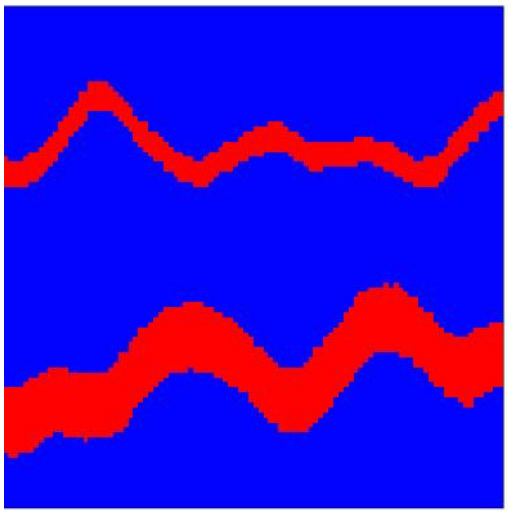

Fig. 5. 3— Fine scale model of 2D channelized reservoir.

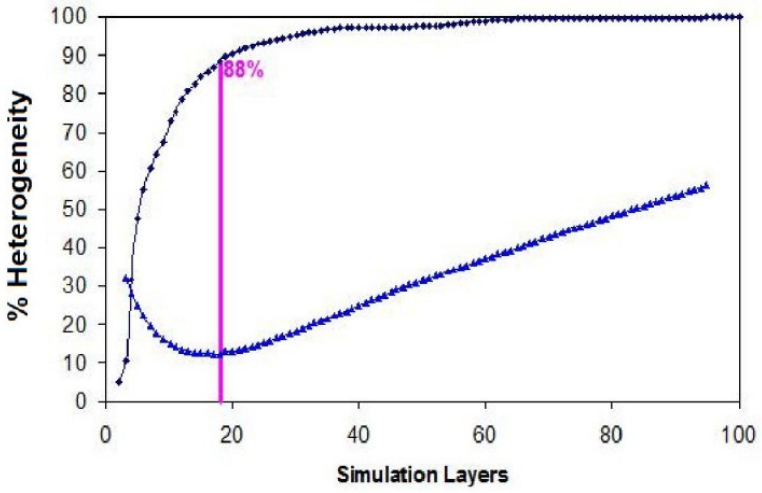

Fig. 5. 4— Between-layer variance and the determination of the optimal layer.

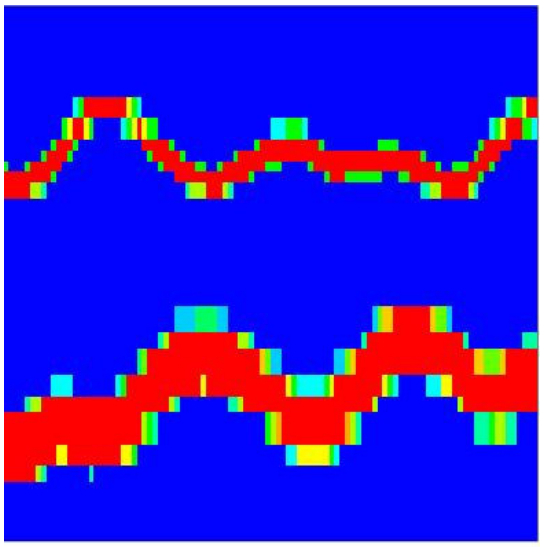

Fig. 5. 5—18-layer optimal model using variance analysis.

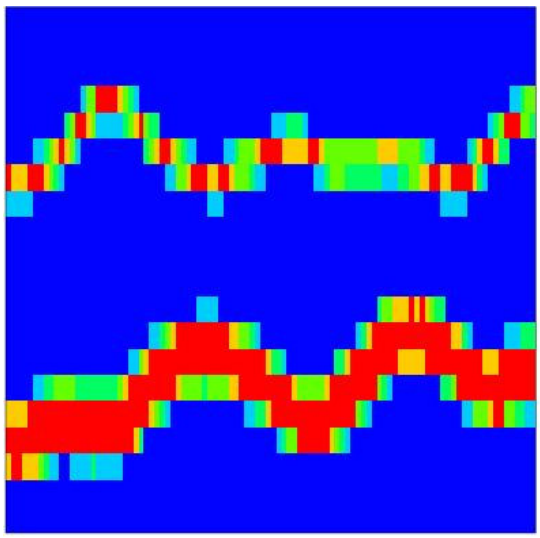

Fig. 5. 6—20-layer model using uniform upgridding.

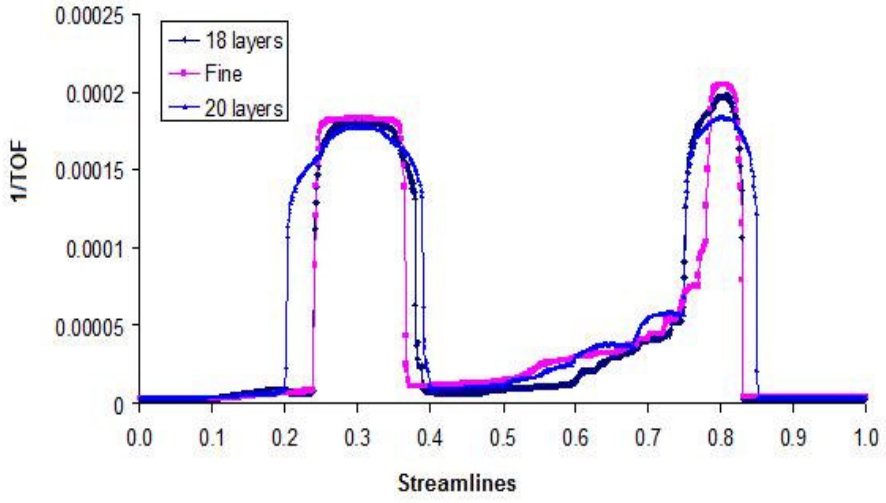

Fig. 5. 7— Distribution of inverse time of flight, showing fine scale (100 layers), the optimal (18 layers) and uniform (20 layers).

5.3 Case Study of 2D Cross-Section

We have used 2D cross-sectional studies for a variety of purposes. It is where we tried different measures of heterogeneity and where we developed the curvature analysis to select the optimal number of layers. 2D also provides a natural validation environment as we can perform more detailed analysis than in the 3D simulator.

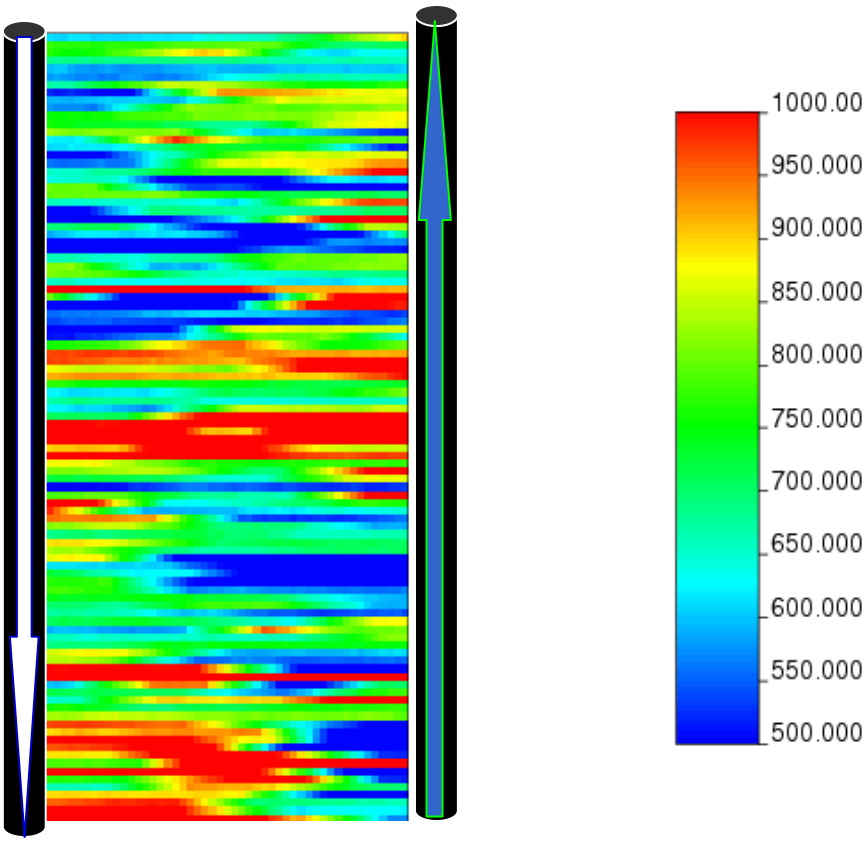

Fig. 5. 8—The heterogeneity has 50x100 2D cross-section generated by sequential Gaussian simulation.

We will exhibit our results on a 50x100 cross-section with permeability developed using Sequential Gaussian Simulation, **Fig. 5.8**. As can be seen in the figure, the lateral correlation length is approximately one half the width of the model and the vertical correlation is a few cells thick. The optimal number of layers is chosen based on the inflection point in 'W' curve. The inflection is determined by analyzing the relationship between the 'within cell variation' and the number of layers as shown in **Fig. 5.1**. Two linear regressions were fit on the two sides of the curve, and then the weighted mean square error of the regressions is calculated by varying the number of points used in the regressions.

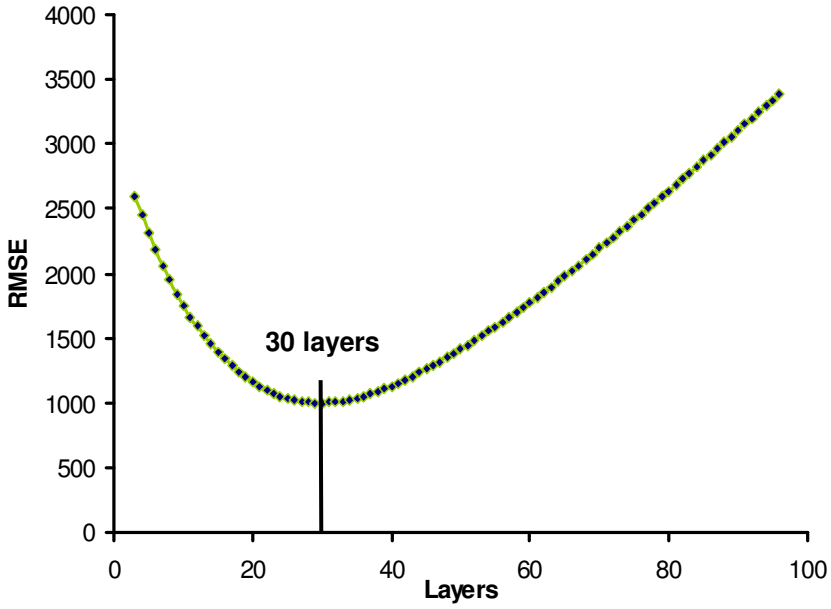

Fig. 5. 9—Regression mean square error analysis.

Fig. 5.9 shows the mean square error and the number layers. The optimal number of layers is the one with the minimal mean square error. In this case, it is 30 layers as the optimal, which preserves *82%* heterogeneity of the fine scale model. This approximately three-fold vertical coarsening is consistent with the correlation length.

As this is a 2D cross-section, it is simple to analyze the results using streamlines (Datta-Gupta and King 2007). 100 lines are introduced from the left boundary of the model and the transit time to the right boundary is calculated for each. The minimum values in time of flight characterize correlated high permeability streaks. The maxima characterize stagnation regions. We display the inverse time of flight, which is the global equivalent of the local velocity error. Results are shown in **Fig. 5.10**. In the first plot, results are contrasted with a higher resolution solution and in the second plot, with lower resolutions. It is clear that the 30 layer solution is excellent. The 20 layer solution is

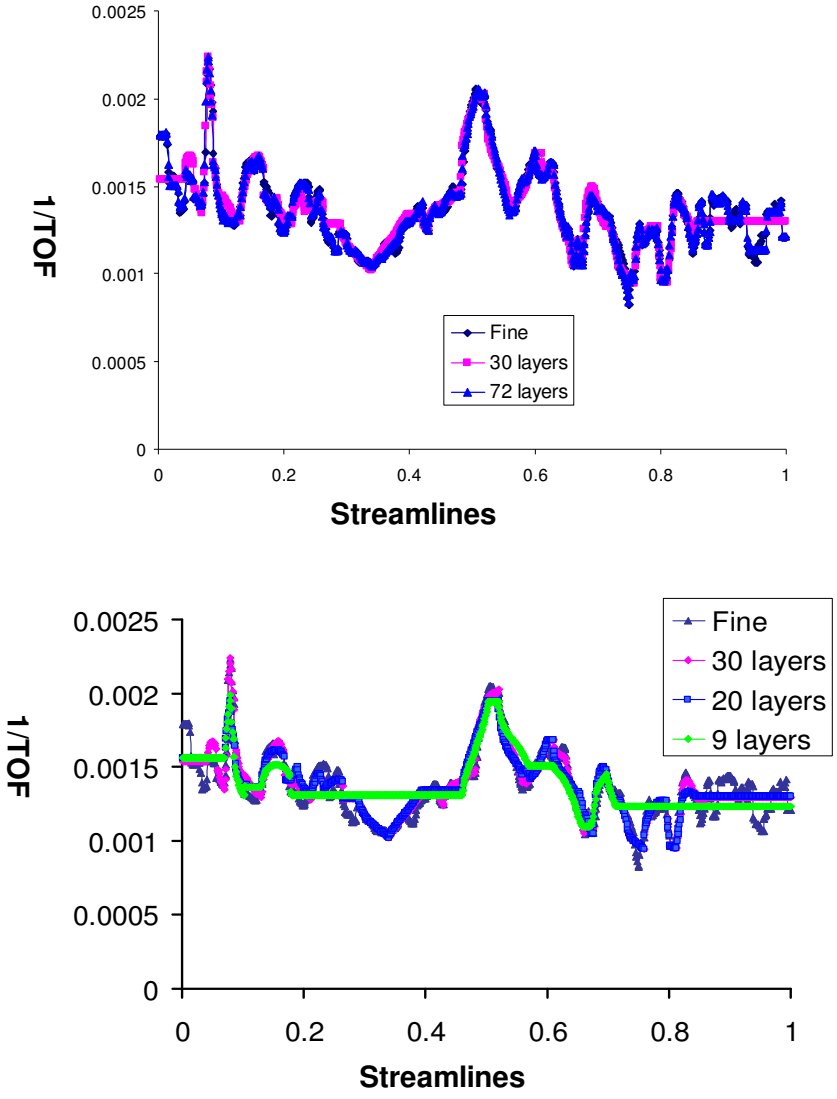

Fig. 5. 10—Distribution of inverse time of flight for 100 streamlines, showing the optimal (30 layers) and fine solutions (100 layers). The first plot further compares the results with a finer 70 layer model. The second includes a 20 layer and a 9 layer model.

fairly good as well. Clearly the 72 layer solution does not need this much resolution and the 9 layer solution is too coarse.

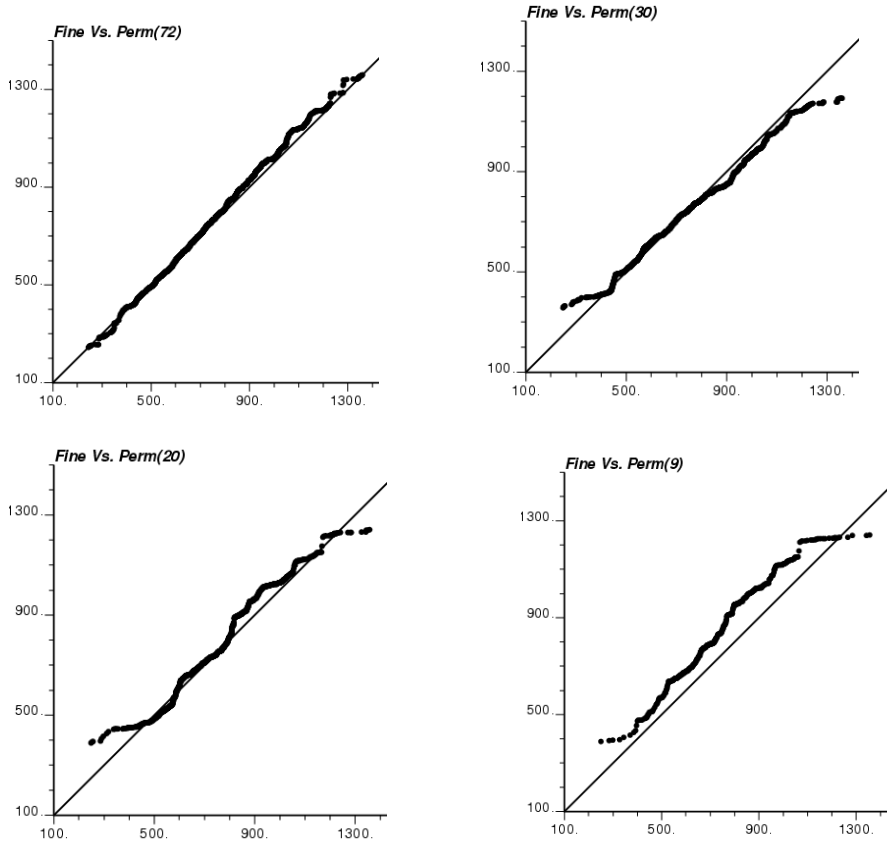

Fig. 5. 11—QQ scatter-plot of averaged versus fine permeability. With the exception of the 72 layer model, all distributions show a loss in the extremes. At 9 layers, a significant bias has also been introduced.

An additional validation is provided with a QQ scatter-plot of the coarsened permeability versus the fine scale permeability, in **Fig. 5.11**. With the exception of the 72 layer model, all distributions show a loss in the extremes. At 9 layers, a significant bias has also been introduced. However, in general, it is hard to ascertain which of these coarse models will perform well, and which will not, using a QQ analysis.

5.4 Case Study of 3D Channelized Reservoir

A South American offshore Eocene reservoir that is composed of sheet and channel sands is used to demonstrate our algorithm (Hohl et al. 2006). The sands are divided into 3 distinctive regions, Sand A, Sand B, and the Main Sand, all with a k_v/k_h ratio of 0.01. The field was initially produced under primary depletion with 2 producers using well productivity and water cut as the tools for monitoring. Eventually the field was converted to a waterflood management through 3 years of field workovers adding 6 producers and 4 injectors. The field has a total 8 producer and 4 injector wells for use in history matching and forecasting in our simulation. The reservoir model was developed as an 81 layer structurally complex and faulted turbiditic oil reservoir with excellent quality sands with high permeability, excellent porosity and distinctive transitions between low and high quality sands (Hohl et al. 2006).

Fig. 5.12 shows the 3D perspective view of the 81 layer model. The channels are visible as higher permeability streaks in the figure. **Fig. 5.13** shows the sand A, sand B, and main sand permeability distribution respectively. It is evident that the reservoir becomes more highly channelized moving down towards the main sand. The Sand A has a fairly smeared permeability distribution and Sand B has a tighter definition of channels in the reservoir. Moving to the main sand we see that there is a highly channelized permeability features in the reservoir.

We have applied the upgridding algorithm to the 81 layer model. **Fig. 5.14** shows the normalized 'within cell variation (W)' as a function of the number of layers. Recall that *W* quantifies the loss of heterogeneity as a result of layer grouping. Clearly, the curve shows a distinct upward trend below about 30 layers. In fact, below 36 layers, the layers across the geologic markers are merged.

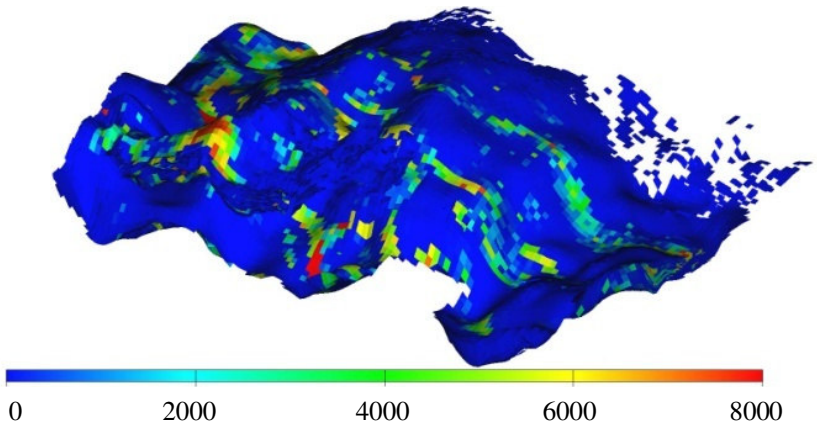

Fig. 5. 12—81 layer, 3D model permeability distribution.

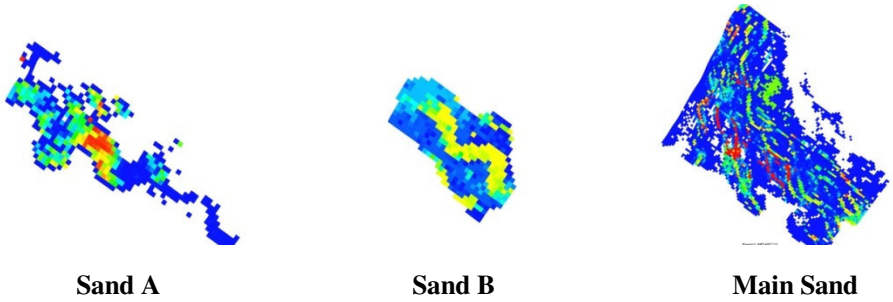

Fig. 5. 13—81 layer model, Sand A shows no channel definition. Sand B shows more channelized reservoir. Main sand shows highly channelized reservoir between pay/non-pay regions.

To avoid this, we chose 36 layers as the optimal in this case. However, if the optimal number of layers is chosen based on the inflection point in '*W*' curve, then we arrive at 26 layers as shown in **Fig. 5.15**, which shows the mean square error and the number layers. The optimal number of layers is the one with the minimal mean square error. In this case, it is 26 layers. However, this violates the geologic markers which can significantly impact the flow response as we will see later. This also underscores the fact the optimal number of layers should be selected based on a combination of geologic insight and the layer statistics rather than purely based on the statistical criterion.

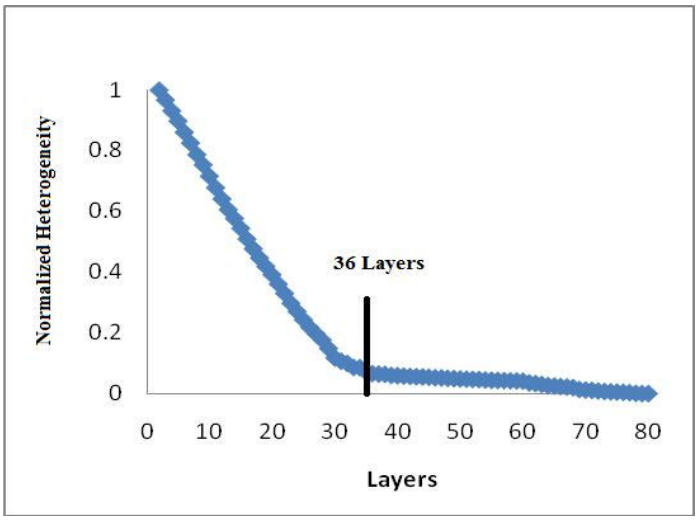

Fig. 5. 14—36 Layers is determined to be the optimal number of layers due to the sharp change in slopes.

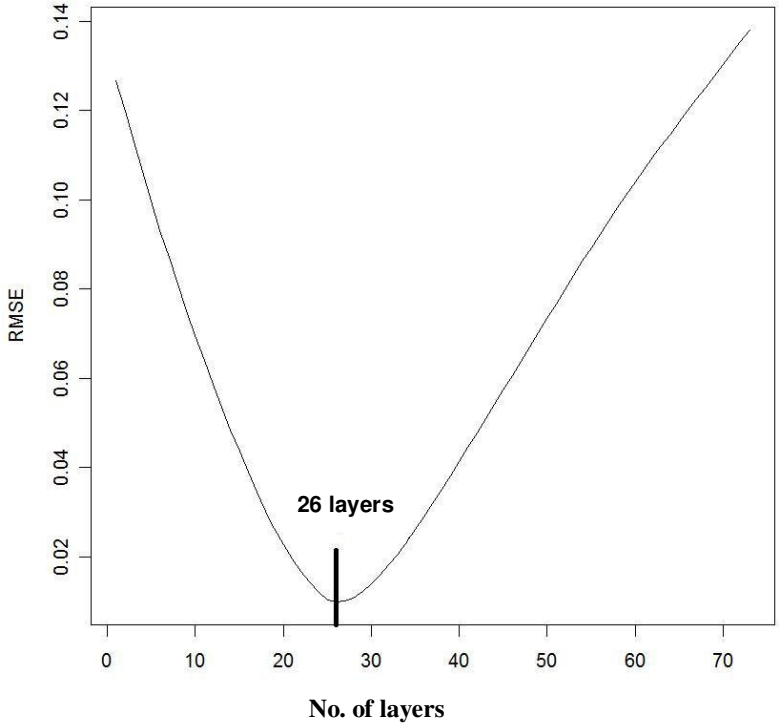

Fig. 5. 15—Regression mean square error analysis is used to determine the minimum number of layers at 26 layers.

Fig. 5.16 shows the 3D perspective view of the 36 layer model. Comparing this 3D view with the original 81 layer model as seen in **Fig. 5.12**, it is evident that the model has maintained the same channel characteristics. The 36 layer model has maintained the local distribution and orientation of the channels as in the original earth model with minimal smearing. As expected the range of property values have been lowered because of averaging. As mentioned before, the optimal number of layers was determined to be 36 layers because this preserves the distinction between Sand A and Sand B. Sand A as seen in **Fig. 5.17** shows a decrease in the permeability values when compared to the 81 layer model. However, the main regions of high permeability have maintained their distinction within the layer. The same conclusion can be drawn for Sand B, shown in **Fig. 5.18,** as the high permeability regions are maintained on the whole. The Main Sand is not altered by the upgridding algorithm and this region with distinct resolution of channels is preserved as in the fine-scale model.

The overall field response in terms of oil production and water-cut as shown in **Fig. 5.19** through **Fig. 5.20** match excellently with minimal deviation from the fine scale model response. We have also included individual well responses for water cut and oil production for a selected number of producers. In these and all subsequent figures, the actual values of the oil production have been suppressed for confidentiality reasons. **Fig. 5.21** through **Fig. 5.23** show the oil production rate and water cut for three wells in our model. These wells were chosen as a representative sample of all producers with significant separation between well locations. Production from all three sands is captured in the analysis of these wells. These plots show that our algorithm maintains individual well response excellently as well as the field wide response.

As mentioned before, an analysis of the 'within the cell variation (W)' curve without regard to the geologic markers will lead to 26 layers as being optimal. The 3-D model with 26 layers as seen in **Fig. 5.24** shows that the reservoir properties have been significantly smeared compared to the original distribution as channels have been removed from the model. The choice of 26 layers results in the loss of the facies distinction between all sands from layer 1 to layer 56 in the fine-scale model. This

merges all of Sand A and Sand B and the top 4 layers of the Main Sand. The reservoir response is also altered because the reservoir properties are smeared and lowered below their appropriate values as layers are merged across geologic boundaries. **Fig. 5.25**, Sand A, and **Fig. 5.26**, Sand B, show the merging of these sand bodies causing a severe lowering of the reservoir properties and loss of channels. The Main Sand, shown in **Fig. 5.27**, compares the permeability of the 81 layer and 26 layer models. This comparison shows a major loss of geologic resolution when merging across sand body markers.

Fig. 5.28 through **Fig. 30** show the reservoir response of the fine scale model compared to the 26 layer model on an individual well basis. The same individual wells are used for comparison as were used in the 36 layer model. It is evident that the reservoir properties are altered significantly causing a significant deviation in water cut and therefore a deviation in oil production rate as seen in all the individual well plots. The field wide response as expected from the individual well analysis is significantly deviated from the fine scale model.

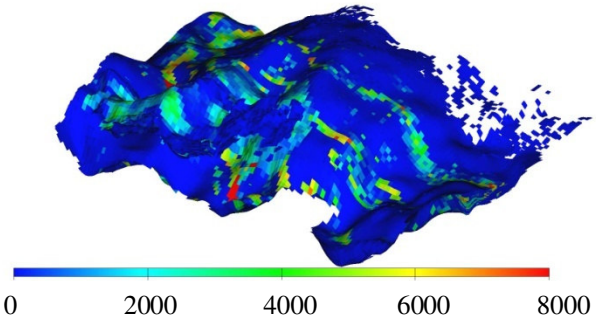

Fig. 5. 16—36 layer, 3D model permeability distribution.

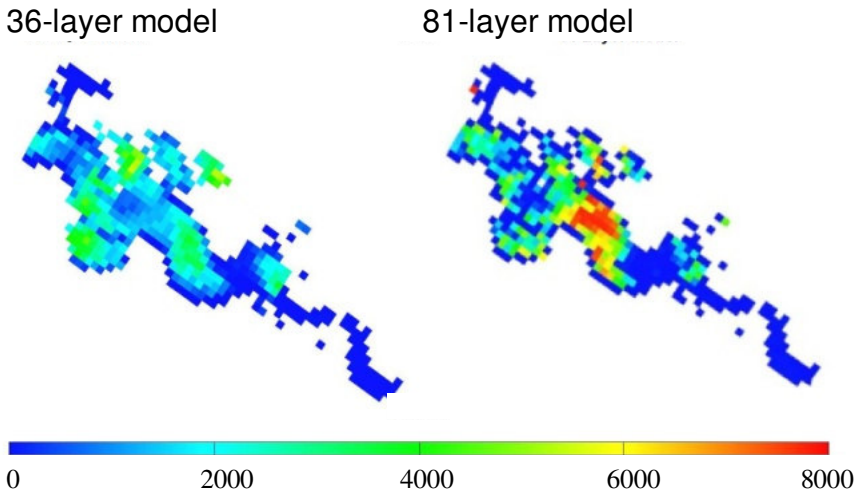

Fig. 5. 17—36 layer model Sand A comparison of permeability distribution shows homogenization of the previous smeared distribution in 81 layer model.

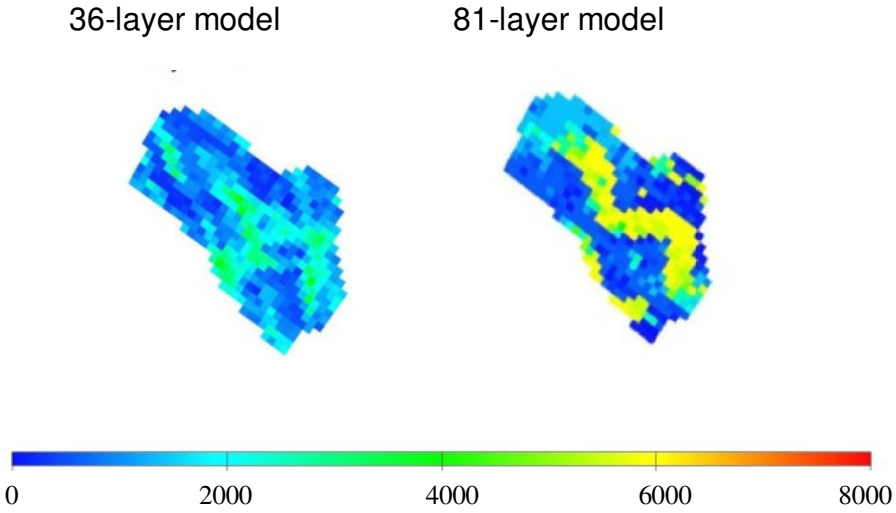

Fig. 5. 18—36 layer model Sand B permeability distribution shows that the channels are being smeared but the regions maintain a high permeability to maintain the pay/non-pay distinction.

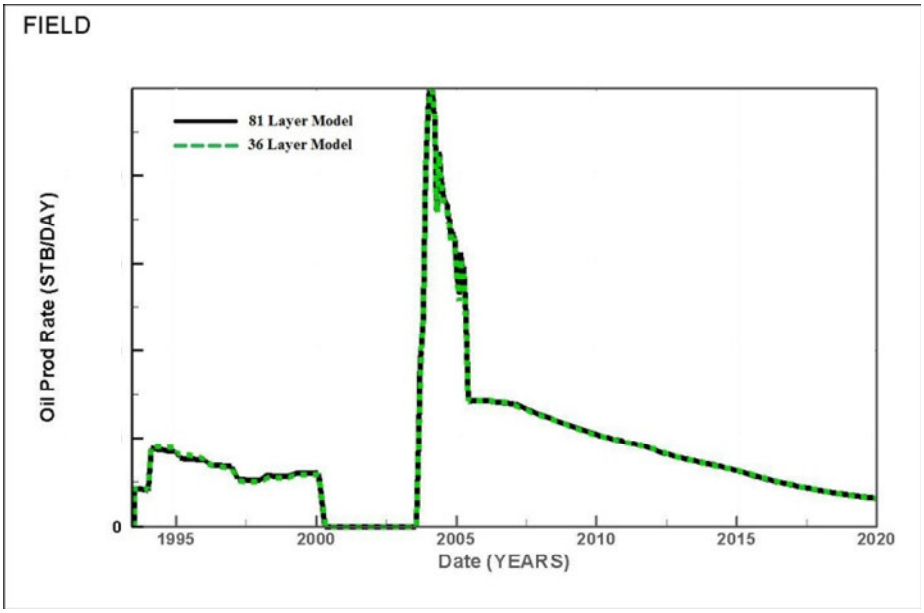

Fig. 5. 19—The field oil production rate is almost identical for both the 36 layer model and the fine 81 layer model.

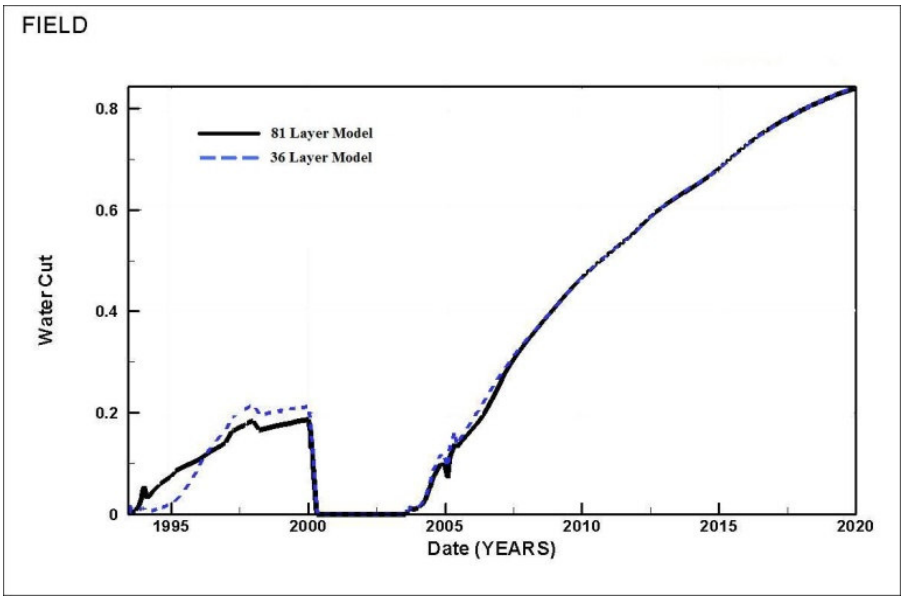

Fig. 5. 20—The water-cut matches in forecasting for both the fine and 36 layer model.

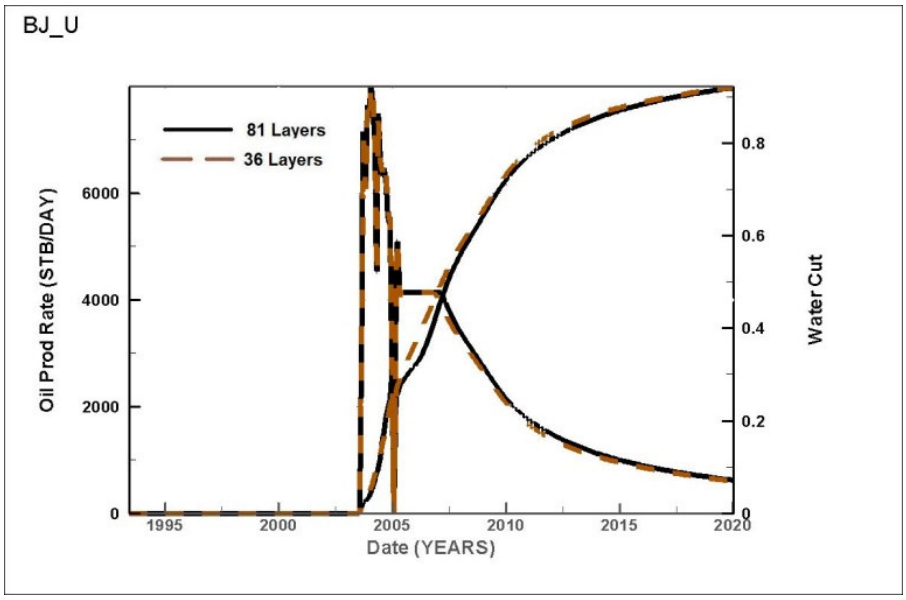

Fig. 5. 21—The oil production rate and wate cut are closely matached for the BJ-U producer.

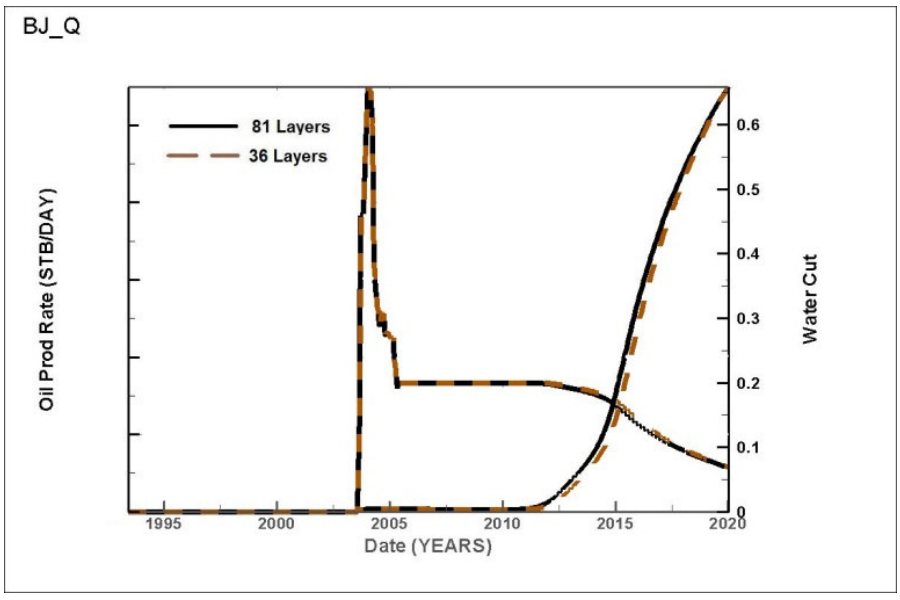

Fig. 5. 22—The oil production rate and water cut are closely matched for the BJ_Q producer.

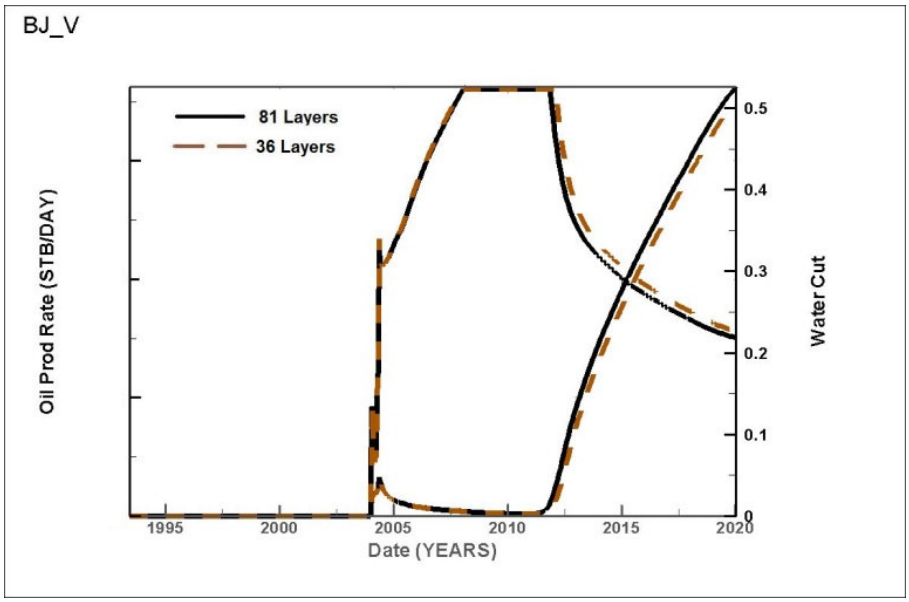

Fig. 5. 23—The oil production rate and water cut are closely matched for the BJ_V producer.

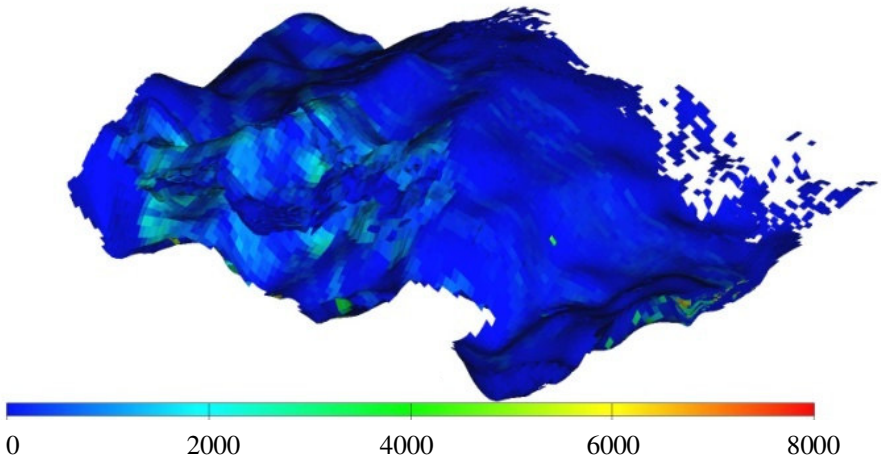

Fig. 5. 24—26 layer 3D model permeability distribution.

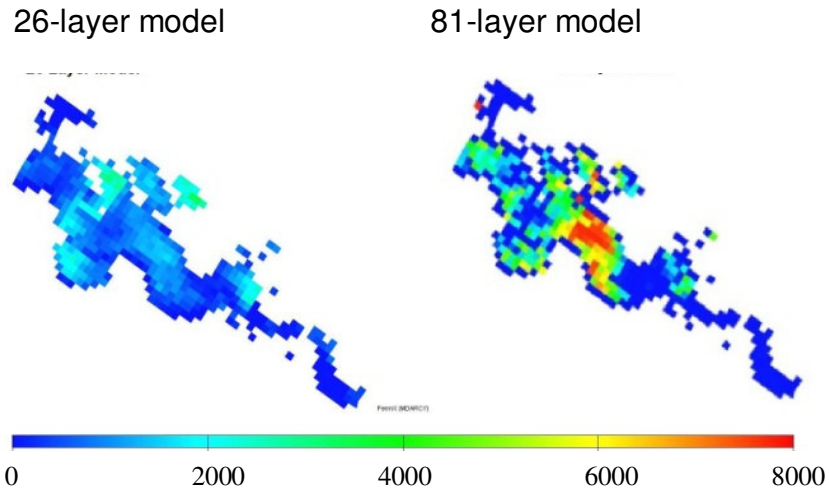

Fig. 5. 25—26 layer model Sand A permeability distribution shows a homogenization of the smeared distribution shown the 81 layer model.

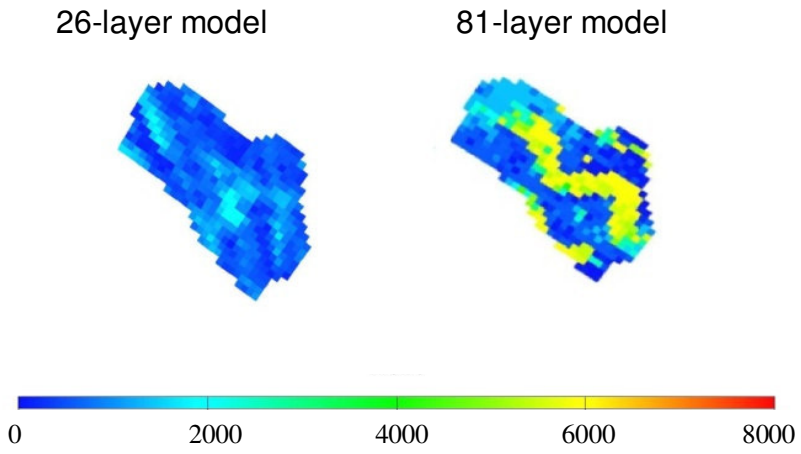

Fig. 5. 26—26 layer model Sand B permeability distribution shows a greater removal of channel definition as compared to the 36 layer model.

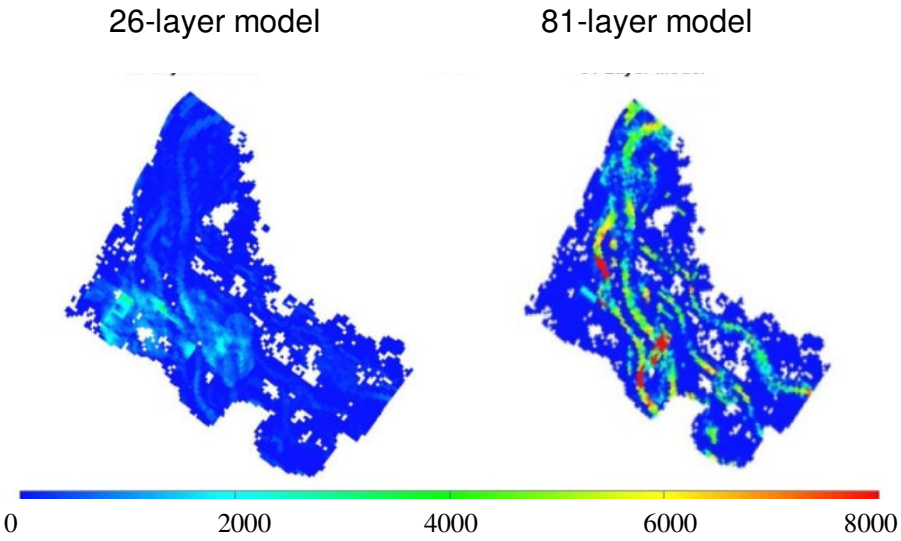

Fig. 5. 27—81 layer model Main Sand permeability distribution shows distinct channels since the upgridding has not entered this zone however, the 26 layer model shows major loss of geologic realism.

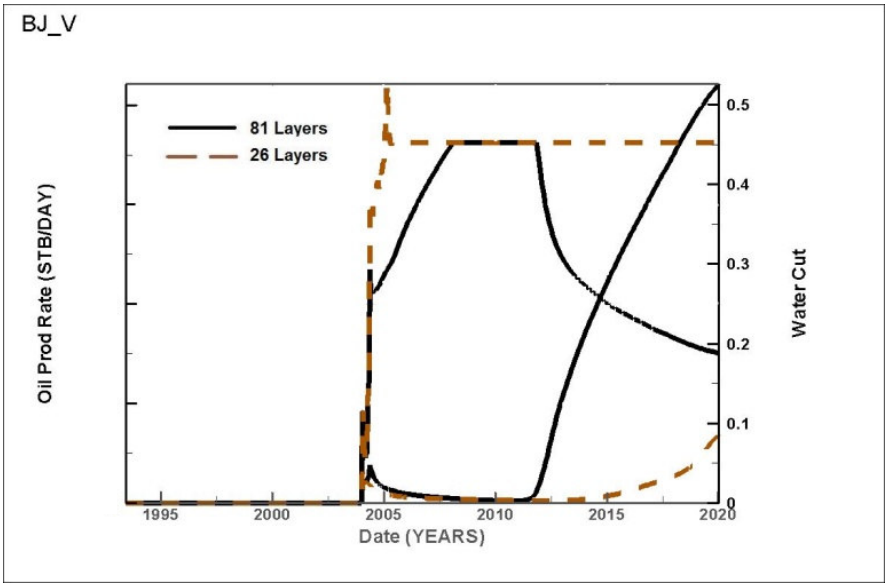

Fig. 5. 28—The oil production rate and water cut for the 26 layer model are severely deviated when compared to the fine scale model.

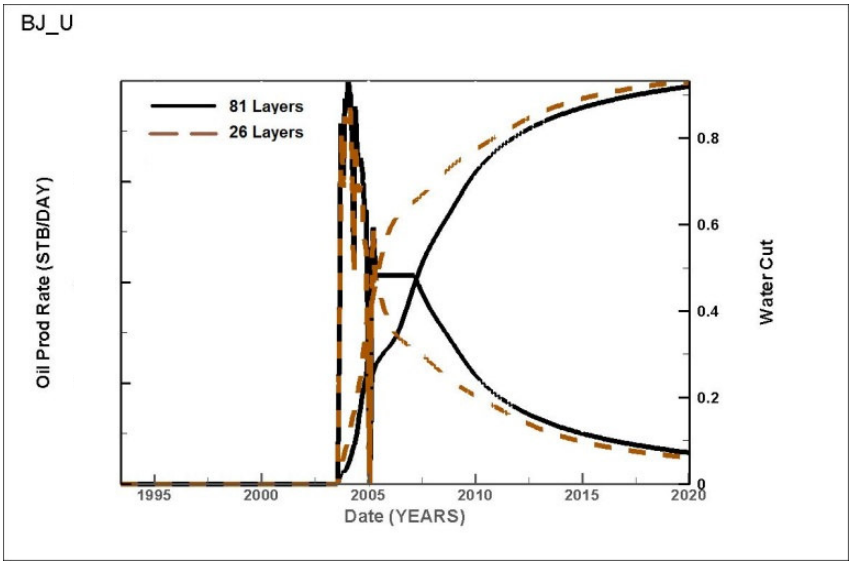

Fig. 5. 29—The oil production rate and water cut for the 26 layer model deviates at approximately 2003 with the water cut significantly higher than the fine scale model causing under production of oil.

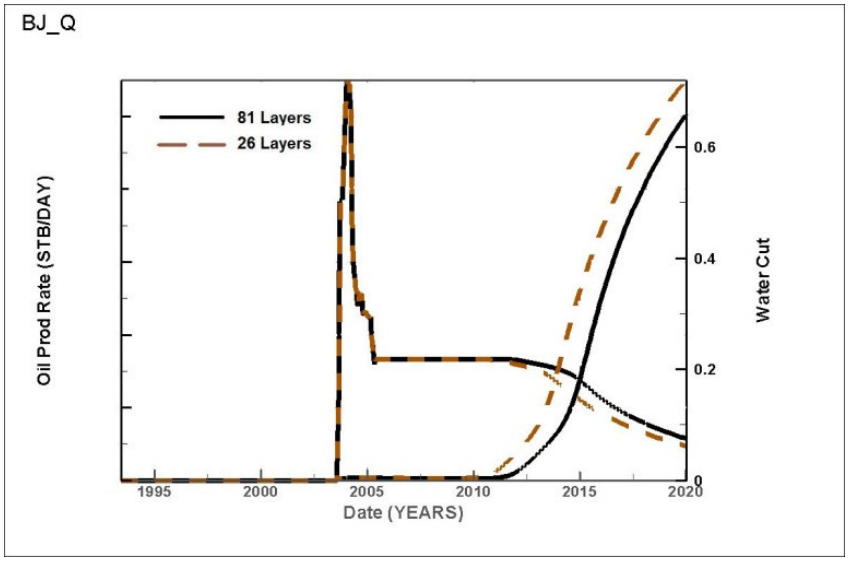

Fig. 5. 30—The water cut in the 26 layer model is higher than the fine scale model starting around 2005 causing a deviation in the oil production rate and lowering the wells response.

CHAPTER VI

CONCLUSIONS AND RECOMMENDATIONS

In this work, we have formulated several two-stage MCMC methods by modifying the instrumental probability distribution that achieves a high acceptance rate while preserving the robustness of the traditional MCMC algorithm. Our proposed method leads to a significant reduction in computation time. Three surrogate models are proposed to approximate the likelihood in the Metropolis-Hastings algorithm. This is then followed by exact likelihood calculations for selected proposals with high potential for acceptance. The power and utility of these techniques have been demonstrated using synthetic and field applications.

6.1 Conclusions

Some specific conclusions can be made from this work:

1. We have formulated a two-stage MCMC using streamline-derived sensitivity. In the first stage, we compute the acceptance probability for a proposed change in reservoir parameters based on a fast linearized approximation to flow simulation in a small neighborhood of the previously computed dynamic data. The method requires a single simulation run to obtain both reservoir response and reservoir parameter sensitivities which substantially reduce the computational cost involved.
2. We have formulated a two-stage MCMC using response surface models. In the first stage, the response surfaces as surrogate models take the place of expensive multiphase flow simulations. The two-stage MCMC formulation allows us to history match three-phase flow match simultaneously and sensitivities are not required. Kriging and Bayesian partition modeling have been applied in the first stage for modeling the response surface.

3. We have formulated a two-stage MCMC using upscaling and nonparametric regression. The proposed method combines coarse- and fine-scale information to improve the efficiency of MCMC methods, and employs offline computations for modeling the relationship between coarse- and fine-scale error responses. The method does not rely on the proximity of approximate and resolved models and can employ much coarser and inexpensive models to guide the fine-scale simulations.
4. Either streamline or finite difference simulators can be used in our work flow which makes the method applicable to existing risk analysis workflows with minor modifications.
5. Since the methods perform an exact likelihood calculation for all proposals accepted by the approximate likelihood step using the same acceptance probability level, the method does not compromise the rigorousness in sampling in the traditional MCMC method.
6. The efficiency of our proposed methods has been demonstrated using both 2-D and 3-D examples with realistic field conditions. The method maintained high acceptance and convergence rates when compared with the full MCMC method which translates into substantial cost savings for high resolution models.
7. We have developed a new approach to the optimal coarsening of 3D reservoir models for flow simulation. The optimization maximally preserves a statistical measure of the heterogeneity of a fine scale model. Constraints arise from the reservoir fluids, well locations, pay/non-pay juxtaposition, and large scale reservoir structure and stratigraphy. We have demonstrated a statistical analysis for layer coarsening based on static properties of a geologic model which predicts the optimal reservoir simulation layering scheme. This method uses a recursive sequential coarsening algorithm which is both more informative of reservoir heterogeneity and faster than previous static analyses.

6.2 Recommendations

Within the Bayesian Framework, uncertainty assessment is typically carried out based on the posterior distribution obtained from Bayes' theorem. Often, the production data arrive sequentially in time and we are interested in performing history matching and uncertainty quantification on a near real-time. Therefore, it is necessary to update the posterior distribution as production data become available. We would like extend the current two-stage MCMC methods to update reservoir models sequentially. Sequential Monte Carlo (SMC) methods such as particle filters are a set of flexible simulation-based methods for sampling from a sequence of probability distributions (Doucet et al. 2001). It is worth combining SMC into two-stage MCMC methods.

Two-stage MCMC methods have been applied to reservoir models simulated by two-point statistics. It is necessary to extend the two-stage MCMC method to channelized and non-stationary permeability distributions, for example reservoirs are generated by multi-point statistics (Caers 2003).

The gradual deformation method and KLE expansion can honor two-point statistics of geological models since we update the models globally. Our experience with history matching indicates that local update is more efficient in obtaining a better overall match and achieving faster convergence. It is necessary to develop a local parameterization method for this purpose.

NOMENCLATURE

B = between variance

BHP = bottom hole pressure

C = covariance matrix

C_D = data error covariance

C_k = prior model parameter covariance

d = data vector

d_{obs} = observed response

f_w = fractional flow of water

f' = Buckley-Leverett speed

I = number of realizations

J = iterations

g = reservoir simulator

G = sensitivity matrix

GOR = production gas/oil ratio

k = permeability vector

k_{prior} = prior permeability vector

m = number of chains

n = samples

$n_{i,j,k}$ = bulk rock volume

NX = number of cells in x axis

NY = number of cells in y axis

NZ = number of cells in z axis

P = probability distribution

p = defined reservoir property

q = proposal distribution

R = region

R_s = solution gas/oil ratio

S = location vector

s = entropy

t = time

Var = variance

W = within variance

ε = random variable

λ = eigenvalues

δ = difference

σ = variance

∇ = gradient

ρ = acceptance probability

π = stationary probability distribution

τ = time-like parameter

θ = random variable

$\Delta\tau$ = time difference

ϕ = porosity

ϕ_k = eigenvector

REFERENCES

Agarwal, B., and Blunt, M., 2004, A Streamline-based Method for Assisted History Matching Applied to an Arabian Gulf Field. *SPE Journal* **9** (4): 437–449.

Armstrong, M., Galli, G.A., Le Loc'h, G., Geffroy, F., and Eschard, R. 2003. *Plurigaussian Simulations in Geosciences*. Berlin: Springer-Verlag.

Aziz, K. and Settari, A. 1979. *Petroleum Reservoir Simulation*. London: Elsevier.

Bissel, R.C., Killough, J.E., and Sharma, Y. 1992. Reservoir History Matching Using the Method of Gradients. Paper SPE 24265 presented at the SPE European Petroleum Computer Conference, Stavanger, 25–27 May.

Brigham, J. and Aquino, W. 2007. Surrogate-Model Accelerated Random Search Algorithm for Global Optimization with Application to Inverse Material Identification. *Comput. Methods Appl. Mech. Engrg* **196** (2): 4561–4576.

Brooks, S. and Gelman, A. 1998. General Methods for Monitoring Convergence of Iterative Simulations. *Journal of Computational and Graphical Statistics* **7** (4): 434-455.

Caers, J. 2003. Geostatistical History Matching Under Training-Image Based Geostatistical Model Constraints. *SPE Journal* **8** (3): 218–226.

Caers, J., Krishnan, S., Wang, Y., and Kovscek, A., 2002, A Geostatistical Approach to Streamline-based History Matching. *SPE Journal* **7** (3): 250–266.

Cheng, H., Oyerinde, D., Datta-Gupta, A., and Milliken, W. 2007. Compressible Streamlines and Three-phase History Matching. *SPE Journal* **12** (4): 475–485.

Christen, J.A. and Fox, C. 2005. MCMC Using an Approximation. *Journal of Computational and Graphical Statistics* **14** (4): 795–810.

Christie, M., MacBeth, C., and Subbey, S. 2002. Multiple History-matched Models for Teal South. *The Leading Edge* **21** (3): 286–289.

Datta-Gupta, A., Yoon, S.S., Nordaas, K., and Vasco, D.W. 2001. Streamlines, Ray Tracing and Production Tomography: Generalization to Compressible Flow. *Petroleum Geoscience* **7** (S): 75–86.

Datta-Gupta, A., King, M.J. 2007. *Streamline Simulation: Theory and Practice*. Houston: SPE.

Denison, D., Holmes, C., Mallick, B. and Smith, A. 2002. *Bayesian Methods for Nonlinear Classification and Regression*. New York: Wiley.

Deutsch, C.V. and Journel, A.G. 1998. *GSLIB: Geostatistical Software Library and User's Guide*. New York: Oxford.

Dostert, P. 2007. *Uncertainty Quantification Using Multiscale Methods and Stochastic Finite Element Methods for Porous Media Flows*. PhD dissertation Texas A&M University.

Doucet, A., Freitas, N., and Gordon, N. 2001. *Sequential Monte Carlo Methods in Practice*. New York: Springer-Verlag.

Durlofsky, L.J., Behrens, R.A., Jones, R.C., and Bernath, A. 1996. Scale Up of Heterogeneous Three Dimensional Reservoir Descriptions. *SPE Journal* **1** (3): 313–326.

Efendiev, Y., Durlofsky, L.J., and Lee, S.H. 2000. Modeling of Subgrid Effects in Coarse-scale Simulations of Transport in Heterogeneous Porous Media. *Water Resources Research* **36** (8): 2031–2041, August.

Efendiev, Y., Datta-Gupta, A., Ginting, V., Ma, X., and Mallick, B. 2005. An Efficient Two-Stage Markov Chain Monte Carlo Method for Dynamic Data Integration. *Water Resources Research* **41** W12423. DOI: 10.1029/2004WR003764.

Efendiev, Y., Datta-Gupta, A., Ma X., and Mallick, B. 2008. Modified MCMC for Dynamic Data Integration Using Streamline Models. *Mathematical Geology*. In press.

Efendiev, Y., Datt-Gupta, A., Ma, X., and Mallick, B. 2008. Efficient Sampling Techniques for Uncertainty Quantification in History Matching Using Nonlinear Error Models and Ensemble Level Upscaling. Submitted to *Water Resources Research*.

Emery, X. 2007. Simulation of Geological Domains Using the Plurigaussian Model: New Developments and Computer Programs. *Computer & Geosciences* **33** (9): 1189–1201.

Fincham, A., Christensen, J., Barker, J., and P. Samier, P. 2004. Up-Gridding from Geological Model to Simulation Model: Review, Applications and Limitations. Paper SPE 90921 presented at Annual Technical Conference and Exhibition, Houston, 26–29 September.

Gelman, A. and Rubin, D. 1992. Inference from Iterative Simulation Using Multiple Sequences. *Statistical Science* **7** (4): 457–511.

Geweke, J. 1992. Evaluating the Accuracy of Sampling-Based Approaches to the Calculation of Posterior Moments. *Bayesian Statistics*. **4** (2): 169–193.

Gu, Y. and Oliver, D. S. 2004. History Matching of the PUNQ-S3 Reservoir Model Using the Ensemble Kalman Filter. Paper SPE 89942 presented at the Annual Technical Conference and Exhibition, Houston, 26–29 September.

Hastings, W. 1970. Monte Carlo Sampling Methods Using Markov Chains and Their Applications. *Biometrika* **57** (1): 97–109.

He, Z., Datta-Gupta, A., and Yoon, S. 2002. Streamline-Based Production Data Integration with Gravity and Changing Field Conditions," *SPE Journal* **7** (4): 423–436.

Hohl, D., Jimenez, E.A., and Datta-Gupta, A. 2006. Field Experiences with History Matching an Offshore Turbiditic Reservoir Using Inverse Modeling. Paper SPE 101983 presented at Annual Technical Conference and Exhibition, San Antonio, 24-27 September.

Hu, L.Y. 2000. Gradual Deformation and Iterative Calibration of Gaussian-Related Stochastic Models. *Mathematical Geology* **32** (1): 87–108.

Jafarpour, B. and McLaughlin, D. 2007. Efficient Permeability Parameterization with the Discrete Cosine Transform. Paper SPE 106453 presented at SPE Reservoir Simulation Symposium, Houston, 26-29 February.

Jones, D., Schonlau, M. and Welch, W. 1998. Efficient Global Optimization of Expensive Black-Box Functions. *Journal of Global Optimization* **13** (4): 455-492.

Killough, J.E. 1995. Ninth SPE Comparative Solution Project: A Reexamination of Black-Oil Simulation. Paper SPE 29110 presented at the 13th SPE Symposium on Reservoir Simulation held in San Antonio, TX, 12-15 February.

King, M., Burn, K., Wang, P., Muralidharan, V., Alvarado, F., Ma, X., and Datta-Gupta, A. 2006. Optimal Coarsening of 3D Reservoir Models for Flow Simulation. *SPE Reservoir Evaluation & Engineering* **24** (10): 317-334.

Kitanidis, P.K. 1995. Quasi-Linear Geostatistical Theory for Inversing. *Water Resource Research* **31** (10): 2411–2420.

Lepine, O.J., et al. 1999. Uncertainty Analysis in Predicative Reservoir Simulation Using Gradient Information. *SPE Journal* **4** (3): 251-259.

Li, D. and Beckner, B. 2000. Optimal Uplayering for Scaleup of Multimillion-Cell Geologic Models. Paper SPE 62927 presented at Annual Technical Conference and Exhibition, Dallas, 1-4 October.

Li, D., Cullick A. and Lake, L. 1995. Global Scale-Up of Reservoir Model Permeability with Local Grid Refinement. *Journal of Petroleum Science and Engineering* **14** (1): 1-13.

Liu, N., Betancourt, S., and Oliver, D.S. 2001. Assessment of Uncertainty Assessment Methods. Paper SPE 71624 presented at the 2001 SPE Annual Technical Conference and Exhibition, New Orleans, 30 September-3 October.

Loeve, M. 1977. *Probability Theory*. Fourth edition, Berlin: Springer-Verlag.

Lophaven, S., Nielsen, H., and Søndergaard, J. 2002. DACE: A Matlab Kriging Toolbox, Version 2.0, Technical Report IMM-REP-2002-12, Informatics and Mathematical Modelling, Technical University of Denmark, Lyngby, Denmark.

Ma, X., Al-Harbi, M., Datta-Gupta, A., and Efendiev, Y. 2008. An Efficient Two-Stage Sampling Method for Uncertainty Quantification in History Matching Geological Models. *SPE Journal* **13** (1): 77-87.

Ma, X. and Journel, A. 1999. An Expanded GSLIB Cokriging Program Allowing for Two Markov Models. *Computer & Geoscience* **25** (6) 627-639.

MacKay, M., Beckman, R., and Conover, W. 1979. A Comparison of Three Methods for Selecting Values of Input Variables in the Analysis of Output from a Computer Code. *Technometrics* **21** (2): 239–245.

Maucec, M., Douma, S., Hohl, D., Leguijt, J., Jimenez, E., and Datta-Gupta, A. 2007. Streamline-Based History Matching and Uncertainty: Markov-chain Monte Carlo Study of an Offshore Turbidite Oil Field. Paper SPE 109943 presented at the Annual Technical Conference and Exhibition, Anaheim, 11-14 November.

Metropolis, N., Rosenbluth, M., Rosenbluth, A., Teller, A. and Teller, E. 1953. Equation of State Calculations by Fast Computer Machines. *Journal of Chemical Physics* **21** (6): 1087-1092

Montgomery, D. 2000. *Design and Analysis of Experiments*. New York: Wiley.

Nævdal, G. 2003. Reservoir Monitoring and Continuous Model Updating Using Ensemble Kalman Filter. Paper SPE 84372 presented at the Annual Technical Conference and Exhibition, Denver, 8-5 October.

Oliver, D.S., Cunha, L.B., and Reynolds, A.C. 1997. Markov Chain Monte Carlo Methods for Conditioning a Permeability Field to Pressure Data. *Mathematical Geology* **29** (1): 61–91.

Oliver, D.S., He, N., and Reynolds, A.C. 1996. Conditioning Permeability Fields to Pressure Data. 5th European Conference on the Mathematics of Oil Recovery, Leoben, Austria, 3–6 September.

Oliver, D.S., Reynolds, A.C., Bi, Z., and Abacioglu, Y. 2001. Integration of Production Data into Reservoir Models. *Petroleum Geoscience* **7** (S): 65-73.

Raftery, A. and Lewis, S. 1992. How Many Iterations in the Gibbs Sampler? *Bayesian Statistics*. **4** (2): 763-773.

Robert, C. and Casella, G. 1999. *Monte Carlo Statistical Methods*. New York: Springer-Verlag.

Sacks, J., Welch, W., Mitchell, T., and Wynn, H. 1989. Design and Analysis of Computer Experiments. *Statistical Science* **4** (4): 409-435.

Sambridge, M. 1999. Geophysical Inversion with a Neighborhood Algorithm-I. Searching a Parameter Space. *Geophysical Journal International* **138** (2): 479–494.

Sen, M.K. Gupta, A.D., Stoffa, P. L., Lake, L. W., and Pope, G.A. 1992. Stochastic Reservoir Modeling Using Simulated Annealing and Genetic Algorithm. *SPE Formation Evaluation* **10** (1): 49-56.

Smith, J. 2007. Boa: An R Package for MCMC Output Convergence Assessment and Posterior Interference. *Journal of Statistics Software* **21** (11): 1-37

Sobester, A., Leary, S., and Keane, A. 2005. On the Design of Optimization Strategies Based on Global Response Surface Approximation Models. *Journal of Global Optimization* **33** (1): 31-59.

Stern, D. and Dawson A. 1999. A Technique for Generating Reservoir Simulation Grids to Preserve Geologic Heterogeneity. Paper SPE 51942 presented at Reservoir Simulation Symposium, Houston, 14-17 February.

Stone, H.L. 1973. Estimation of Three-Phase Relative Permeability and Residual Oil Data. *Journal of Petroleum Technology* **12** (3): 53-61.

Tarantola, A. 1987. *Inverse Problem Theory: Methods for Data Fitting and Model Parameter Estimation*. New York: Elsevier.

Testerman, J.D. 1962. A Statistical Reservoir-Zonation Technique. *Journal of Petroleum Technology* **14** (8): 889-893.

Vasco, D.W., Yoon, S., and Datta-Gupta, A. 1999. Integrating Dynamic Data into High-Resolution Reservoir Models Using Streamline-Based Analytic Sensitivity Coefficients. *SPE Journal* **4** (4): 389-399.

Wu, X., Efendiev, Y., and Hou T. 2002. Analysis of Upscaling Absolute Permeability. *Discreet and Continuous Dynamical Systems Series B* **2** (3): 185-204.

Wu, Z. and Datta-Gupta, A. 2002. Rapid History Matching Using a Generalized Travel Time Inversion Method. *SPE Journal* 7 (2): 113-122.

Yoon, S., Malallah, A., Datta-Gupta, A. and Vasco, D. 2001. A Multiscale Approach to Production Data Integration Using Streamline Models. *SPE Journal* **6** (2): 182-192.

APPENDIX A

CONVERGENCE OF MODIFIED MARKOV CHAIN

First we note that there is no need to compute the modified proposal distribution $Q(k_n \mid k)$ and $Q(k \mid k_n)$ separately in (2.17). The acceptance probability (2.17) can be simplified as

$$\rho(k_n, k) = \min\left(1, \frac{\pi(k)\pi^*(k_n)}{\pi(k_n)\pi^*(k)}\right). \quad \text{.....(A.1)}$$

For simplicity, we demonstrate this for a discrete chain. Let k_n and k be ith and jth states of Markov chain. We will consider the case $i \neq j$. The case $i = j$ can be derived easily. The transition probability of Markov chain after the first stage of MCMC is given by

$$Q_{ij} = a_{ij} q_{ij}. \quad \text{……..……..(A.2)}$$

Then

$$\rho_{ij} = \min(1, \frac{\pi_j Q_{ji}}{\pi_i Q_{ij}}) = \min(1, \frac{\pi_j a_{ji}}{\pi_i a_{ij}}). \quad \text{……..(A.3)}$$

Assume for simplicity $\pi_j^* q_{ji} > \pi_i^* q_{ij}$. Then $a_{ij} = 1$ and $a_{ji} = \frac{\pi_i^* q_{ij}}{\pi_j^* q_{ji}}$. Using these relationships for a_{ij} and a_{ji}, we obtain

$$\rho_{ij} = \min(1, \frac{\pi_j \pi_i^*}{\pi_i \pi_j^*}). \quad \text{.....(A.4)}$$

If $\pi_j^* q_{ji} <= \pi_i^* q_{ij}$, then $a_{ji} = 1$ and $a_{ij} = \frac{\pi_j^* q_{ji}}{\pi_i^* q_{ij}}$. With these values of a_{ij} and a_{ji}, we get

$$\rho_{ij} = \min(1, \frac{\pi_j \pi_i^*}{\pi_i \pi_j^*}). \quad \text{.....(A.5)}$$

Next, we show that the detailed balance condition is satisfied. Again, we will demonstrate this for the discrete chain for simplicity. Denote by K_{ij} the transition matrix of modified MCMC. Then, it is given by

$$K_{ij} = \rho_{ij} Q_{ij}, \quad \text{.....(A.6)}$$

where $Q_{ij} = a_{ij} q_{ij}$, if $i \neq j$. If $i = j$, then $K_{ii} = 1 - \sum_{j \neq i} K_{ij}$. We need to show that

$$K_{ij} \pi_i = K_{ji} \pi_j. \quad \text{.....(A.7)}$$

This trivially holds for $i = j$. For $i \neq j$, we need to show that

$$\rho_{ij} Q_{ij} \pi_i = \rho_{ji} Q_{ji} \pi_j. \quad \text{.....(A.8)}$$

Taking into account the form for Q_{ij} and ρ_{ij}, (Eq. A.8) becomes

$$\min(1, \frac{\pi_j \pi_i^*}{\pi_i \pi_j^*}) \min(1, \frac{\pi_j^* q_{ji}}{\pi_i^* q_{ij}}) q_{ij} \pi_i = \min(1, \frac{\pi_i \pi_j^*}{\pi_j \pi_i^*}) \min(1, \frac{\pi_i^* q_{ij}}{\pi_j^* q_{ji}}) q_{ji} \pi_j \text{.....(A.9)}$$

First we note the following identity

$$\frac{\min(1,\frac{\pi_j\pi_i^*}{\pi_i\pi_j^*})}{\min(1,\frac{\pi_i\pi_j^*}{\pi_j\pi_i^*})}=\frac{\pi_j\pi_i^*}{\pi_i\pi_j^*}\text{.....(A.10)}$$

Applying this identity to the first terms on the right and left hand side of (Eq. A.9) we obtain

$$\frac{\pi_j\pi_i^*}{\pi_i\pi_j^*}\min(1,\frac{\pi_j^*q_{ji}}{\pi_i^*q_{ij}})q_{ij}\pi_i=\min(1,\frac{\pi_i^*q_{ij}}{\pi_j^*q_{ji}})q_{ji}\pi_j\text{. .....(A.11)}$$

or equivalently

$$\frac{\pi_i^*}{\pi_j^*}\min(1,\frac{\pi_j^*q_{ji}}{\pi_i^*q_{ij}})q_{ij}=\min(1,\frac{\pi_i^*q_{ij}}{\pi_j^*q_{ji}})q_{ji}\text{.....(A.12)}$$

The latter is detailed balance condition for Metropolis-Hasting MCMC and can be directly verified using (Eq. A.12).

Denote the supports of the distributions as

$$\begin{aligned}&E=\{k;\pi(k)>0\},\\&E^*=\{k;\pi^*(k)>0\},\\&D=\{k;q(k\mid k_n)>0\text{ for some }k_n\in E\}.\end{aligned}\qquad\text{.....(A.13)}$$

To sample from $\pi(k)$ correctly, it is necessary that E is a subset of E^*. Otherwise, there will exist a subset $A\subset(E\setminus E^*)$ (i.e., the region A will be a subset of E^*, while it will not belong to E^*) such that

$$\pi(A) = \int_A \pi(x)dx > 0 \qquad \text{and} \qquad \pi^*(A) = \int_A \pi^*(x)dx = 0. \ldots\ldots\ldots\ldots..(A.14)$$

As a result, the chain $\{k_n\}$ will never visit (sample from) A since the element of A will never be pass the first stage. For the same reason, it is necessary to require that E is a subset of D. For most practical proposals $q(y \mid x)$, in particular, the ones used in the paper (random walk and independent sampler), E^* is a subset of D is true. In this case, E^* is also the support of the effective proposal $Q(k \mid k_n)$:

$$E^* = \{k; Q(k \mid k_n) > 0 \text{ for some } k_n \in E\}. \ldots\ldots\ldots\ldots\ldots\ldots\ldots\ldots\ldots\ldots\ldots\ldots\ldots(A.15)$$

In general, the support D of the proposal $q(k \mid k_n)$ is much larger than the support E of the target distribution $\pi(k)$.

Next we will discuss the irreducibility and aperiodicity of two-stage MCMC. In our numerical results, the proposal $q(y \mid x)$ is chosen to satisfy

$$q(y \mid x) > 0 \text{ for every } (x, y) \in E \times E. \ldots\ldots\ldots\ldots\ldots\ldots\ldots\ldots\ldots\ldots\ldots\ldots\ldots(A.16)$$

This guarantees that Metropolis-Hasting MCMC method is irreducible. Modified MCMC is reducible of

$$Q(y \mid x) > 0. \ldots\ldots\ldots\ldots..\ldots\ldots\ldots\ldots..\ldots\ldots\ldots\ldots..(A.17)$$

This is not difficult to verify. Again for simplicity, we do it for a discrete chain, where $Q_{ij} = a_{ij} q_{ij}$. It can be easily verified that if $q_{ij} > 0$ then $Q_{ij} > 0$.

To prove the convergence of the distribution, we need to show that the chain is aperiodic. Recall that a simple sufficient condition for the aperiodicity is that $K(k_n, \{k_n\}) > 0$ for some $k_n \in E$. For a discrete chain, this is equivalent to $K_{ii} > 0$ for

some i. This is always true except in a case where $\pi(k) \equiv \pi^*(k)$, and $\pi(k)$ happens to be the stationary distribution of the proposal $q(k \mid k_n)$. In this case, it doesn't make sense to use MCMC method since we can sample $\pi(k)$ directly from the distribution $q(k \mid k_n)$. So in practice, we can always safely assume that the chain $\{k_n\}$ generated by the modified MCMC method is aperiodic. As a result, the modified Markov chain converges to the posterior distribution.

APPENDIX B

ACCEPTANCE PROPERTIES FOR LANGEVIN ALGORITHM IN LINEAR PROBLEMS

We want to sample from the following posterior probability distribution:

$$\pi(k) \propto \exp\left(-\frac{(k-k_{\text{obs}})^2}{2a^2} - \frac{(F(k)-F_{\text{obs}})^2}{2b^2} \right). \quad \text{.....(B.1)}$$

Our goal here is to show that the Langevin algorithm has an acceptance probability of unity for linear problems. Denote

$$U(k) = \frac{(k-k_{\text{prior}})^2}{2a^2} + \frac{(F(k)-F_{\text{obs}})^2}{2b^2}, \quad \text{.....(B.2)}$$

$$dk(\tau) = -\frac{1}{2}\frac{\partial U(k)}{\partial k} d\tau + dw_\tau. \quad \text{.....(B.3)}$$
$$k(0) = k_0$$

Consider the following discretization for Eq. B.3:

$$\frac{k_{n+1}-k_n}{\Delta\tau} = -\frac{1}{4}\left(\frac{\partial U(k_{n+1})}{\partial k} + \frac{\partial U(k_n)}{\partial k} \right) + \sqrt{\Delta\tau} N(0,1). \quad \text{.....(B.4)}$$

For the linear case, we consider $F(k) = Ak$. It follows that

$$k_{n+1} = k_n - \frac{\Delta\tau}{4}\left(\frac{1}{a^2} + \frac{A^2}{b^2} \right)(k_n + k_{n+1}) + \frac{\Delta\tau}{2}\left(\frac{k_{obs}}{a^2} + \frac{AF_{obs}}{b^2} \right) + \sqrt{\Delta\tau} N(0,1). \quad \text{.....(B.5)}$$

For a special timestep of $\Delta\tau = \frac{4a^2b^2}{b^2 + a^2A^2}$, we get

$$k_{n+1} = \frac{ab}{\sqrt{b^2 + a^2A^2}} N(0,1) + \frac{b^2 k_{obs} + a^2 A F_{obs}}{b^2 + a^2A^2} \quad \text{.....(B.6)}$$

It can be shown that k_{n+1} in Eq. B.6 is a valid sample from the distribution in Eq. B.1 by setting $F(k) = Ak$ after some simplifications. We note that k_{n+1} is independent of k_n. Thus, in the linear case, the Langevin approach has acceptance probability of unity, as in the case of the RML method.

APPENDIX C

SAMPLING PROPERTIES OF RML

In this Appendix, we discuss the sampling characteristics of the RML. To start with, we briefly describe the RML approach following Oliver et al. (1996). For clarity of exposition, we will restrict ourselves to a 1D problem. First, a pair of unconditional realization of the model and the data, (k_{us}, F_{us}) is generated from the Gaussian distribution,

$$\rho(k,F) \propto \exp(-\frac{(k-k_{\text{obs}})^2}{2a^2}-\frac{(F-F_{\text{obs}})^2}{2b^2}). \quad \text{.....(C.1)}$$

Note that the variable F is treated as independent of k at this moment. Next, a calibrated sample k_{cal} is computed by solving the following minimization problem:

$$L(k_{\text{cal}}) = \min_k \frac{(k-k_{us})^2}{a^2}+\frac{(F(k)-F_{us})^2}{b^2}. \quad \text{.....(C.2)}$$

In general, the calibrated sample k_{cal} will not satisfy the desired stationary distribution $\pi(k)$ in Eq. C.1. To correct the error, k_{cal} is used as a proposal for the MCMC method (Oliver et al. 1996). At state k_n, the proposal k_{cal} is accepted as a new sample with the probability

$$p(k_n,k_{\text{cal}}) = \min\left(1, \frac{\pi(k_{\text{cal}})q(k_n)}{\pi(k_n)q(k_{\text{cal}})}\right), \quad \text{.....(C.3)}$$

where $q(k_{\text{cal}})$ is the probability of proposing k_{cal} in the above procedure. Note that the proposal distribution $q(k_{\text{cal}})$ does not depend on the current state, k_n. Because k_{cal} is proposed by solving a nonlinear minimization problem in Eq. C.2, the analytical formula of $q(k_{\text{cal}})$ is not readily available. However, the proposal distribution $q(k_{\text{cal}})$ is well defined and can be derived theoretically. Following Oliver et al. (1996), consider the following map:

$$k_{us} = h(k_{\text{cal}}, F_{us}). \quad \text{.....(C.4)}$$

In Eq. C.4, we treat F_{us} as a parameter (i.e., conditioning on the variable F_{us}). Denote the distribution of F_{us} as $\rho_F(F_{us})$, and the conditional distribution of k_{us} on F_{us} as $\rho_{k|F}(k_{us})$. Then the map between k_{us} and k_{cal} will introduce a conditional probability measure for k_{cal}, which we denote as $q(k_{\text{cal}} \mid F_{us})$. By simple chain rule, we have

$$\rho_{k|F}(k_{us})dk_{us} = \rho_{k|F}(k_{us})Jdk_{\text{cal}} = q(k_{\text{cal}} \mid F_{us})dk_{\text{cal}}, \quad \text{.....(C.5)}$$

where

$$J(k_{\text{cal}}, F_{us}) = \left| \frac{\partial(k_{us})}{\partial(k_{\text{cal}})} \right| \quad \text{.....(C.6)}$$

is the Jacobian. It follows that (Oliver et al. 1996):

$$q(k_{\text{cal}}) = \int q(k_{\text{cal}} \mid F_{us})\rho_F(F_{us})dF_{us} = \int \rho(k_{us}, F_{us})JdF_{us} \quad \text{.....(C.7)}$$

For general nonlinear problems, it is very difficult to compute the map $k_{us} = h(k_{\text{cal}}, F_{us})$ and hence the Jacobian *J*. As an approximation, Oliver et al. (1996) suggest either to accept all the proposals k_{cal}, or to modify the acceptance criteria as

$$p(k_n, k_{\text{cal}}) = \min\left(1, \frac{\pi(k_{\text{cal}})}{\pi(k_n)}\right). \quad \text{……..……..(C.8)}$$

The common practice is to accept all the proposals, k_{cal}. This approximation is equivalent to assuming that k_{us} is sufficiently close to k_{cal}. This is a potential limitation, because this assumption can be violated easily in practice.

The RML approach is easier to visualize when we cast the algorithm in a geometric framework. The minimization problem in Eq. C-2 is to find a point $(k_{\text{cal}}, F(k_{\text{cal}}))$ on the surface $F = F(k)$ which is "closest" to (k_{us}, F_{us}) with respect to a particular distance,

$$d(\vec{x}, \vec{y}) = \frac{(x_1 - y_1)^2}{a^2} + \frac{(x_2 - y_2)^2}{b^2}. \quad \text{……..……..……..(C.9)}$$

This is illustrated in **Fig. C.1**. In fact, one can obtain an expression for the distribution, $q(k_{\text{cal}})$. From the minimization in Eq. C.2, k_{cal} satisfies (assuming $a = b = 1$ for simplicity) ,

$$F'(k_{\text{cal}})(F(k_{\text{cal}}) - F_{us}) + (k_{\text{cal}} - k_{us}) = 0. \quad \text{……..…(C.10)}$$

From Eq. C-10, we have

$$k_{us} = k_{\text{cal}} + F'(k_{\text{cal}})(F(k_{\text{cal}}) - F_{us}). \quad \text{……..(C.11)}$$

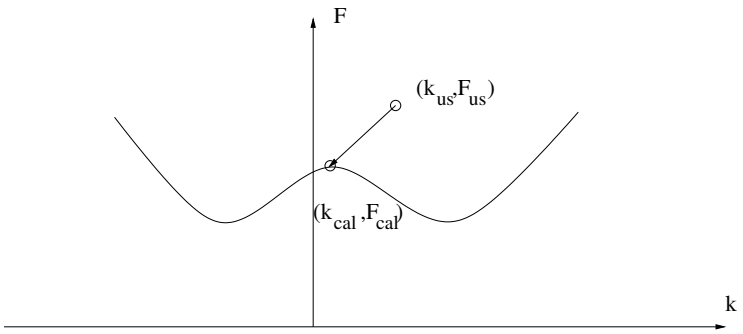

Fig. C. 1—Geometric interpretation of RML.

Also,

$$J = \left| \frac{\partial k_{\text{obs}}}{\partial k_{\text{cal}}} \right| = \left| 1 + F''(k_{\text{cal}})(F(k_{\text{cal}}) - F_{us}) + F'(k_{\text{cal}})^2 \right| . \quad \text{(C.12)}$$

For simplicity, assuming $k_{us} = F_{us} = 0$, we obtain from Eq. C.7, after some manipulations,

$$q(k_{cal})=\int \exp(-(k_{cal}+F'(k_{cal})(F(k_{cal})-F_{us})-k_{obs})^2-(F_{us}-F_{obs})^2)JdF_{us}=$$

$$\int \exp(-(k_{cal}+F'(k_{cal})F(k_{cal}))^2+2(k_{cal}+F'(k_{cal})F(k_{cal}))F'(k_{cal})F_{us}-(F'(k_{cal})^2+1)F_{us}^2)JdF_{us}=$$

$$\int \exp(-(\sqrt{F'(k_{cal})^2+1}F_{us}-\frac{F'(k_{cal})(k_{cal}+F'(k_{cal})F(k_{cal}))}{\sqrt{F'(k_{cal})^2+1}})^2)$$

$$\exp(-\frac{(k_{cal}+F'(k_{cal})F(k_{cal}))^2}{F'(k_{cal})^2+1})JdF_{us}=$$

$$\int \exp(-(\sqrt{F'(k_{cal})^2+1}F_{us}-\frac{F'(k_{cal})(k_{cal}+F'(k_{cal})F(k_{cal}))}{\sqrt{F'(k_{cal})^2+1}})^2)$$

$$\exp(-\frac{(k_{cal}+F'(k_{cal})F(k_{cal}))^2}{F'(k_{cal})^2+1})|1+F''(k_{cal})(F(k_{cal})-F_{us})+F'(k_{cal})^2|dF_{us}=$$

$$\exp(-\frac{(k_{cal}+F'(k_{cal})F(k_{cal}))^2}{F'(k_{cal})^2+1})\times$$

$$\int \exp(-(\sqrt{F'(k_{cal})^2+1}F_{us}-\frac{F'(k_{cal})(k_{cal}+F'(k_{cal})F(k_{cal}))}{\sqrt{F'(k_{cal})^2+1}})^2)$$

$$|1+F''(k_{cal})(F(k_{cal})-F_{us})+F'(k_{cal})^2|dF_{us}.$$

……..(C-12)

It is unlikely that Eq. C-12 will be equivalent to the desired posterior distribution in Eq. C-1,

$$\pi(k) \propto \exp(-F(k)^2-k^2),\ \text{…….……} \quad \text{(C-13)}$$

for general $F(k)$. In general, the limits of integrations in Eq. C-11 are not the whole real line and one needs to restrict the integration. Some of these integrations can be computed explicitly and $q(k_{cal})$ involves high order derivatives of objective functional and is unlikely to be equal to $\pi(k)$.

VITA

Xianlin Ma
1500 Louisiana, Houston, TX 77002
xianlinm@yahoo.com

Education

Ph.D., Petroleum Engineering, Texas A&M University, College Station, TX, USA, Aug. 2008
M.S., Statistics, University of Waterloo, Ontario, Canada, October 2003
M.S., Applied Geophysics, China University of Petroleum, Beijing, China, May 1990
B.S., Applied Geophysics, China University of Geosciences, Wuhan, China, July 1987

Journal Articles

1. Ma, X., Al-Harbi, M., Datta-Gupta, A., and Efendiev, Y. 2008. An Efficient Two-Stage Sampling Method for Uncertainty Quantification in History Matching Geological Models. *SPE Journal* **13** (1): 77-87.
2. King, M., Burn, K., Wang, P., Muralidharan, V., Alvarado, F., Ma, X., and Datta-Gupta, A. 2006. Optimal Coarsening of 3D Reservoir Models for Flow Simulation. *SPE Reservoir Evaluation & Engineering* **24** (10): 317-334.
3. Efendiev, Y., Datta-Gupta, A., Ma, X., and Mallick, B. 2008. In Press. Modified MCMC for Dynamic Data Integration Using Streamline Models. *Mathematical Geosciences.*
4. Efendiev, Y., Datta-Gupta, A., Ginting, V., Ma, X., and Mallick, B. 2005. An Efficient Two-Stage Markov Chain Monte Carlo Method for Dynamic Data Integration. *Water Resources Research* **41** W12423.
5. Caers, J. and Ma, X. 2002. Modeling Conditional Distribution of Facies from Seismic Using Neural Nets. *Mathematical Geology* **34** (2): 143-167.
6. Ma, X. and Yao, T. 2001. A Program for 2D Modeling (cross) Correlogram Tables Using Fast Fournier. *Computer & Geoscience* **27** (7) 763-774.
7. Ma, X. and Journel, A. 1999. An Expanded GSLIB Cokriging Program Allowing for Two Markov Models. *Computer & Geoscience* **25** (6): 627-639.

This dissertation was typed by the author.